OBSERVATIONS OF FATIGUE CRACK GROWTH RATE AND CLOSURE BEHAVIOR IN 7475-T731 ALUMINUM UNDER VARIABLE AMPLITUDE LOADING*

Charles C. Turner
Graduate Research Assistant

and

B. M. Hillberry
Professor

School of Mechanical Engineering
Purdue University
West Lafayette, IN 47907

NASA Research Grant NAG-1-231
"Constraint Effects on Fatigue Crack Propagation"
National Aeronautics and Space Administration
Langley Research Center
Hampton, Virginia 23665

* This report is essentially Charles C. Turner's M.S. thesis.

TABLE OF CONTENTS

Page

LIST OF TABLES

LIST OF FIGURES

Figure Page

Appendix
Figure Page

Figure Page

Figure Page

LIST OF SYMBOLS

Symbol	Description
A	cross sectional area of specimen
a	crack length
a_{ol}	overload affected zone size
b	constant
c	constant
CMOD	crack mouth opening displacement
CTOD	crack tip opening displacement
$\frac{da}{dN}$	fatigue crack growth rate
$\frac{da}{dN}\Big\|_{1IF}$	interaction free growth rate for K_1 cycle
$\frac{da}{dN}\Big\|_{IF}$	interaction free fatigue crack growth rate
$\frac{da}{dN}\Big\|_{min}$	minimum fatigue crack propagation rate
$\frac{da}{dN}\Big\|_{ol}$	pre-overload fatigue crack propagation rate
E	modulus of elasticity
K_I	mode I stress intensity factor
K_{II}	mode II stress intensity factor
K_{III}	mode III stress intensity factor
K_{bmax}	maximum stress intensity in a loading block
K_{bmin}	minimum stress intensity in a loading block
K_{max}	maximum stress intensity factor
K_{min}	minimum stress intensity factor

K_{ol}	overload stress intensity factor
K_{op}	stress intensity factor at crack opening
ΔK	stress intensity factor range
ΔK_{eff}	effective stress intensity factor range
m	constant
N	number of cycles
N_D	number of delay cycles
N_2	number of fatigue cycles between overloads
n	constant
P	applied load
P_{max}	maximum applied load
P_{min}	minimum applied load
P_{ol}	applied overload
ΔP	cyclic load range
Q_{ol}	overload ratio, K_{ol}/K_{max}
R	stress ratio, K_{min}/K_{max}
R_{cut}	stress ratio above which closure is not observed
R_f	stress ratio of the fatigue cycles
R_{ol}	overload stress ratio, K_{min}/K_{ol}
$r_{y\varepsilon}$	plane strain plastic zone radius
$r_{y\varepsilon\|ol}$	overload plane strain plastic zone radius
$r_{y\sigma}$	plane stress plastic zone radius
$r_{y\sigma\|ol}$	overload plane stress plastic zone radius
$\Delta r_{y\varepsilon}$	cyclic plane strain plastic zone radius
t	specimen thickness
ε	strain

π	ratio of circumference to diameter of a circle
σ	stress
σ_{ys}	yield stress
ν	Poisson's ratio

ABSTRACT

Turner, Charles Christopher. M.S.M.E., Purdue University. May 1986. Observation of Fatigue Crack Growth Rate and Closure Behavior in 7475-T731 Aluminum Under Variable Amplitude Loading. Major Professor: Dr. B.M. Hillberry, School of Mechanical Engineering.

Simultaneous measures of fatigue crack propagation rate and crack closure were taken from 7475-T731 aluminum alloy center cracked tensile specimens under variable amplitude loading conditions. Variable amplitude servo hydraulic machine control and data acquisition were performed using commercially available microprocessor and analog-to-digital equipment. Crack tip opening measurements using an Elber type extensometer were combined with load data to determine the crack opening load levels using the compliance technique. Digital load and crack tip opening displacement data were numerically analyzed to optimize crack opening load using a least squares non-linear regression algorithm.

Results indicate the presence of load interaction in a variety of repeated variable amplitude loading blocks. Constant amplitude tests conducted by Daiuto provide an

interaction free data base by which observed rates were compared. Load interaction results in retardation of propagation rate for most loading blocks examined in the study. Growth rate acceleration was not observed for any of the loading blocks studied. In cases where load interaction is observed, measured crack opening loads correlate well with observed propagation rate data using a growth rate expression based on effective stress intensity range. Closure did not explain observed delay behavior associated with high stress ratio, single peak overloads. Primary influences on the crack opening stress intensity level include the maximum stress intensity of the repeated loading block, the minimum stress intensity of the block, and the number of fatigue cycles between overloads in a block.

CHAPTER 1 - INTRODUCTION

Fatigue cracks and their growth have been recognized as a significant factor in the failure of many types of structures. In recent history, much attention has been focused on the mechanics of crack growth and the role which it plays in the service life of a structure. Toward this end, numerous physical and phenomenological models have been developed to predict the role of crack growth under service loading conditions. The predictive capabilities of early crack growth models suffered, primarily due to their inability to quantify one important physical phenomenon which has been experimentally verified by numerous investigators; the load interaction effect. The acceleration or retardation of crack growth rate due to the sequence and magnitude of the loads in a given loading spectrum has proven to be a difficult phenomenon to explain with mathematical models. To date, crack growth models remain inadequate in their ability to account for the interaction in random loading patterns which are typical in many service loading conditions.

Current theories concerning the effect of load interaction on crack growth suggest that the predictive

accuracy could be substantially improved with an understanding of the crack closure phenomenon. While the concept of crack closure proposed by Elber [2] is over 15 years old, it has proven to be a difficult concept to quantify in various materials. This is likely the result of the acute instrument sensitivity needed to accurately detect crack opening stress intensity. As a result, there is contradiction in the literature as to exactly how the crack opening stress intensity behaves under variable amplitude loading conditions.

In the following pages, the author will describe the investigative procedure and results of a study conducted to examine the load interaction effect in an aircraft aluminum alloy. The objective of this investigation was to gather accurate crack opening stress intensity and crack growth rate data simultaneously from cracks in center-cracked 7475-T731 aluminum specimens subjected to variable amplitude loading conditions. Crack growth rates will be related to the effective stress intensity range to establish crack closure as the primary mechanism of load interaction in low R-ratio loading.

CHAPTER 2 - LITERATURE SEARCH

As mentioned previously, fatigue crack growth and its effect on the service life of structures has been the focus of many experimental and analytic studies since being recognized as a primary cause for mechanical failure. A review of contemporary literature in the fields of fracture mechanics and crack growth indicates that, at the very least, the physical process of crack growth is a complex phenomenon which is affected by a number of interelated factors. While many of these factors undoubtedly affect the rate of fatigue crack growth in structural materials, it is essential to identify the first order contributors to fatigue crack growth if significant contributions to the prediction of growth rates are to result from subsequent research efforts. Although this study is primarily concerned with the factors affecting fatigue crack propagation (FCP) rates under variable amplitude loading, a review of the literature affirms that an understanding of the factors affecting constant amplitude FCP is essential in quantifying more complex loading spectrums. Before proceeding to a more detailed presentation of the factors affecting both

constant and variable amplitude FCP, two concepts of historical significance to the understanding of crack growth will be presented.

2.1 Historic Contributions to Contemporary FCP Theory

In 1961, Paris et al. [1] proposed a mathematical relation based on experimental data which related the FCP rate in fractured specimens under constant amplitude loading to the applied stress intensity range (ΔK). This relation,

$$\frac{da}{dN} = C\left[\Delta K\right]^m \tag{2.1}$$

employs two empirically obtained constants, C and m, which correspond to the y-intercept and slope of constant amplitude FCP rates when plotted against ΔK on a log-log scale. While this relation has been popularly recognized as a major advancement in the prediction of FCP rates, it does not explain the observed influence of the stress ratio (R) on the rate of crack growth under constant amplitude loading conditions. The experimentally confirmed R effect is the phenomenon wherein higher FCP rates are observed at higher R ratios given the same ΔK in constant amplitude loading.

In a series of papers presented in the late 1960's, Elber [2,3] proposed a modification to the Paris law which

accounted for the R effect on constant amplitude FCP rates. Based on observations of load versus crack tip opening displacement plots recorded for 2024-T3 aluminum sheets under tension-tension loading, Elber concluded that, in many cases, the crack tip was closed for a significant portion of the loading cycle. In a description of a typical plot of his experimental data, shown in Figure 2.1, Elber illustrated that in loading from A to B the compliance of the cracked specimen was equal to that of an uncracked specimen of the same geometric configuration.

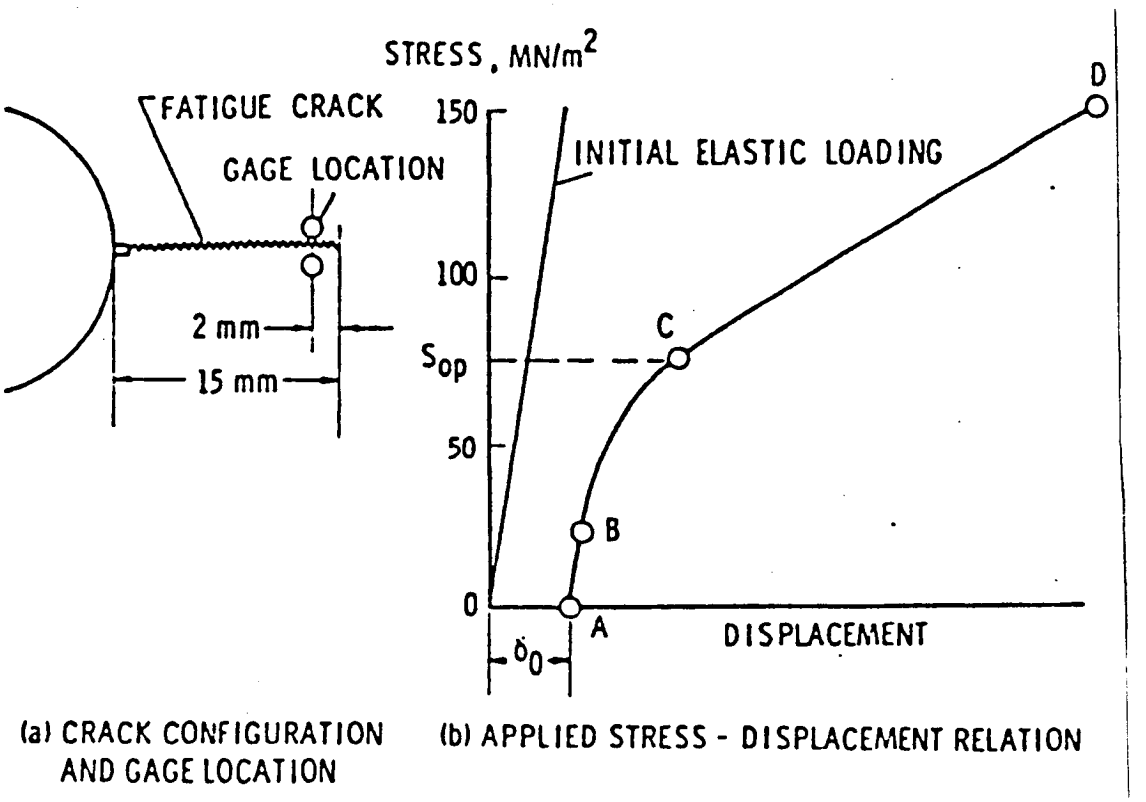

Figure 2.1 Elber's load versus CTOD profile for defining K_{op}. [2]

For loads higher than the load corresponding to point C the crack is fully open, thus, the compliance from point C to point D is that of a fully opened crack. Elber called the load associated with point C the crack opening load and its corresponding stress the crack opening stress (S_{op}). Since the crack tip is not open until S_{op} is achieved, Elber concluded that crack extension should not occur at stress intensities below that point. A new parameter, ΔK_{eff}, was formulated such that:

$$\Delta K_{eff} = K_{max} - K_{op} \tag{2.2}$$

where,

ΔK_{eff} = the effective stress intensity range,

K_{max} = the maximum stress intensity of a fatigue cycle,

K_{op} = the crack opening stress intensity,

and the closure based growth rate equation is given by

$$\frac{da}{dN} = C\left[\Delta K_{eff}\right]^m \tag{2.3}$$

or

$$\frac{da}{dN} = C\left[\Delta KU\right]^m \tag{2.4}$$

where U is a material dependent function of stress ratio.

Elber conducted a series of experiments at different stress ratios in order to determine the effect of R on the parameter U in equation 2.4. Under plane stress loading

conditions, Elber's data indicated that U, the ratio of ΔK_{eff} to ΔK, was a linear function of R for 2024-T3 aluminum. This functional relationship between U and R is

$$U = 0.5 + 0.4R \qquad (2.5)$$

When equations 2.4 by Elber and 2.5 were combined and used to predict constant amplitude FCP rates in 2024-T3 aluminum sheet the results affirmed the superiority of the closure based growth rate equation in predicting the effects of the stress ratio on fatigue crack growth.

The concept of fatigue crack closure is widely accepted as a significant factor affecting fatigue crack growth under both constant and variable amplitude loading conditions. However, in order to employ the closure concept in a cycle-by-cycle crack growth model such as Johnson's MPYZ model [4] for service life prediction, a thorough understanding of the factors affecting the behavior of K_{op} in constant and variable fatigue loading must be attained. It is in this explanation of the primary factors affecting K_{op} that the author finds wide disagreement in the literature.

2.2 Factors Affecting K_{op}

Elber concluded that the closure phenomenon was a result of residual compressive stresses left in the wake of

an advancing crack. These stresses, he suggested, serve to close the crack over varying portions of the loading cycle depending on its relative minimum and maximum stress intensity values. Studies conducted since Elber's work suggest that R may not fully describe the behavior of K_{op}. In addition, investigators have shown the prescence of closure effects generated from asperities and oxides on the fracture surface. A proper review of the observed factors affecting K_{op} under variable amplitude loading requires a survey of the literature addressing these factors under constant amplitude loading.

2.2.1 Stress Ratio and Surface Effects

The effect of stress ratio on U which was first observed by Elber was confirmed in tests conducted by Katcher and Kaplan [5]. Using compact tension specimens from 2219-T851 aluminum and Ti-6Al-Cu titanium, Katcher and Kaplan ran a series of constant amplitude crack growth tests at different stress ratios. During these tests, closure was measured using a strain gage extensometer at a distance of 0.05 inches behind the crack tip. These tests showed that the characteristic shift in FCP rate curves with R could be explained with equation 2.4 when a unique $U=f\left[R\right]$ for each material was found using load versus CTOD data. Their linear expressions for U in terms of R are given for the aluminum and titanium alloys in equations 2.6

and 2.7, respectively. It is important to note that no closure was observed at stress ratios above 0.35 in these materials.

2219-T851: $U = 0.68 + 0.91R$ when $0.08 < R < 0.32$ (2.6)

Ti-6Al-Cu: $U = 0.73 + 0.82R$ when $0.08 < R < 0.35$ (2.7)

McEvily [6] finds flaw in explaining closure in terms of stress ratio for several reasons. Based on observations of constant amplitude FCP rate curves at different stress ratios in En30A steel, McEvily points to a pronounced difference in the R effect on FCP rates which apparently result from different material hardnesses due to heat treatment. Observing that R has a greater effect on FCP rates in the material with lower toughness values, it is suggested that this is inconsistent with the idea of R influenced closure. Viewing closure as a surface asperity phenomenon, McEvily suggests that closure exerts its greatest effect at low ΔK values, regardless of the stress ratio. At this low ΔK value, McEvily asserts, the effect of microscopic Mode II displacements result in surface asperities which approach the size of the crack tip opening displacement. To substantiate this supposition, he points to plots of K_{op} / K_{max} versus ΔK which show the diminishing effect of K_{op} as ΔK increases in constant amplitude tests for AISI 1018 steel (Figure 2.2).

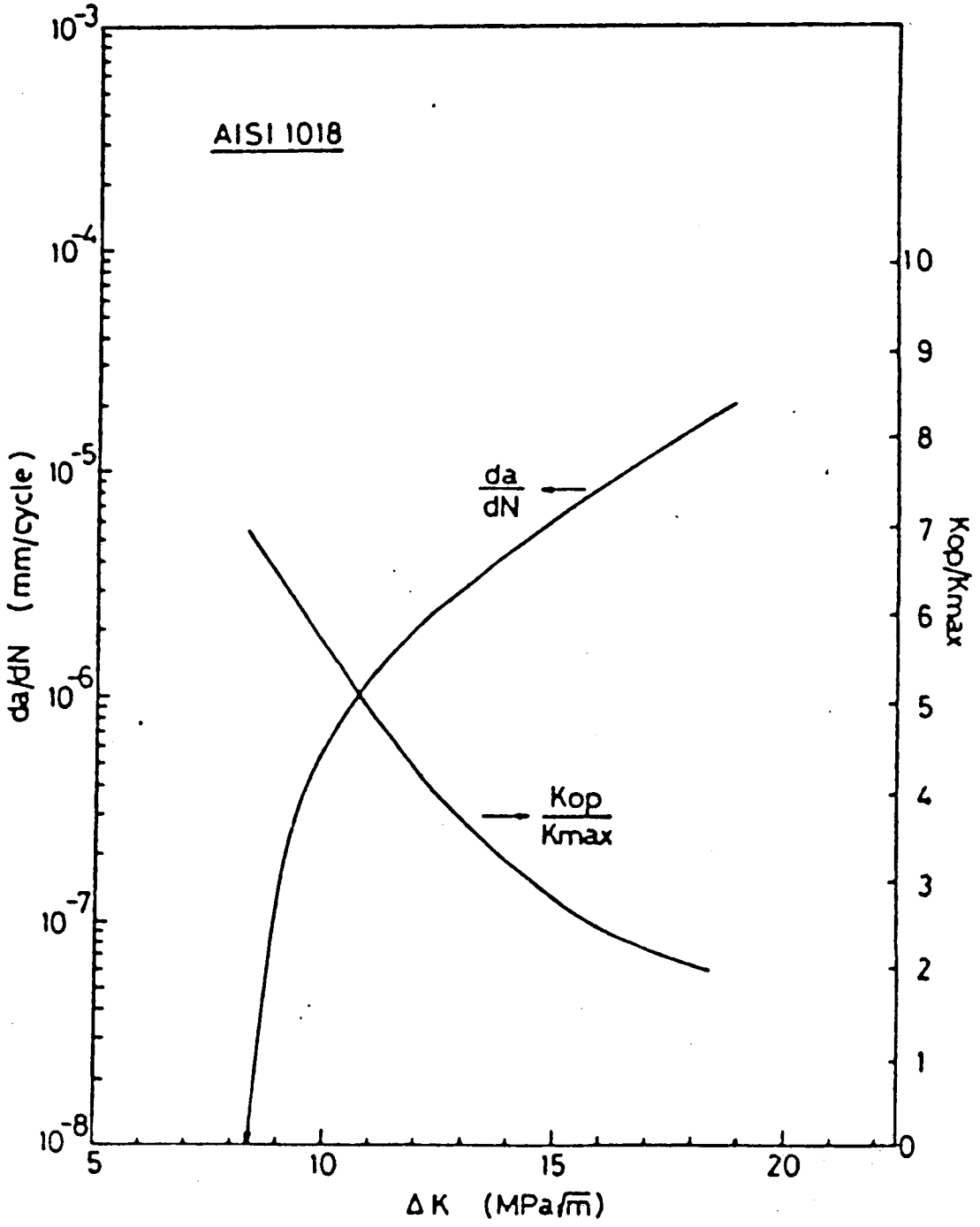

Figure 2.2 Observed K_{op}/K_{max} versus crack length using CMOD gage. [6]

In an effort to study Elber's observations of stress ratio on U at low ΔK values, Yu and Topper [7] performed a series of constant amplitude tests with different stress ratios in the near threshold FCP region. Using 2024-T351 aluminum, constant amplitude tests were run at an assortment of stress ratios ranging from -1.0 to 0.7. These tests showed that the R effect was present at near threshold FCP rates and that equations 2.4 and 2.5 could be used to collapse the growth rate curves at different R values onto one FCP rate versus ΔK_{eff} curve. These results indicate that the mechanism of closure at low growth rates near the fatigue threshold is similar to that observed in the mid growth rate region. Since the effects of surface asperities or oxides are assumed to have a greater influence at low ΔK values, this evidence seems more consistent with the plasticity induced closure theory.

Frenot and Gasc [8] investigated the significance of surface roughness on closure near the threshold ΔK range. In order to do this, 7075 aluminum was age hardened in two different conditions so as to induce a relatively smooth and rough surface in separate fracture specimens. Observations of the rough fracture surface under fatigue cycling indicated that the crack was opening gradually under stress while the smooth fracture surface appeared to behave more like a hinge, opening simultaneously all along the fracture surface. Using the potential drop technique to determine

when the crack tip opened in each of these specimens, a high U value was observed in the specimen with the rougher fracture surface. From these observations it was concluded that the surface asperities had resulted in friction forces which seemed to hold the crack closed, thereby resulting in a primary mechanism of fatigue crack closure.

Both Frenot and McEvily draw conclusions about the significance of asperity induced closure based on observations made of materials which have been aged or heat treated to different hardnesses. This raises obvious questions in the author's mind about the effect of increased yield strength with increased hardness. It seems that all of the effects witnessed in these surface asperity arguments may also be explained by the same plasticity induced closure theory proposed by Elber. While this by no means refutes the significance of the asperity induced closure theory, it is important to note when weighing the relative merits of each proposed closure mechanism.

2.2.2 Stress State and Maximum Stress Intensity

If plastic deformations in the wake of an advancing crack are considered as the primary source of fatigue crack closure, specific attention must be focused on the factors affecting crack tip plasticity. Irwin [9] related yield stress and stress intensity to the size of the plastic zone at the crack tip in the relations given in equations 2.8

and 2.9. For plane stress conditions where constraint effects due to the free surface are a dominant factor in this stress state, the radius of the plastic zone is given by

$$r_{y\sigma} = \frac{K^2}{2\pi\sigma_y^2} \tag{2.8}$$

and in plane strain conditions,

$$r_{y\varepsilon} = \frac{K^2}{6\pi\sigma_y^2} \tag{2.9}$$

where σ_y is the yield strength material.

Daiuto and Hillberry [10] observed thickness effects on crack propagation rates in 7475-T731 aluminum sheet due to stress state transitions at the crack tip. However, there is some question as to whether this thickness effect is primarily the result of increased plasticity at the crack tip resulting in fatigue crack closure. In their work it was concluded that the observed difference in constant amplitude FCP rates at R=0.05 was the result of increased Mode II stress intensity due to the characteristic slant of the fracture surface. Observed rate differences at R=0.75 could not be attributed to the fracture mode transition, indicating that another mechanism was in play.

Lindley and Richards [11] used microscopic evaluations of the fracture profile to show that crack tip closure in

mixed mode stress states was predominate at the surface of the specimen where plane stress conditions are dominant. Shaw and LeMay [12] verified these results using scanning electron microscopy in experiments conducted on AISI 4010 steel. In this study, single edge notched specimens were subjected to constant amplitude loading while closure measurements were taken using extensometers to measure crack tip and crack mouth opening displacements. Fractographic analyses of the fracture surface showed evidence of closure induced abrasion at the free surface while the interior, plane strain portions of the fracture surface appeared to be free of abrasion. Thus, the phenomenon of surface closure associated with the plane stress slant of the fracture surface was recognized as an important factor in the determination of K_{op}. This type of closure was substantiated by Shaw and Lemay using crack tip extensometers since evidence in their study indicated that K_{op} measurements made with a crack mouth opening gage were increasingly unreliable as the crack increased in length. This would seem to explain the observations made by McEvily concerning the diminishing effect of crack closure as the crack grows.

Fleck [13] evaluated many contemporary closure measuring devices in an effort to confirm closure at the crack tip under plane strain conditions. Concluding that many of the techniques used in previous studies yield inherently erroneous results, Fleck proposed to measure closure at the

crack tip directly by using a push-rod assembly which was inserted into holes in the fractured specimen. The holes were drilled in order to establish locating surfaces above and below the crack surface on which the push rods could rest. In constant amplitude, plane strain, R=0.05 loading conditions U was measured in B54460-50B steel to be a constant value of 0.81. From his observations Fleck concluded that the crack-closed increment in plane strain conditions is much smaller than that in plane stress conditions. For this reason, it is much more difficult to measure using conventional techniques. However, it was shown that the bulk closure behavior of the material could be measured using a surface type crack tip extensometer if it was placed at least 1.5 plastic zones behind the crack tip. [13]

In a series of constant amplitude tests conducted to determine the effect of K_{max} on ΔK_{eff} Vasques and Morrone [14] concluded that K_{max} alone could be used to describe the behavior of K_{op}. In tests conducted from R = 0.05 to 0.6, it was shown that ΔK_{eff} maintains a linear relationship with K_{max} and was independent of stress ratio. These results indicate the significance of crack tip plasticity in the closure phenomenon. However, in plots of K_{op} / K_{max} versus K_{max} their results show a characteristic curve associated with each material tested (Figure 2.3). It was concluded from their work that these curves were

material dependent and considered as material properties when calculating crack growth rates.

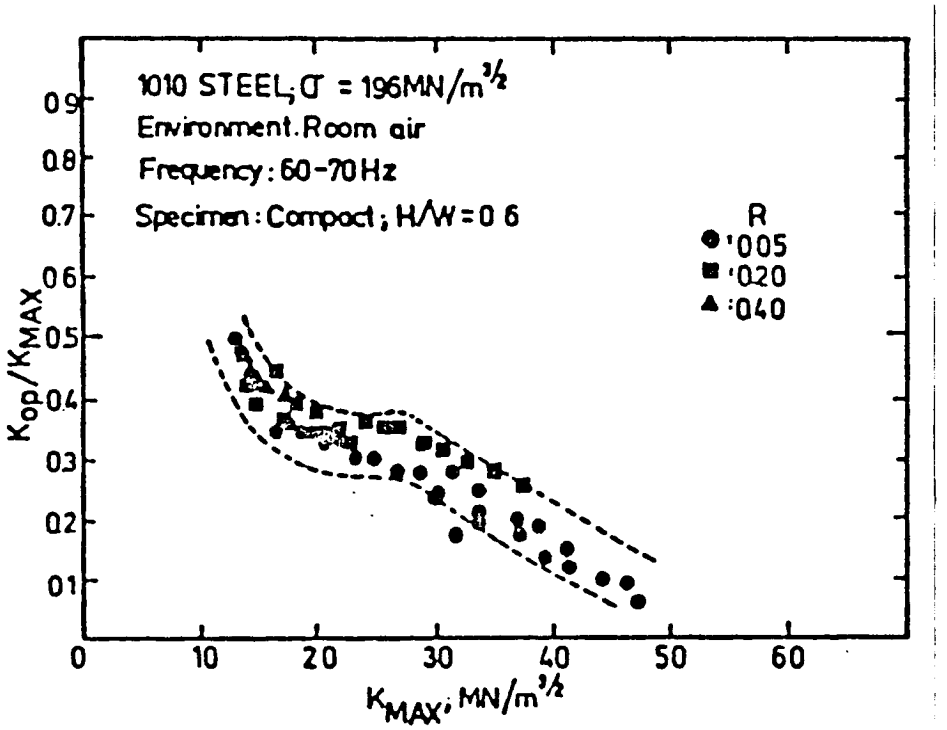

Figure 2.3 Vasques and Morrone K_{op}/K_{max} vs. K_{max} results. [14]

2.3 Variable Amplitude Loading Effects on K_{op}

Load interaction and its effects on FCP rates has been the focus of numerous studies over the past 20 years. A representative body of work compiled by Hillberry and associates [15-18] may be use to characterize the effect of

single peak overloads on the FCP rates of subsequent fatigue cycles. In these studies, numerous overloads have been applied to 2024 and 7475 aluminum alloys while their effects on crack growth rate were measured using an optical microscope along with a digital cycle counter. A summary of the observations in these studies with respect to load interaction is provided as follows:

1. Following the application of an overload during a constant load amplitude or constant K fatigue test, a brief period of acceleration in FCP rate is followed by a significant period of retardation.

2. The period of delay in FCP rate may be related to the Irwin plastic zone size and larger overloads produce longer delays.

3. Crack arrest may result from the application of an overload of sufficient magnitude. The ratio of the overload stress intensity to the maximum stress intensity of the fatigue cycles, Q_{ol}, required to produce crack arrest is a function of the stress ratio of the fatigue cycles.

4. Underloads applied following an overload serve to reduce the delay effect or eliminate it entirely, depending on the magnitude of the underload.

These observed effects of load interaction on FCP do not lend themselves to simple predictions which base FCP rates on the ΔK as seen in constant amplitude growth tests. Elber [3] conducted the first tests which indicated that these delay effects are the result of fluxuations in ΔK_{eff} resulting from changes in K_{op}. Elber's experiments showed that K_{op} sharply decreased immediately after overloads and then gradually increased to a maximum corresponding to the period of maximum retardation in the FCP rate as show in Figure 2.4.

It was shown that the original dip in K_{op} resulted from plastic deformations caused by the overload which were larger than the displacements at the crack tip recorded prior to the overload. This large plastic deformation served to hold the crack tip open thus reducing K_{op}. However, as the accelerating crack grows into the plastic zone produced by the overload, residual compressive stresses close in its wake and gradually raise K_{op} until maximum delay occurs. Eventually, the crack grows sufficiently beyond the plastic zone of the overload such that its delay effect is not present as K_{op} returns to its constant amplitude value at the given stress ratio.

Subsequent investigations into the load interaction effect on FCP rate revealed that the number of delay cycles, N_D, resulting from an overload could be increased

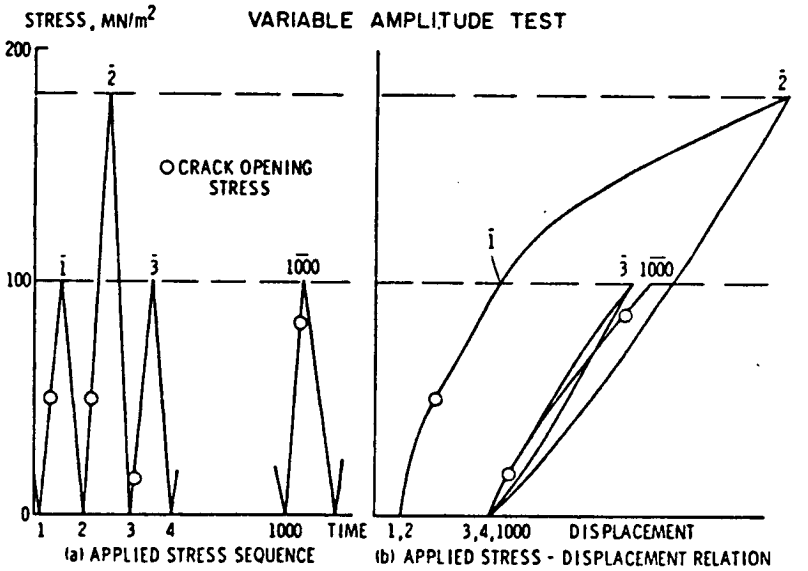

Figure 2.4 Elber's observations of K_{op} behavior following an overload. [2]

if multiple overloads were applied. Chehimi et al. [19] recently presented their observations of this effect in E36 steel at different values of Q_{ol} and R_f=0.1. Their results are shown graphically in Figure 2.5. It should be noted that for Q_{ol} of 1.9 and 2.2 arrest was induced by the application of multiple overloads where it did not occur for single overloads. Trebules [20] and Chang and Lemay

[21] have also noted this phenomenon in an assortment of aircraft aluminum alloys.

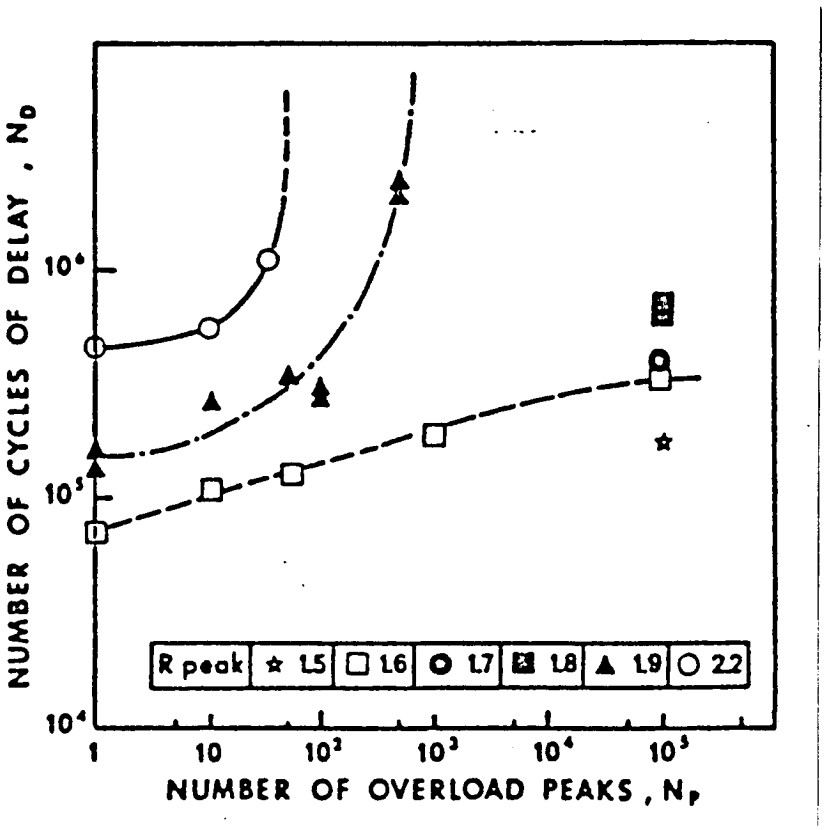

Figure 2.5 Chehimi's arrest results. [18]

Topper and Yu [22] measured K_{op} for cracks in various steels and 2024-T351 aluminum while subjecting them to the high-low block loading sequences described above. Their observations of K_{op} indicated that delay associated with this loading sequence is at least partially attributable to closure mechanisms. In Figure 2.6 their observations of K_{op} during loading are presented graphically.

Crack opening levels in these experiments were determined using crack tip extensometers.

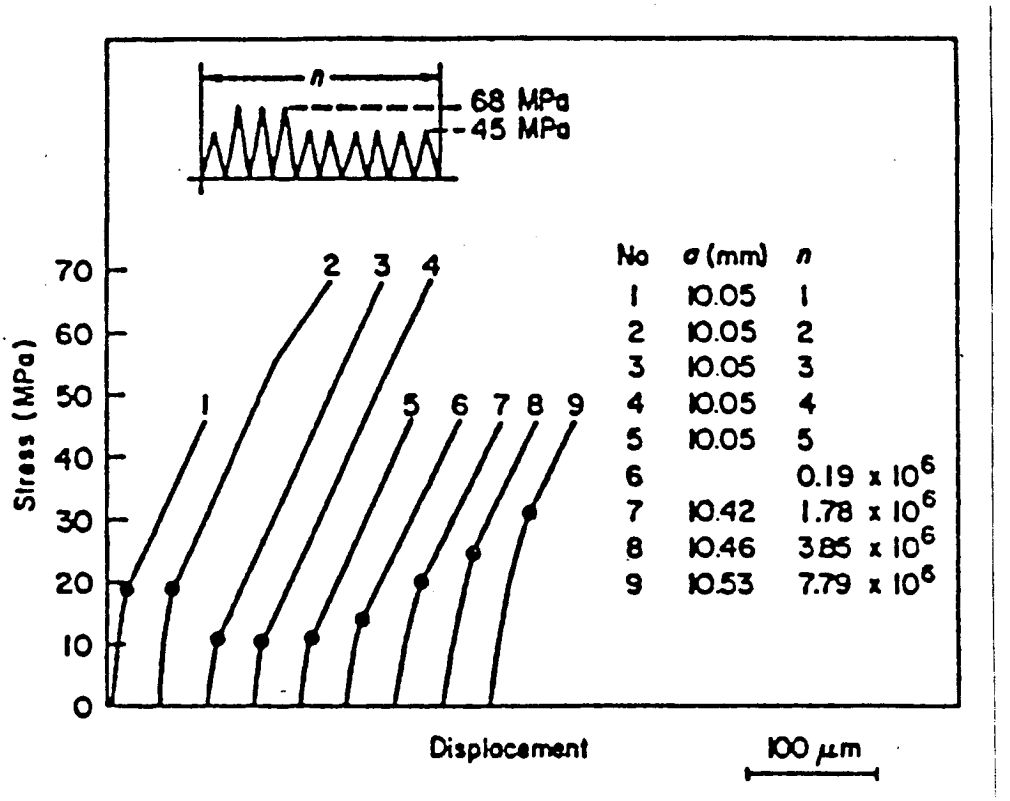

Figure 2.6 Observed behavior of K_{op} in block loading.[22]

Despite the apparent significance of crack closure in explaining the effect of load interaction on FCP rates, there are few studies which document the behavior of K_{op} under variable amplitude loading histories. According to Fleck, many of the studies which have been conducted suffer from inconsistent K_{op} data due to improper gage placement or faulty experimental technique. With the knowledge of

K_{op} behavior as it stands today, a number of proven mathematical models which predict the effects of load interaction quite well have been developed. A number of these models use finite element methods to account for the effects of K_{max}, the minimum stress intensity (K_{min}), and material hardening characteristics on K_{op} [23-25]. These models tend toward high complexity and their use at this time is primarily limited to their developers. In order for more simple load interaction models to be perfected for day to day use, the literature indicates a pressing need for more experimental data concerning the effect of load interaction spectrum and variable amplitude loading sequences on the FCP rate and K_{op}.

CHAPTER 3 - TEST PROGRAM

In response to the recognized need for a broader experimental data base, the objective of this investigation is to study the effects of variable amplitude loading on the fatigue crack propagation and K_{op} behavior of 7475-T731 aluminum alloy. Since it seems that a number of factors influence the FCP behavior under variable amplitude loading conditions, an effort was made to single out and study those factors which exert a first order effect on the measured quantities of FCP rate and K_{op}. With these goals and guidelines in mind, a test program consisting of four unique and simple variable amplitude loading conditions or cases was defined and executed. In all of the cases, the effect of $\frac{dK}{da}$ observed by Marrisen [26] was minimized or controlled by maintaining constant ΔK conditions within three percent of the applied load. In addition, the effects of crack length on measured K_{op} was minimized by using a crack tip extensometer at a distance of approximately one and one half plastic zones behind the crack tip as suggested by Fleck [13]. Where possible, mixed mode and plane strain permutations of each case were planned in an

effort to study the effect of stress state on load interaction behavior.

The 7475-T731 aluminum alloy used in the current study is from the same lot of material used by Daiuto [10] in his constant amplitude and overload studies. The quality of Daiuto's constant amplitude and delay arrest data for this lot of alloy made it an ideal choice for subsequent variable amplitude studies. For this reason, his data was used in the formulation of the test program and subsequent data analyses. However, the limited quantity of the remaining material in this lot proved to be a factor in the development of the test program. When possible, several unique loading blocks were run in the same specimen. Inter-block interaction was minimized by separating each unique variable amplitude loading block by five plane stress plastic zones. Care was taken in the test development stage to insure that FCP rate and K_{op} data were extracted at crack lengths beyond the five plastic zone buffer. Detailed numeric listings of stress intensities and loads at specified crack lengths are provided in Appendix A.

3.1 Case I: Multi-Step Loading

In an effort to study the relative effect of K_{min} on FCP rate and K_{op}, the three unique loading blocks presented in Figure 3.1 were proposed for testing. In his closure

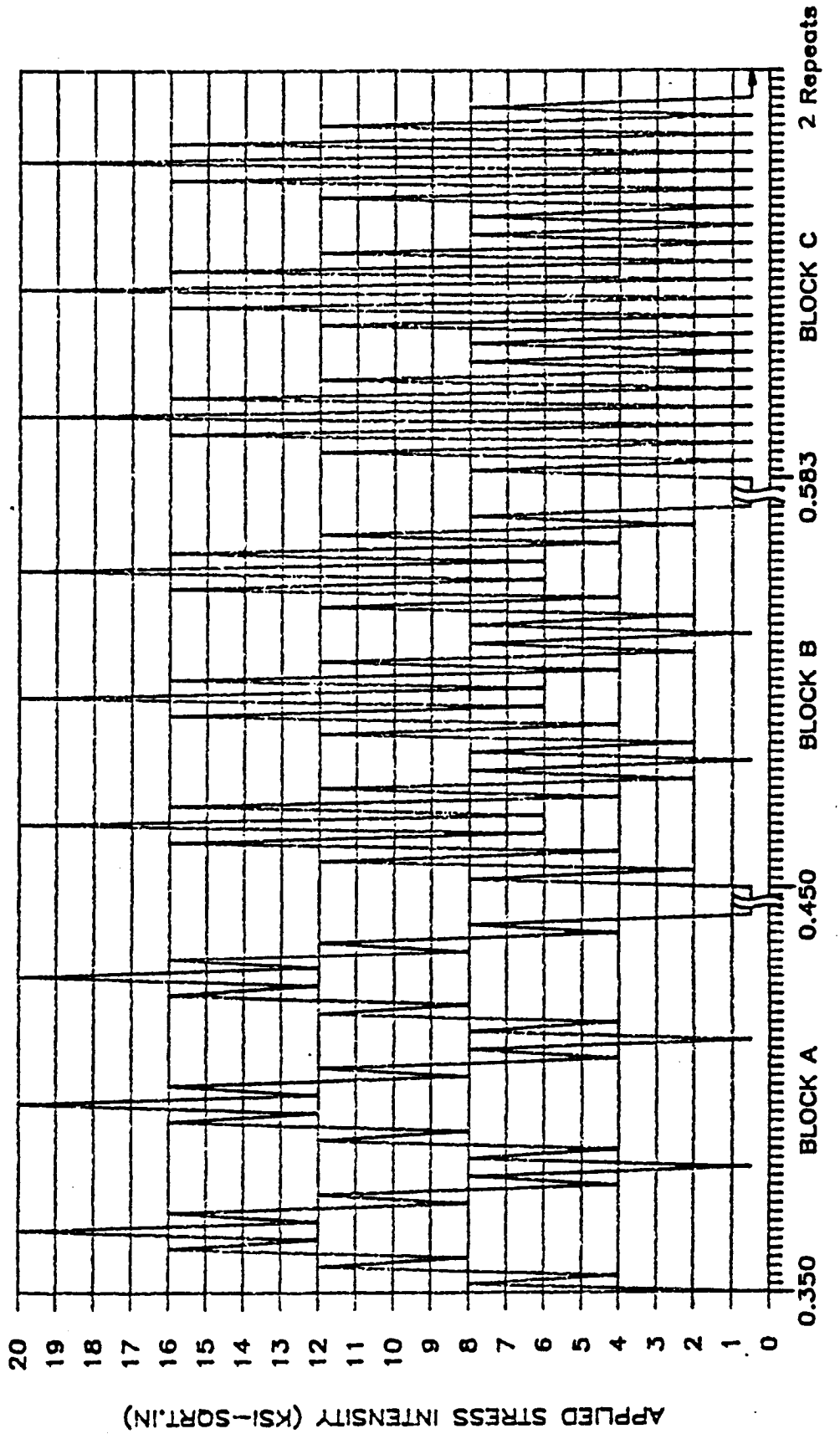

Figure 3.1 Multi-step loading test program.

model, DeKoning indicates that K_{min} plays a significant role in the establishment of K_{op} while most researchers tend to characterize K_{op} and the parameter U by the stress ratio as first proposed by Elber. In the load profiles displayed in Figure 3.1, it can be seen that while the load profiles are markedly different, K_{max} is the same for all three loading blocks. However, the cyclic value of K_{min} varies from a high mean value in block A to a constant low value in block C. Assuming that there is a single, constant K_{op} value for each repeated loading block in Figure 3.1, observations of K_{min} and R would indicate that K_{op} should decrease as the loading profile changes from A to C. This should be accompanied by appropriate changes in the FCP rate.

A single 0.17 inch thick specimen was used in examining the multi-step load form. Three repeats of blocks A, B, and C were performed in order to observe experimental error. The test was designed such that a 0.1 inch FCP rate data range for each loading block was separated by five plastic zones of K_{max} from the preceding loading block. Crack growth rate data was taken over this data range at 0.2 millimeter intervals, yielding approximately 13 crack length versus cycle count data points. At the end of each data range, crack tip opening versus load profiles were taken and later were reduced to obtain K_{op} data. The loading blocks were run sequentially in this manner such that

the overall loading sequence on the specimen in terms of block identification symbols was A-B-C-A-B-C-A-B-C.

3.2 Case II: Bi-Harmonic Loading

It was suggested by Katcher and Kaplan [5] that, under constant amplitude loading, K_{max} could be used to predict K_{op}. For variable amplitude loading, a question concerning the relative significance of K_{max} and stress ratio remains. Using the constant K_{op} assumption described previously for multi-step loading, one must assume that each cycle in a loading spectrum contributes to the level at which this constant K_{op} value is set. In order to determine the relative contributions of K_{max} and stress ratio for each cycle in a variable amplitude loading block, the bi-harmonic, high-low loading block pictured in Figures 3.2 and 3.3 were proposed for experimental study. In the bi-harmonic series of tests, a two cycle loading block described by the parameters K_1, K_2, and K_{min} was repeated continuously while rate data was taken. The parameter K_1 was the maximum stress intensity of the first and K_2 was the maximum stress intensity of the second loading cycle. Both cycles shared a common K_{min} which maintained the stress ratio of both cycles very near 0.05. Thus, the block to block effects of K_{min} and R were essentially eliminated as variables in this loading case.

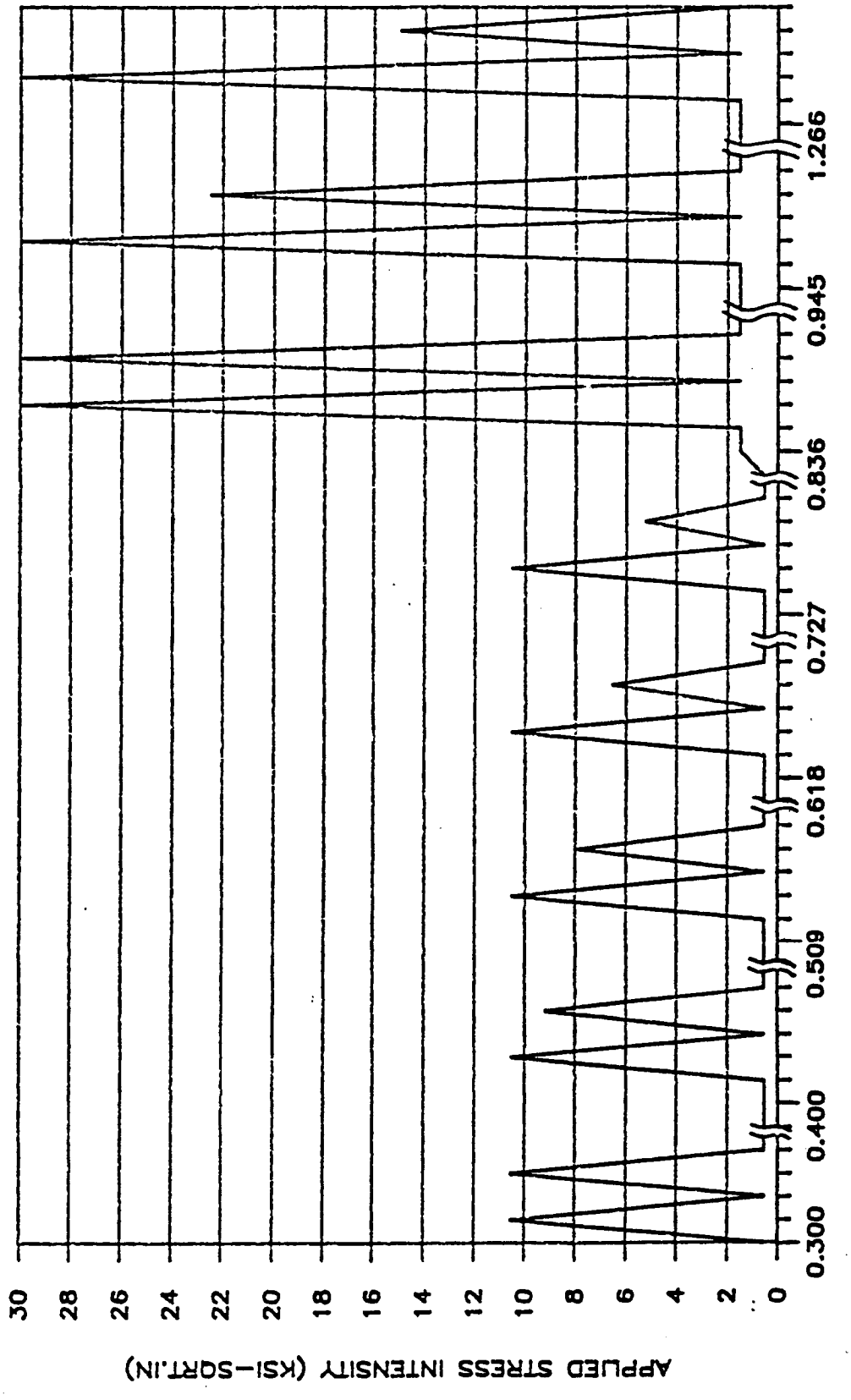

Figure 3.2 Bi-harmonic constant loading test program.

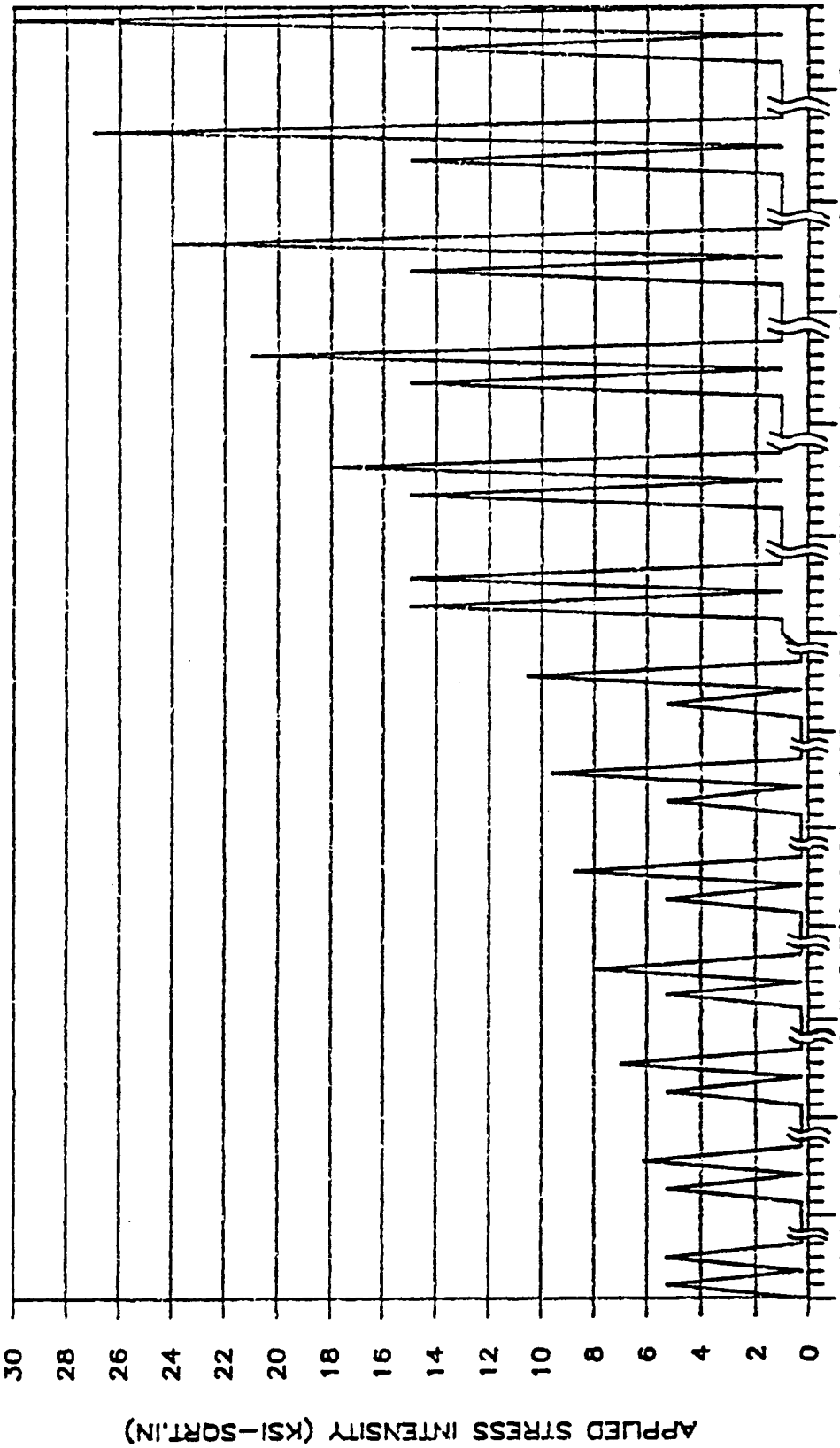

Figure 3.3 Bi-harmonic ascending loading test program.

In preparing this testing program, the relative effects of K_1 and K_2 on the value of K_{op} was examined by varying the ratio K_2 / K_1 from values of 1.0 to 0.5 in uniform increments. Since this required a variation of K_{bmax}, the maximum stress intensity in each repeated loading block, the effect of $\frac{dK}{da}$ had to be considered. Therefore, when developing the test program, the desired K_2 / K_1 ratios were selected in two different ways so as to leave different plastic wakes behind the crack tip. In the ascending K_{bmax} bi-harmonic tests K_2 and K_1 were initially fixed at equal, low values. The value of K_1 was then increased on each successive block until K_2 / K_1 was equal to 0.5. In the constant K_{bmax} bi-harmonic test K_2 and K_1 were initially fixed at equal, high values and K_2 was lowered until K_2 / K_1 was equal to 0.5. By testing in this manner, the influence of $\frac{dK}{da}$ on the constant K_{bmax} test was considered to be minimal since K_1 was constant throughout the test and $\frac{dK}{da}$ was approximately zero. However, in the ascending K_{bmax} tests $\frac{dK}{da}$ maintained a constant positive value from block to block as the crack grew. This $\frac{dK}{da}$ pattern is similar to that seen in constant amplitude growth tests.

At low stress ratios, Daiuto [10] correlated observed changes in the shape of the constant amplitude growth rate curve with stress state transitions at the crack tip using the stress state model presented in Figure 3.4. Since

these stress state transitions seemed likely to effect the growth rates in these low stress ratio tests an effort was made to insure that separate mixed mode and plane strain conditions at the crack tip were maintained for both ascending and descending bi-harmonic loading blocks. Plane stress testing conditions were placed at the longer crack lengths and behind plane strain portions to insure a minimal effect of plastic wake between loading conditions of different stress states.

Two testing patterns resulted from the concerns detailed above. The first pattern, shown in Figure 3.2 shows the bi-harmonic descending tests with the plane strain loading blocks preceding the mixed mode loading blocks. A similar graphic for the bi-harmonic ascending test is given in Figure 3.3. Inter-block interaction reduction and data acquisition was performed in a manner identical to that described for the multi-step loading condition. Two replicates of each test were performed on 0.17 inch thick specimens, resulting in four sets of experimental data for this loading case.

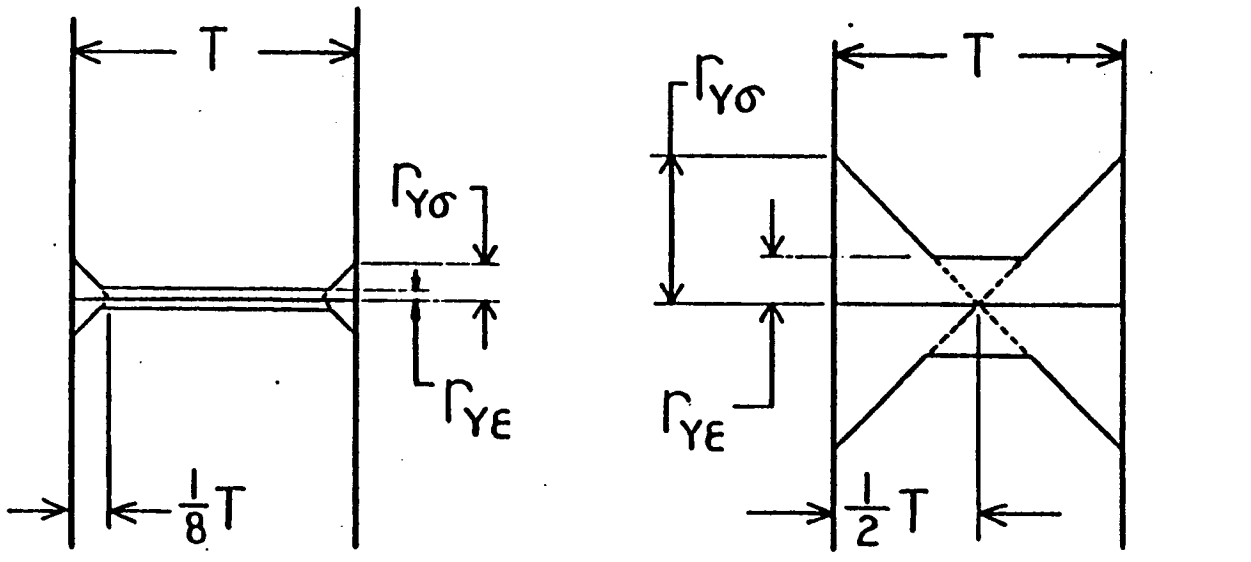

PLANE STRAIN

$$\frac{r_{y\sigma}}{T} \leq .125$$

PLANE STRESS

$$\frac{r_{y\varepsilon}}{T} \geq .5$$

Figure 3.4 Stress state model used in test program definition. [10]

3.3 Case III: Variable Fatigue Cycling

Elber and others have observed significant reductions in K_{op} and associated increases in FCP rate directly following the application of single peak overloads. Assuming that this drop in K_{op} is the result of plastic deformations at the crack tip larger than the CTOD previously required to open the crack tip prior to the overload, the resulting increase in growth rate due to greater ΔK_{eff} in the fatigue cycles is to be expected. Assuming the same mechanism, it seems likely that a sustained period of acceleration would be attainable if overloads were applied periodically between a fixed number of fatigue cycles. This assumes a loading history effect limited to the overload and the fatigue cycles associated with it. However, if the proper number of fatigue cycles between overloads (corresponding roughly to the cyclic "memory" of the crack) were applied one would expect to observe the sustained acceleration effect. The author now assumes a cyclically dynamic K_{op} which is maintained at an artificially low value by periodic overloads.

In order to study post overload acceleration and retardation effects, a series of variable fatigue cycling test were developed. The repeated loading blocks in these tests may be described with four parameters; K_1 , K_2 ,K_{min}, and N_2. The maximum stress intensity of the overload and

the subsequent fatigue cycles are given by K_1 and K_2, respectively. The minimum stress intensity (K_{min}) for all cycles in the test was maintained at a constant low value such that the stress ratio for all cycles executed in the tests is approximately 0.05. The number of fatigue cycles between overloads in a repeated loading block is given by N_2. The values of N_2 proposed for this study were 10, 30, 100, 300, and 1000. Graphics describing the variable fatigue cycling test programs for mixed mode and plane strain loading conditions are presented if Figures 3.5 and 3.6, respectively. The mixed mode test sequence required one 0.08 inch thick specimen for each of the three repetitions performed. All three replicates of the plane strain loading sequences were performed with a single 0.248 inch thick specimen. Crack growth rate and K_{op} data were obtained at the end of each block as described in previous cases.

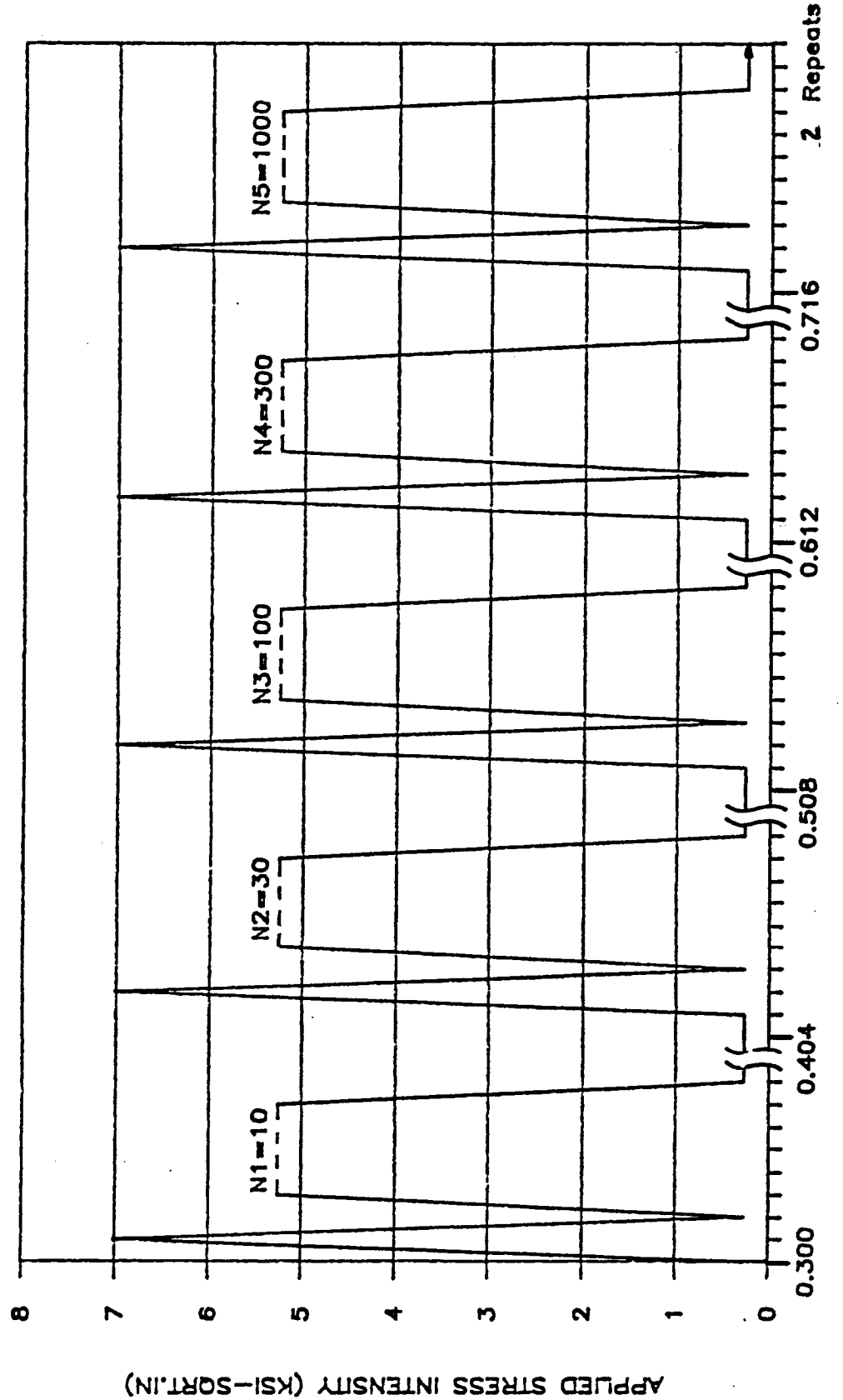

Figure 3.5 Variable fatigue cycling test program with plane strain stress states.

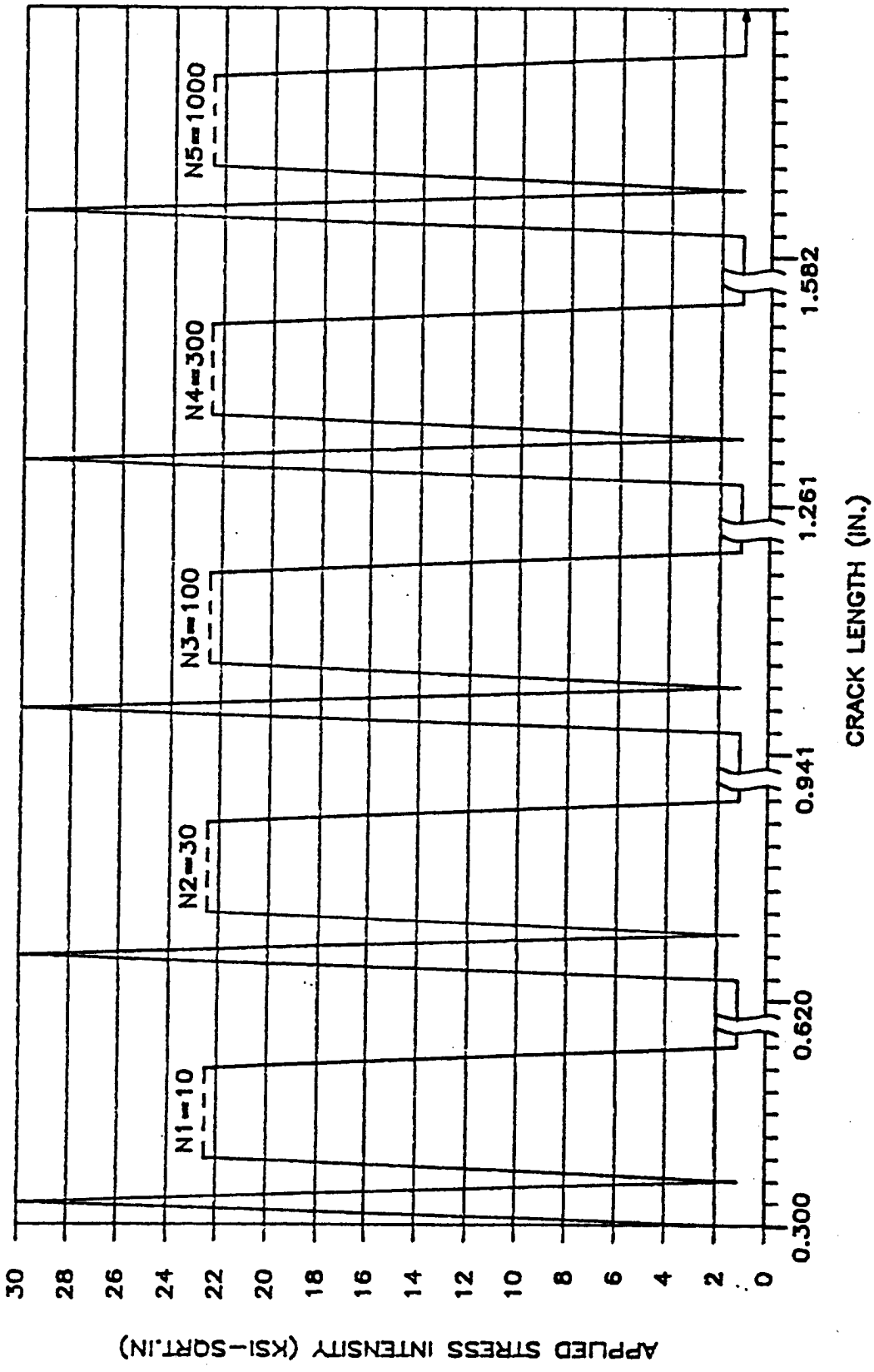

Figure 3.6 Variable fatigue cycling test program with mixed mode stress states.

3.4 Case IV: High R-Ratio Overload Tests

The mechanism of post overload delay at low stress ratios is thought to be largely the result of plasticity induced closure. At high stress ratios where closure is not an active mechanism in the FCP process under constant amplitude loading conditions, there remains some doubt as to the mechanism of delay. In earlier tests, Daiuto observed marked differences in the post overload FCP rate data for single overloads applied at different fatigue stress ratios. Specifically, he noted a much more abrupt decline in the FCP rate after overloads applied at high stress ratios than those applied at lower stress ratios. He observed that delayed retardation is primarily a phenomenon which may be observed at low stress ratios but is less apparent at higher stress ratios. These observations seem to support the closure mechanism of delay discussed throughout this chapter. At high stress ratios, where K_{op} is less than K_{min} acceleration, or delayed arrest effects resulting from overloads should not be expected since ΔK_{eff} is equal to ΔK prior to the overload. At high stress ratios the crack tip growth rate displays delay immediately as it grows into the plastic zone without the accelerating effects of the residual plastic overload strains which are apparent at lower stress ratios.

In an effort to support the discussion presented above, a series of high stress ratio overload tests were conducted. The fatigue cycles in these tests were maintained at a stress ratio of 0.7, a ratio considered to be free of closure effects. Overloads were applied with Q_{ol} ranging from 1.1 to 1.5. The maximum Q_{ol} applied was determined from experimental delay/arrest data gathered by Daiuto and was chosen such that maximum delay would occur. Prior to and following the overload, crack tip opening displacement versus load profiles were taken at uniform cyclic intervals throughout the delay region. The number of cycles between K_{op} data points ranged from 200 to 1000 depending on the severity of the overload and its associated delay period. Crack growth rate data was taken at 0.02 millimeter intervals in the post overload delay region and at 0.2 millimeter intervals elsewhere in the tests. A mixed mode test was run on one 0.08 inch thick specimen. A plane strain test was run on one 0.248 inch thick specimen. The stress ratio for the overload and fatigue cycles in both the mixed mode and plane strain tests tests were held near 0.05. A graphic illustrating the cyclic stress intensities applied for both specimens is presented in Figure 3.6. A summary of the loading cases studied in this investigation is presented in Figure 3.8.

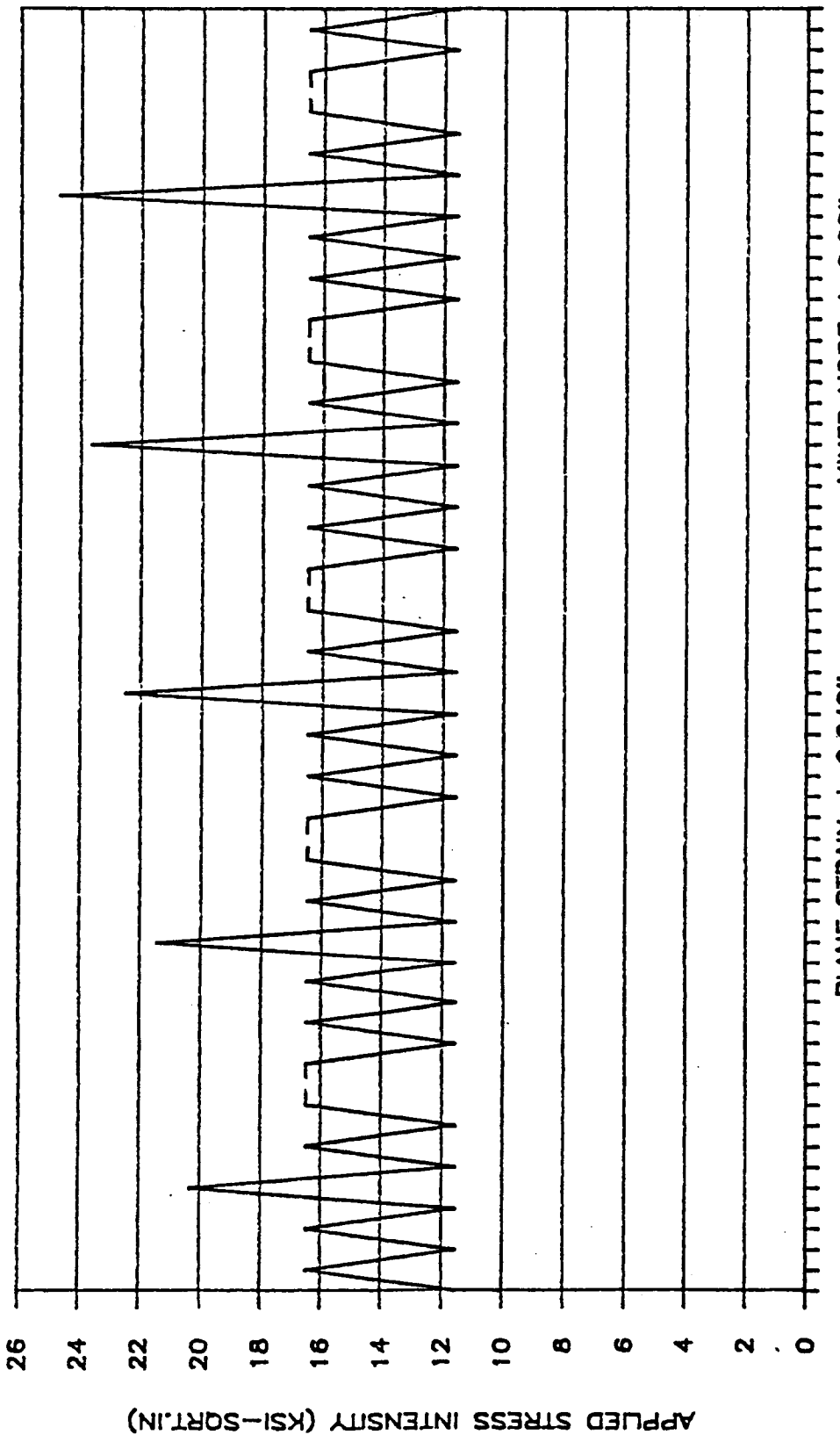

Figure 3.7 High R-ratio overload test program.

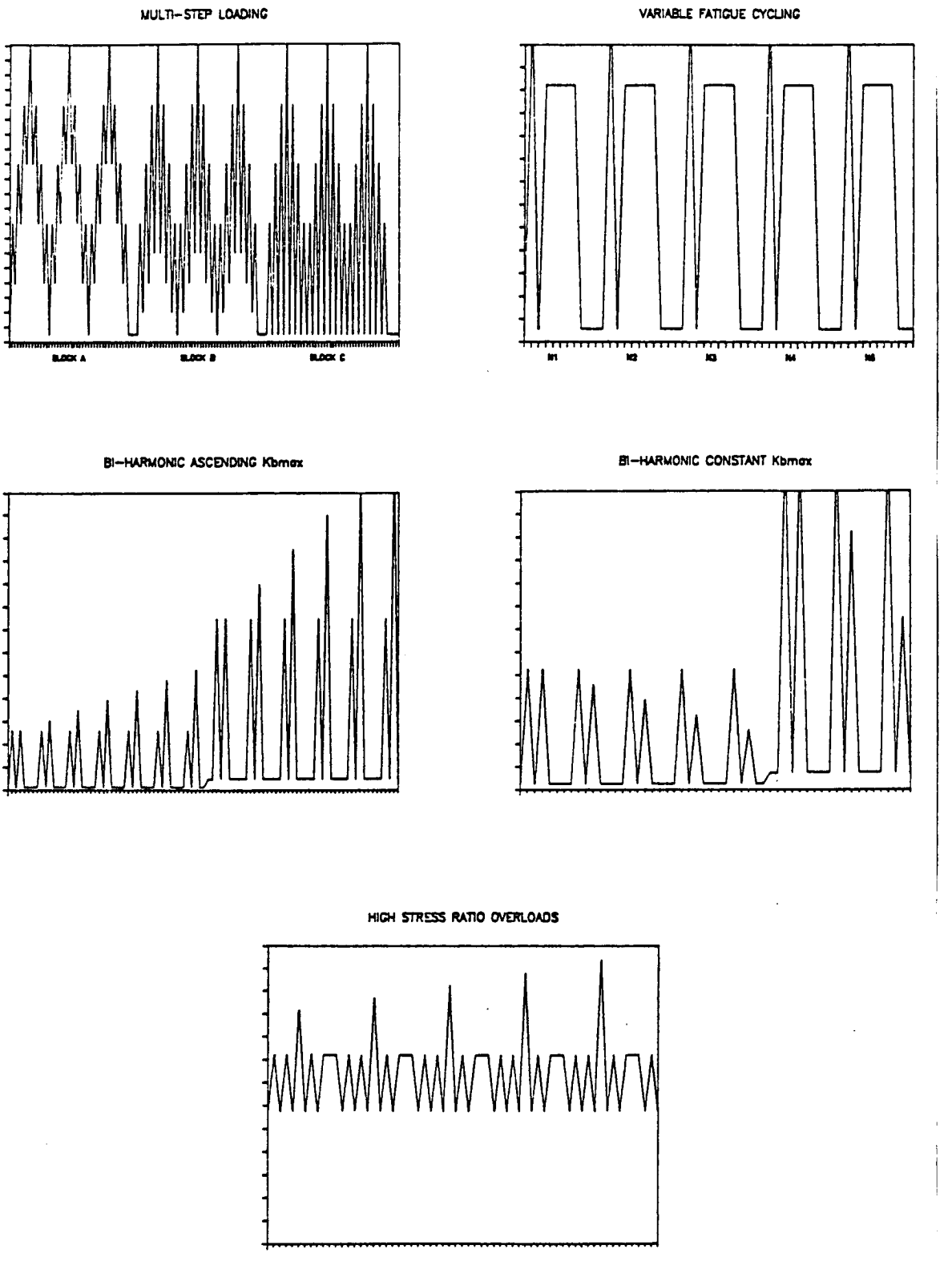

Figure 3.8 Summary of variable amplitude loading conditions.

CHAPTER 4 - TEST EQUIPMENT AND PROCEDURE

Cyclic loading was conducted using a Material Testing Systems (MTS) 20 KIP electro-hydraulic load frame and model 442 controller in conjunction with an external microprocessor. The load frame, load cell, controller and associated signal amplifiers were aligned or calibrated in accordance with MTS specifications. These elements of the testing equipment are the same which were used by Daiuto [10] in conducting his experiments. In order to generate and control the variable amplitude loading blocks required for this study a closed-loop microprocessor control loop was added external to the standard MTS servo control loop.

A schematic of the testing equipment is shown in Figure 4.1. During testing a variable amplitude command signal was incrementally generated by the microprocessor and input to the servo controller. Responding to the programmed command signal, the controller applied the proper loads to the specimen mounted between the load cell and the actuator by using the amplified load cell signal to close the controller feedback loop. The load cell voltage was also routed through filters and into the microprocessor,

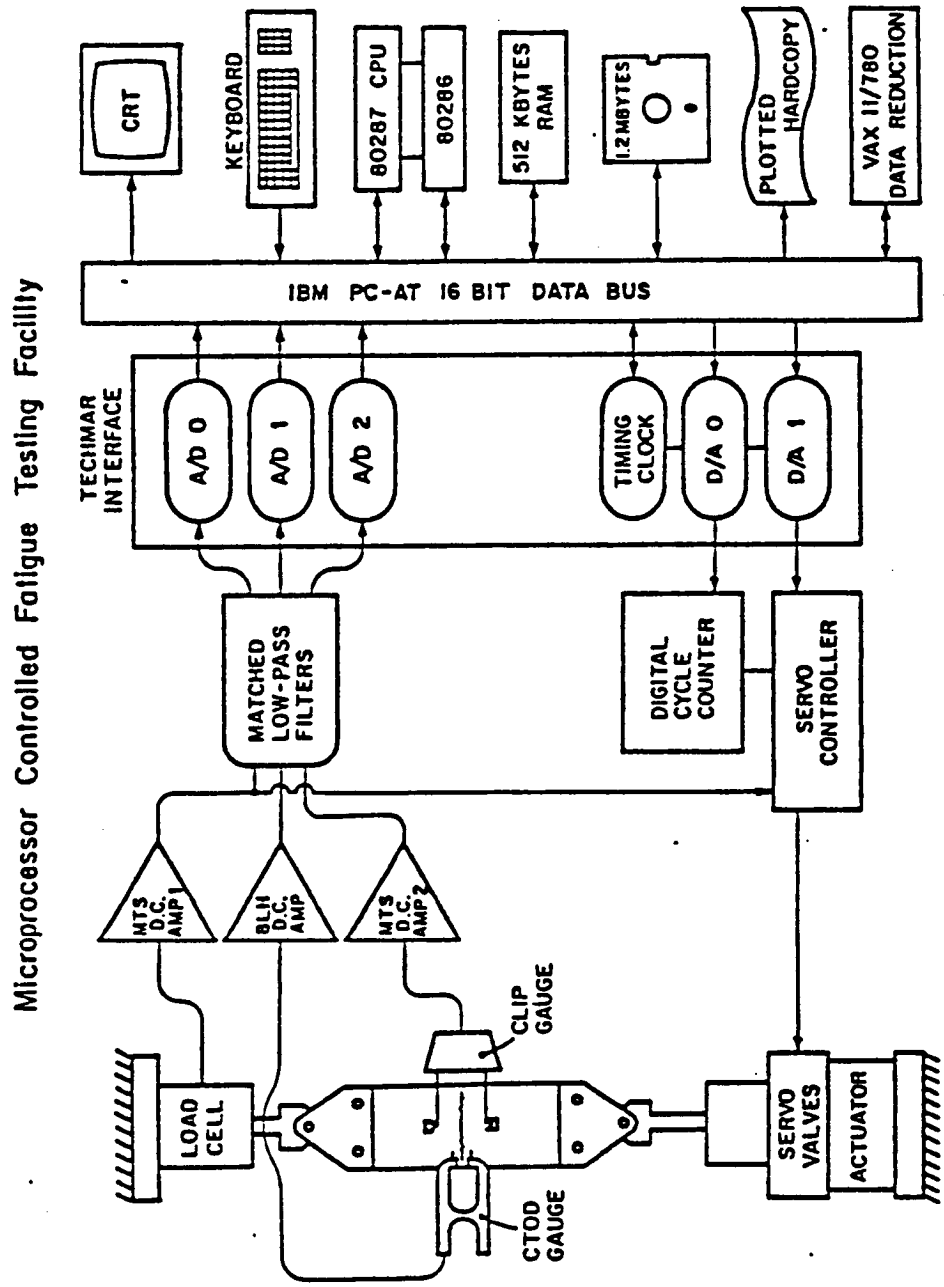

Figure 4.1 Microprocessor controlled fatigue testing facility.

thus closing its feedback loop. Digital computations performed by the microprocessor on the feedback signal permitted compensations in the outgoing command signal for the dynamic response of the specimen and the MTS system such that the desired loading block was attained at the specimen. The net result was a variable amplitude fatigue testing apparatus which maintained load levels to within one percent of the desired load value at frequencies from 0.5 to 18.0 hertz.

During the acquisition of load versus crack opening displacement profiles, the microprocessor served as a data recorder. Signals from crack mouth and crack tip extensometers were filtered and fed into the microprocessor. While generating a 0.5 hertz command signal, the microprocessor recorded and stored the crack tip, crack mouth, and load signal voltages until the data acquisition cycle was completed. Following completion of the data acquisition cycle, software options allowed for plotting of the data to a cathode ray tube or a hardcopy device in addition to the option of storing the data on a floppy disk.

4.1 Test Equipment

The microcomputer selected for variable amplitude load control and data acquisition was the Advanced Technology Personal Computer manufactured by International Business

Machines (PC/AT). The PC/AT used in the study was fitted with an Intel 80287 math co-processor to increase its computational speeds beyond those available with its standard 80286 processor. The Intel 80286 microprocessor is a 16 bit processor with "specially optimized capabilities...for multi-tasking systems" [27] which interfaces with a 16 bit data bus to provide significant speed increased over its commonly used 8088 counterpart. Disk storage devices on the PC/AT consisted of two floppy disk drives.

A Tecmar PC-Mate Lab Master provided the digital to analog interface between the microcomputer and the servo controller, respectively. The analog-to-digital converter provided 8 true differential, 12 bit input channels and two 12 bit digital- to-analog output channels. Both the A/D and D/A functions of the board were used in the I/O mapped, 0 to 10 volt range as calibrated from the manufacturer.

Measurements of critical interest to the objectives of this study involved the load placed on the specimen, the crack mouth opening displacement (CMOD), the crack tip opening displacement (CTOD) and the length of the crack. An optical microscope (150X) on a traveling base was used in conjunction with a strobe light syncronized to the loading frequency in order to measure the crack length to within one micron. The remaining physical quantities were measured using a load cell and strain gage extensometers as

transducers for load and crack opening displacements, respectively. The load transducer, a 20/30 KIP Lebow load cell was used in conjunction with an MTS model 440.21 direct current signal conditioner to provide calibrated load signals ranging from zero to ten volts.

The crack mouth opening displacement was measured with an MTS model 632.03B-30 clip-on extensometer. This extensometer uses four strain gages (350 ohm) in a full bridge configuration with one active gage mounted on the outboard surface of each cantilever in this dual beam gage. Notches machined in the outboard surfaces of both cantilevers were used to locate the gage between knife edge fixtures which were mounted above and below the starter crack at the centerline of the specimen as shown in Figure 4.2. Once mounted in the knife edge fixtures, the clip-gage remained in place for the duration of the test. A second MTS direct current (d.c.) amplifier identical to the load cell amplifier was used to provide excitation voltage to the clip-gage, resulting in a linear, zero to ten volt, signal over the 0.15 inch range of the transducer between 0.075 and 0.225 inches.

The crack tip opening displacement was measured using an extensometer identical to that used by Reuping and Hillberry [28] in their earlier work with fatigue crack closure. Modeled after a gage initially used by Elber [3],

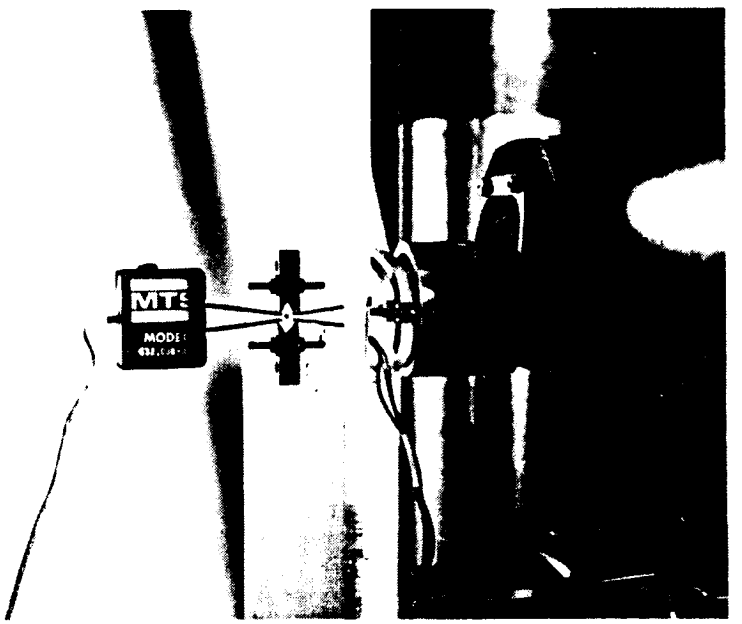

Figure 4.2 Clip gage mounting fixtures.

this extensometer was machined from a single piece of 2024-T6 aluminum into the configuration shown in Figure 4.3. It employs four foil type strain gages (120 ohm) in a full bridge configuration. The active gages in this gage are placed on adjacent links in the bridge circuit and are located on the two internal radii of the gage. Compensating gages are mounted on low strain surfaces of each cantilever. Sharpened steel points fixed at the end of each cantilever were pressed into the cracked specimen at approximately half the material thickness behind the crack tip when CTOD versus load profiles were to be taken. Uniform normal pressure and accurate crack tip location were insured using a spring fixture mounted to the lens of the optical microscope as shown in Figure 4.4. Excitation voltage for the CTOD gage was provided by a BLH model 5100 d.c. amplifier at a gain of 2000.

The material coupons provided by ALCOA were machined into center cracked tensile specimens for use in this study. Details of the specimen geometry are provided in Figure 4.5. The stress raiser detailed in Figure 4.5 was machined using the electric discharge method. Two holes with a diameter of 0.0625 inches were machined into the specimen to accommodate mounting bolts for the knife edges which were required by the clip gage extensometer.

PRECEDING PAGE BLANK NOT FILMED

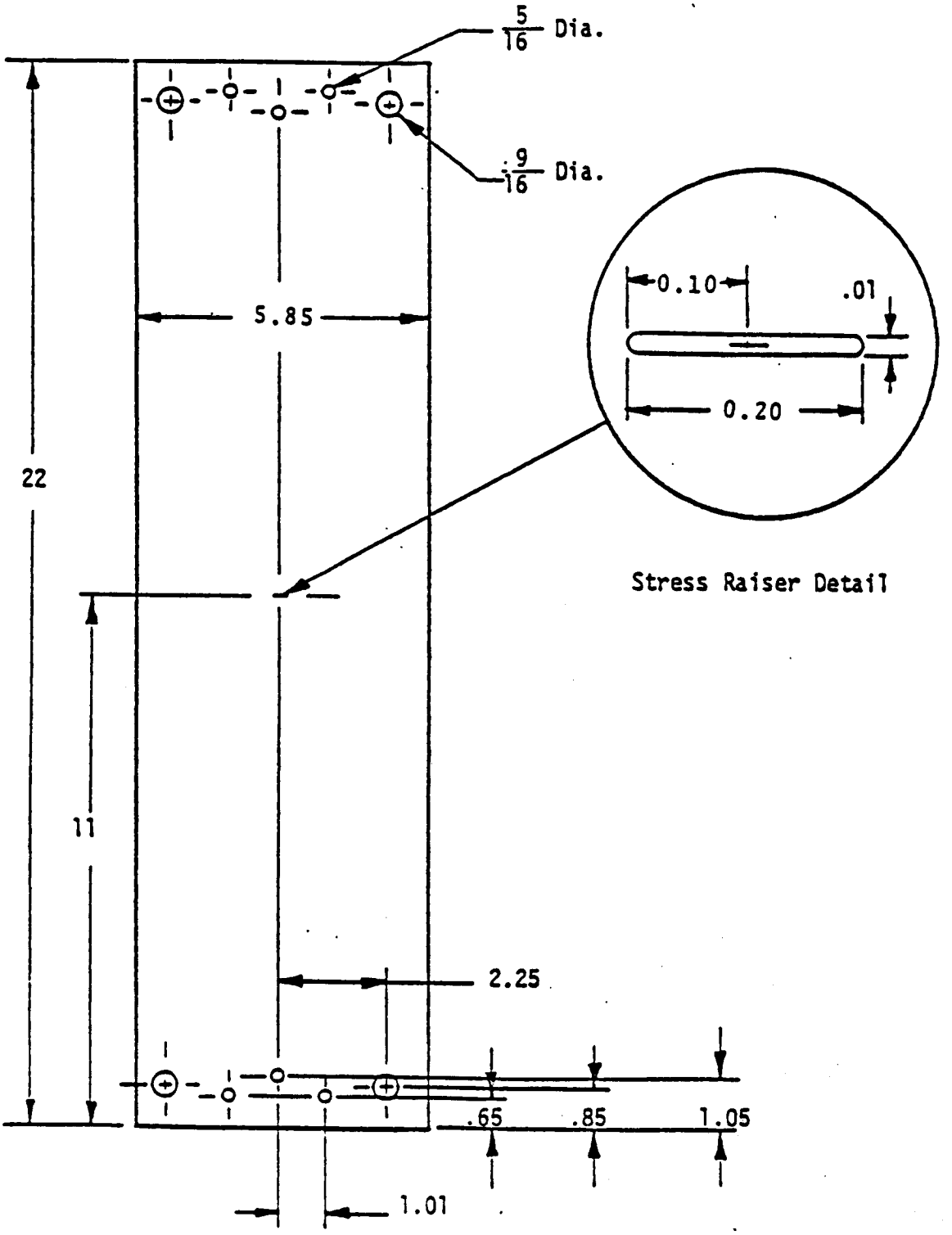

Figure 4.5 Middle tension specimen geometry.

4.4 Procedure

Specimens were precracked to a length of 0.3 inches in accordance with ASTM E647 [29]. All of the tests were conducted under constant ΔK load shedding conditions in which loads were manually reduced when they deviated from the stress intensity solution by more than three percent. The stress intensity solution proposed by Fedderson [30] for center cracked tensile specimens was used in this study and is presented in equation 4.1.

$$K_I = \sigma \sqrt{\left[\pi a\right] \sec\left[\frac{\pi a}{w}\right]} \qquad (4.1)$$

Testing was performed in room air with temperatures ranging from 68 to 72 degrees Fahrenheit. Humidity measurements taken with a wet and dry bulb thermometers indicated relative humidities ranging from 38 to 42 percent during the testing program which was conducted during the early winter months.

Crack growth rate data were obtained using the optical microscope mounted on a traversing base fitted with a digital resolver. When the crack tip was observed to reach the crosshair in the optics of the microscope, the observer triggered a data recorder which logged the digitally monitored crack length and cycle count. With the exception of the overload tests, crack length versus cycle count data were taken at 0.2 millimeter intervals. Overload data were

taken at 0.02 millimeter intervals.

Crack closure data were taken at intervals defined by the test program. Before taking load versus CMOD/CTOD profiles the real-time load control software was halted at the microprocessor and a data acquisition program was executed. The data acquisition software performed low frequency load control and data recording functions as dictated by the operator. After starting the data acquisition program the operator sited the crack at the crosshair in the microscope and then affixed the CTOD gage retainer over the optical lens at the front of the microscope as shown in Figure 4.6. Once the retainer was in place, the tips of the CTOD gage were pressed into place on each side of the crack by slowly advancing the rough focus traverse of the microscope. At this time the operator commonly directed the microprocessor to run from one to ten calibration cycles in order to insure that the gage was properly seated in the indentations made by its sharpened tips. Load versus CTOD profiles made during these cycles were observed on a storage screen oscilloscope to insure that the CTOD signal indicated that the gage was functioning properly. After confirming the placement and operation of the CTOD gage, a data acquisition cycle was executed and the recorded data then written to disk. These data files consisted of 360 sets of load, CMOD, and CTOD data points collected through one loading cycle on the specimen. Following completion of

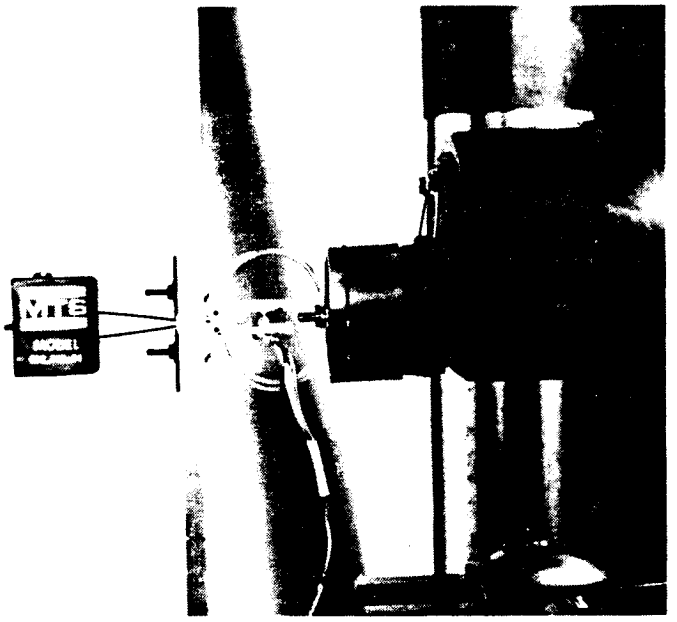

Figure 4.6 CTOD data acquisition assembly.

a test, the load profiles and crack length versus cycle count data were entered into a VAX 11/780 computer for subsequent data reduction and analyses.

A different data acquisition procedure was followed during the high stress ratio overload tests in order to collect accurate FCP rate and K_{op} data simultaneously during the entire period of observed delay. In experimental trials it was determined that 0.008 inch accuracy required in the microscope traverse could not be reliably maintained if large motions of the rough traverse were made. This excluded the use of the previously described CTOD gage retainer since its installation required such movements of the microscope. To overcome this problem, Reuping's [28] wire retaining assembly was attached to the specimen as shown in Figure 4.7. This allowed CTOD data to be taken from one end of the crack in the specimen while the other end was used for crack length versus cycle data.

Inherent problems with the wire retainer assembly resulted in its omission from the general testing equipment in the early stages of equipment development. Using this retainer, pressure is applied to the CTOD extensometer by tightening two wing-nuts located at the fulcrum of the wire cantilever assemblies. As a result, the balance and magnitude of the force applied to each side of the gage was subjectively determined by the operator based on observations

of the quality of the signal resulting from the calibration cycles. Viewed as the only available means by which to gather the needed data in the overload series, this retainer assembly was used only in these tests.

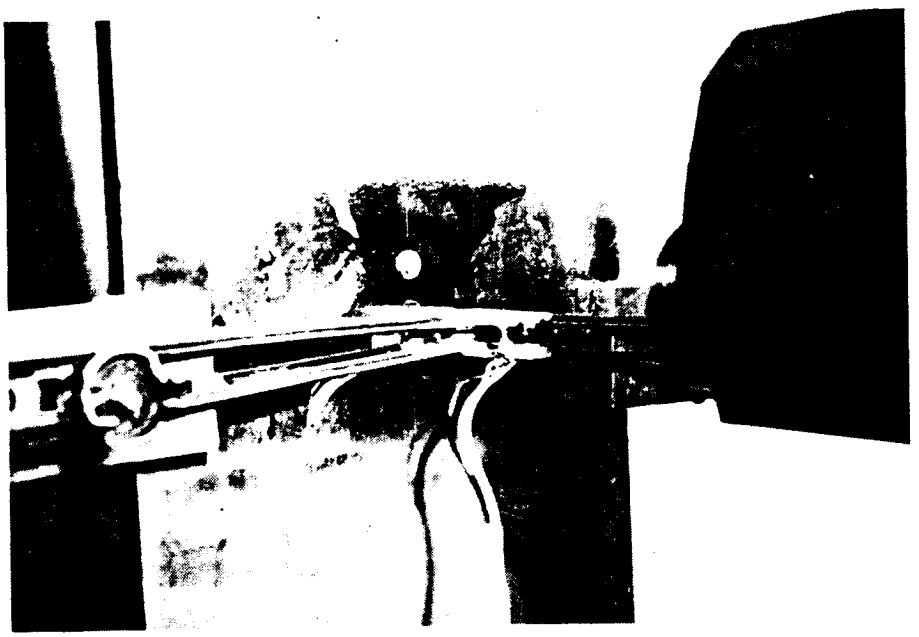

Figure 4.7 Reuping's cantilever wire CTOD gage retainer assembly.

CHAPTER 5 - DATA REDUCTION

5.1 Fatigue Crack Growth Rates

Crack length and cycle count data taken from all test cases were converted to growth rate data using the seven point incremental polynomial methods described in ASTM E647 [29]. In the first three loading cases of the test program, the characteristic growth rate for a unique loading block was obtained by averaging the seven middle $\frac{da}{dN}$ data points in the 13 point, 0.1 inch data range. In the overload tests, rate data were plotted against crack length and cycle count in order to determine the characteristic values of a_{min} and N_D for each overload.

5.2 Determination of Crack Opening Stress Intensity

The digital records of load versus crack tip opening displacement were analyzed to determine K_{op} using a programmed library subroutine on the Purdue University Computing Center's CDC-6500 mainframe computer. The ZXSSQ subroutine is a non-linear, finite difference, least squares curve fitting algorithm in the commercially available

International Mathematics and Statistical Library (IMSL) [31]. The subroutine optimizes a finite number of parameters using residuals which are supplied by a user written, external function. In applying ZXSSQ to the problem of determining K_{op} from the recorded load and CTOD data, the four parameter model presented in equation 5.1 was chosen to calculate the residual values.

$$F_i = y_i - \left[C_1 + C_2 x_i + C_3 \left[C_4 - x_i\right]^2\right] \quad \text{for } x_i < C_4 \tag{5.1a}$$

$$F_i = y_i - \left[C_1 + C_2 x_i\right] \quad \text{for } x_i > C_4 \tag{5.1b}$$

where,

x_i = the normalized load values,

y_i = the normalized CTOD values,

F_i = the calculated residual for the ith pair of data,

C_{1-4} = the optimized model parameters.

Supplied with rough initial guesses for the C parameters, the algorithm optimized the parameters to fit the normalized experimental data such that the sum of the squared errors value was typically 0.0001 in magnitude.

The form of the model presented in equation 5.1 and the parameters associated with it serve to describe the

physical processes associated with the opening crack. The parameters C_2 and C_1 are the slope and CTOD axis intercept of the linear region associated with the compliance of the open crack. The parameter C_3 is the coefficient of the second order term describing the curvature of the load versus CTOD profile as the crack is physically opening. Finally, the C_4 parameter is the normalized value of load which marks the boundary between the linear and the non-linear data. This fourth parameter, when converted back into units of pounds, was considered to be the crack opening load.

In order for this model to accurately describe the opening behavior of the crack, the order of the non-linear term in equation 5.1a must closely match that of the physical process involved. Based on the interferometric crack opening measurements in polycarbonate made by Ray et al [32], a simple mathematical model which supports a second order relationship between externally applied stress and CTOD is proposed. Ray's data linearly relates the length of the open crack at the free surface, a_{op}, to the stress intensity calculated using the physical crack length, a. Thus, using his data

$$a_{op} = mK + b \tag{5.2}$$

where,

$$K = \sigma\sqrt{\pi a \alpha} \tag{5.3}.$$

Combining equations 5.2 and 5.3 yields,

$$a_{op} = m\sigma\sqrt{\pi a\alpha} + b \tag{5.4}$$

Using the elliptic crack opening assumption for center cracked tensile specimens [34], CTOD may be related to a_{op},

$$CTOD = \frac{4\sigma}{E}\left[a_{op}^{2} - x^{2}\right]^{1/2} \tag{5.5}$$

where x, the distance from the centerline at which the CTOD is measured.

Finally, by inserting the expressions for a_{op} from equation 5.4 into the compliance relation in equation 5.5 the resulting expression for the opening crack length in terms of external stress is

$$CTOD = \frac{4\sigma}{E}\left[\left[m\sigma\sqrt{\pi a} + b\right]^{2} - x^{2}\right]^{1/2} \tag{5.6}$$

At a fixed crack length the values of x, m, b, and are constants, leaving CTOD as a second order function of the externally applied stress, σ. Therefore,

$$CTOD \ \alpha \ \sigma^{2} \tag{5.7}$$

Visual inspections throughout the data reduction process indicated that the second order model fit the non-linear portion of the data quite well. The K_{op} values determined by the ZXSSQ algorithm agreed within five percent to the visually determined values . While the visual

technique of determining K_{op} appeared equally as accurate as the digital technique, the author suggests that the objectivity and consistency inherent in the digital method yielded data which more accurately depict the physical phenomenon of crack closure.

CHAPTER 6 - RESULTS AND OBSERVATIONS

Using the data reduction techniques defined in the previous chapter, FCP rate and K_{op} results for all of the loading cases were calculated from the test data. Observations of the relationship between these two sets of results for each case will be made using the closure based growth rate equation presented in equation (2.3). The proper, closure-free coefficient and exponent for this relation were extracted from Daiuto's constant amplitude data for the appropriate thickness at a stress ratio of 0.75. The absence of closure at this stress ratio was verified by Carman [35], who conducted a series of tests which indicated an R_{cut} of 0.45 above which closure does not occur for this material. Daiuto concluded that his constant amplitude, high stress ratio FCP rate versus ΔK data indicated a bi-linear behavior which was not a function of stress state. Therefore, two coefficient-exponent pairs were extracted from his data to accommodate this bi-linearity. The C and m parameters were optimized from each linear data segment using a Hooke-Jeeves, finite integral optimization algorithm [33]. In the analyses presented in

this study the appropriate C and m values were selected based on the magnitude of the ΔK_{eff} values resulting from the observed values of K_{op}. Daiuto also showed that stress state did not explain the bi-linear transition point in high stress ratio constant amplitude data. As a result, the proper C and m coefficients were selected based on the range of ΔK_{eff} observed in the tests. If ΔK_{eff} exceeded the ΔK value associated with the bi-linear transition point observed in Daiuto's data, the C and m pair associated with large ΔK high stress ratio data was used. Similarly, if ΔK_{eff} was lower than the transition point, the C and m values fitting the low ΔK data were used in the closure based growth rate calculations.

6.1 Case I: Multi-Step Loading Results

Data for the three multi-step loading blocks shown in Figure 3.1 are presented in Table 6.1. A single K_{op} value is presented for each loading block. The K_{op} value presented is the mean of four separate readings taken in four unique cycles for each loading block. The data acquisition cycles performed for each block were essentially four cyclic components of the block, each having different stress ratios and K_{max} values. For a given loading block, it is significant that the opening load determined from these four load versus CTOD profiles did not differ from one another by more than five percent.

Averages of the replicates for each block indicate the major trends observed in the data. As one might anticipate, growth rate increases as the load form is varied from the smallest ΔK values in block A to the largest ΔK values in block C. This trend is apparent in the graphical presentation of the FCP rate data shown in Figure 6.1. The K_{op} values obtained for each loading block are presented graphically in Figure 6.2. Since each loading block maintained the same K_{max} and the same K_{bmin} values, the data were normalized using the largest stress intensity value in each block, $K_{bmax} = 20\ ksi\sqrt{inches}$, in order to show the effect of the intermediate, varying K_{min} values on K_{op}. In Figure 6.2 the decreasing trend in the K_{op}/K_{bmax} ratio illustrates the effect of K_{min} on K_{op}. This trend indicates that significant changes in the intermediate K_{min} values, as the loading block varies from A to C, are accompanied by changes in K_{op} / K_{bmax} from 0.42 to 0.35. This trend refutes the assumption made by DeKoning [25] that K_{op} is strictly a function of K_{bmax} and K_{bmin} values.

6.1.1 Rate Comparisons Using Opening Stress Intensity

Using Daiuto's data as described previously, growth rates were calculated with the K_{op} values presented above. These calculations are presented in Appendix B. The results are presented graphically in Figure 6.3. In this figure it may be seen that the observed change in K_{op} may

be used to describe the FCP rate quite well if the inherent scatter in fatigue data from test to test is also considered.

Table 6.1 FCP rate and K_{op} results for multi-step loading. Shown in Figure 3.1, detailed in Appendix A.

Repeat Number	Block Identification					
	Block A		Block B		Block C	
	da/dN (in./cycle)	K_{op} (ksi$\sqrt{in.}$)	da/dN (in./cycle)	K_{op} (ksi$\sqrt{in.}$)	da/dN (in./cycle)	K_{op} (ksi$\sqrt{in.}$)
1	6.6E-06	8.0	1.0E-05	8.6	1.3E-05	7.4
2	6.9E-06	8.8	9.4E-06	8.1	1.3E-05	7.4
3.	6.5E-06	8.3	9.6E-06	6.9	1.2E-05	6.2

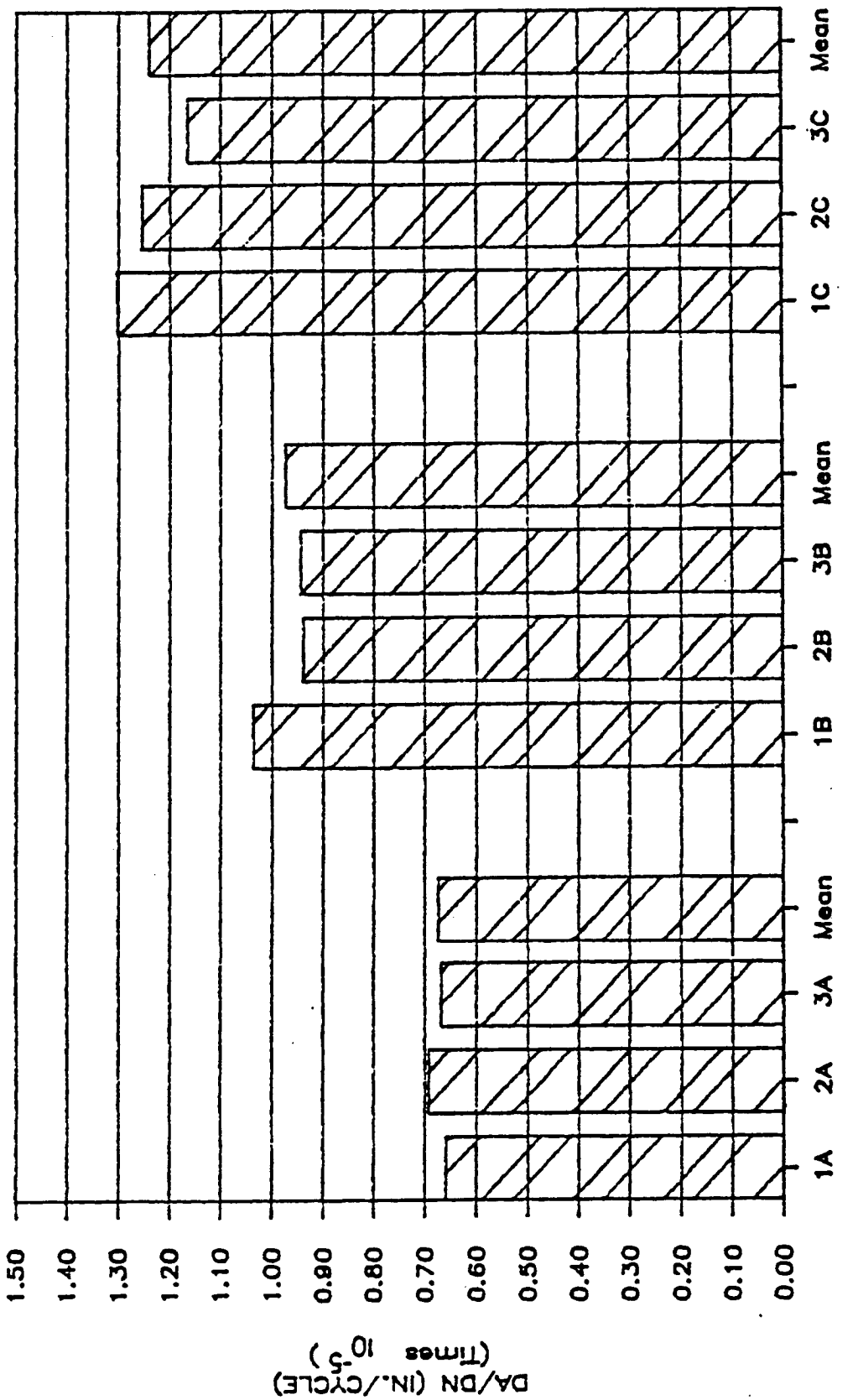

Figure 6.1 FCP rate results for multi-step loading.

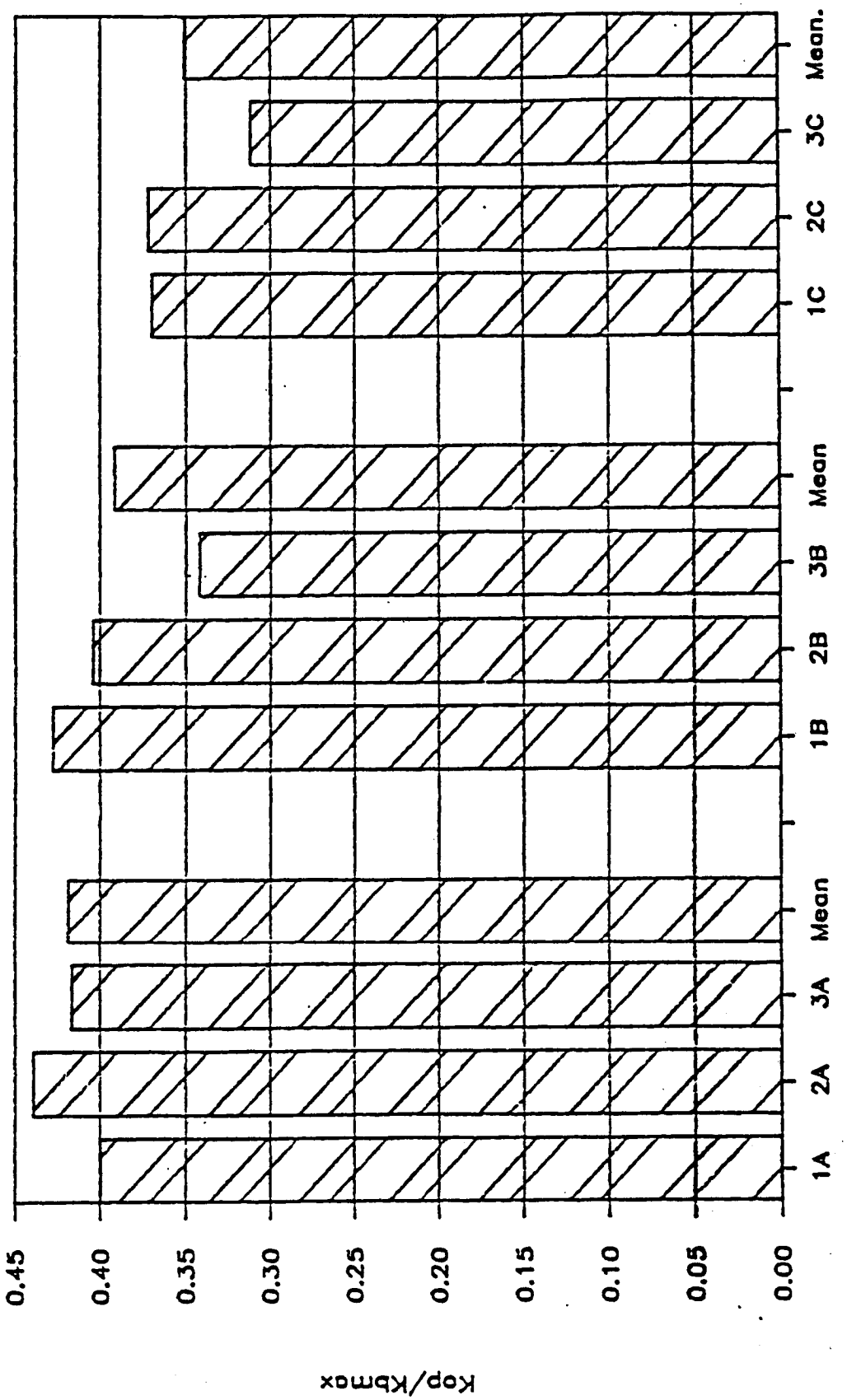

Figure 6.2 K_{op}/K_{bmax} results for multi-step loading.

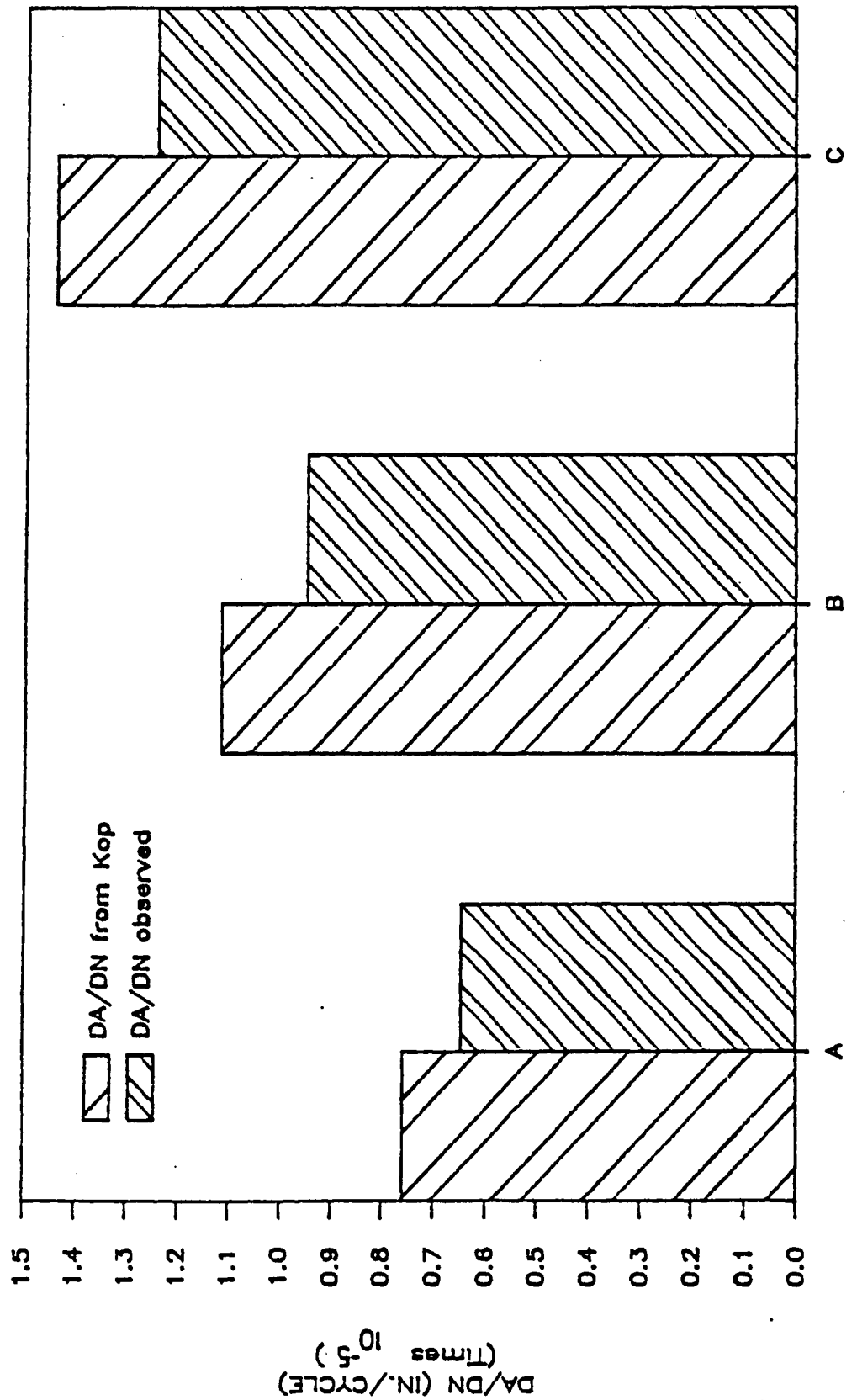

Figure 6.3 FCP rate comparison for multi-step loading K_{op} results.

6.2 Case II: Bi-Harmonic Loading Results

Test results for the bi-harmonic loading case are presented in Tables 6.2 through 6.5. The data is subdivided according to the two major closure influences discussed in Chapter 3: stress state and dK/da. Thus, there are four major divisions of the data, each with a unique combination of mixed mode or plane strain stress state and ascending K_{bmax} or constant K_{bmax}. The K_{op} values presented for each loading block are the mean values calculated from K_{op} loads extracted from load versus CTOD data for the high and low data acquisition cycles in each block. The K_{op} values associated with K_1 and K_2 components of any given bi-harmonic loading block typically differed from one another by no more than six percent.

Observations regarding the influence of dK/da may be made by examination of the data in the tables. Recalling the intent of the test program to examine the influence of dK/da resulting from different plastic wakes, the influence of the effect should be evident in comparisons of FCP rate at $K_2/K_1=0.5$ for ascending and constant K_{bmax} cases. For both the mixed mode and plane strain cases, the load forms at $K_2/K_1=0.5$ were identical and were preceded by markedly different plastic wakes (Figures 3.2 and 3.3). In the plane strain tests, FCP rate replicate average values for ascending and and constant K_{bmax} cases are 3.07E-05 and

3.11E-05, respectively. These values differ by 1.9 percent. For mixed mode data, the discrepancy between the rate values is 9.5 percent. Observations of the variance among replicates indicates that experimental error or uncontrolled process variables resulted in rate differences as high as 7.6 percent. These observations indicate that the effect of dK/da is minimal in these loading conditions.

6.2.1 Normalized K_{op} Results

The behavior of K_{op} for this loading case is best explained by normalizing it with respect to K_{bmax}. Calculations for this normalization are presented in Appendix C. Replicate averages of K_{op}/K_{bmax} for plane strain and mixed mode loading conditions are presented graphically in Figure 6.4. Visual inspection of this data indicates that K_{op}/K_{bmax} ratio maintained a constant value near 0.40 regardless of stress state or load history. An average of this ratio for each of the four loading cases is presented in Table 6.6.

6.2.2 Load Interaction Effects on FCP Rate

FCP rate data for the bi-harmonic loading test matrix are presented graphically in Figures 6.5 through 6.8. Accompanying the observed experimental data in each plot are two additional sets of calculated rate data. The interaction free data were calculated for each load form

using constant amplitude data generated for this material. Cyclic ΔK components of the load blocks were correlated to constant amplitude FCP rate data to obtain a net rate which was based on data free from load interaction effects. The third set of data visible in the graphs is the result of calculations using observed K_{op} values and the closure based growth rate equation, as discussed previously. These graphs reflect the minimal effect which load interaction had on the FCP rates in this loading case. In all cases, the interaction free model fits the observed date better than does the closure based growth rate equation using the selected parameters from high stress ratio data.

Table 6.2 FCP rate and K_{op} results for plane strain, ascending K_{bmax} bi-harmonic loading. Shown in Figure 3.3, detailed in Appendix A.

Plane Strain: Ascending K_{bmax}				
	T252C		T271C	
K_2/K_1	da/dN (in./cycle)	K_{op} (ksi$\sqrt{in.}$)	da/dN (in./cycle)	K_{op} (ksi$\sqrt{in.}$)
1.00	3.48E-07	2.65	3.30E-07	2.53
0.86	4.63E-07	3.30	4.64E-07	3.14
0.75	6.95E-07	3.22	8.81E-07	2.70
0.67	1.00E-06	3.20	1.20E-06	3.34
0.60	1.51E-06	5.22	1.60E-06	3.72
0.55	1.76E-06	4.89	2.00E-06	4.33
0.50	2.85E-06	3.88	3.07E-06	3.79

Table 6.3 FCP rate and K_{op} results for plane strain, constant K_{bmax} bi-harmonic loading. Shown in Figure 3.2, detailed in Appendix A.

Plane Strain: Constant K_{bmax}				
	T231C		T264C	
K_2/K_1	da/dN (in./cycle)	K_{op} (ksi$\sqrt{in.}$)	da/dN (in./cycle)	K_{op} (ksi$\sqrt{in.}$)
1.00	6.39E-06	4.93	5.11E-06	3.56
0.87	3.62E-06	4.68	4.01E-06	3.79
0.75	3.48E-06	4.20	3.90E-06	3.47
0.62	3.21E-06	4.52	3.07E-06	3.88
0.50	3.00E-06	4.26	3.22E-06	3.51

Table 6.4 FCP rate and K_{op} results for mixed mode, ascending K_{bmax} bi-harmonic loading. Shown in Figure 3.3, detailed in Appendix A.

Mixed Mode: Ascending K_{bmax}				
	T231C		T264C	
K_2/K_1	da/dN (in./cycle)	K_{op} (ksi$\sqrt{in.}$)	da/dN (in./cycle)	K_{op} (ksi$\sqrt{in.}$)
1.00	2.05E-05	5.60	2.08E-05	4.62
0.83	2.38E-05	7.12	2.41E-05	5.74
0.71	2.87E-05	7.33	3.17E-05	7.98
0.63	3.91E-05	9.12	3.61E-05	8.23
0.56	3.86E-05	11.35	3.83E-05	10.59
0.50	4.60E-05	11.76	4.17E-05	10.47

Table 6.5 FCP rate and K_{op} results for mixed mode, constant K_{bmax} bi-harmonic loading. Shown in Figure 3.2, detailed in Appendix A.

Mixed Mode: Constant K_{bmax}				
	T231C		T264C	
K_2/K_1	da/dN (in./cycle)	K_{op} (ksi$\sqrt{in.}$)	da/dN (in./cycle)	K_{op} (ksi$\sqrt{in.}$)
1.00	8.77E-05	17.26	8.13E-05	12.19
0.75	5.81E-05	14.60	5.79E-05	11.31
0.50	4.05E-05	9.99	5.03E-05	12.73

Table 6.6 Average values of K_{op}/K_{bmax} for bi-harmonic loading.

	Plane Strain	Mixed Mode
Ascending K_{bmax}	0.46	0.38
Constant K_{bmax}	0.39	0.44

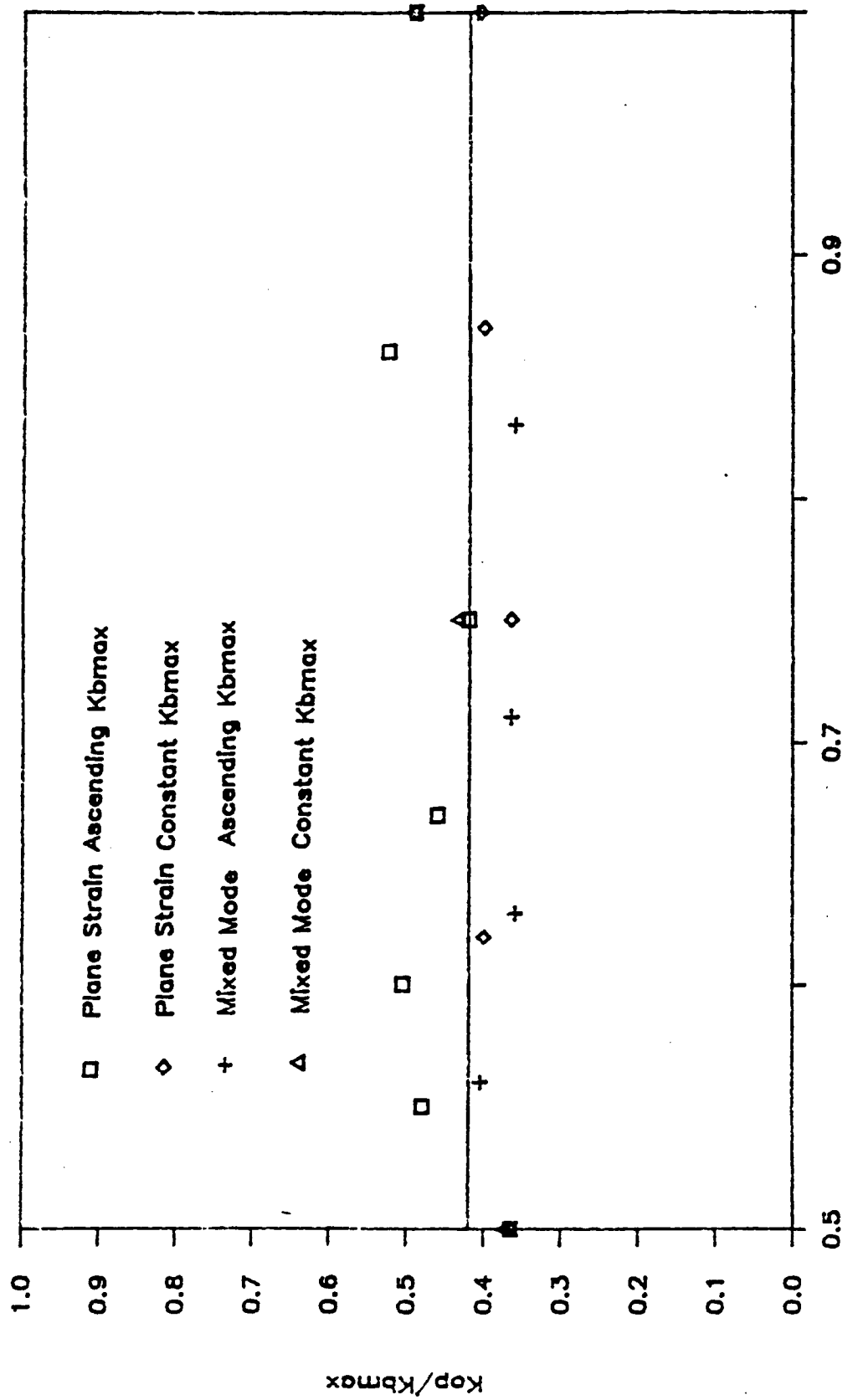

Figure 6.4 Normalized K_{op} results for bi-harmonic loading.

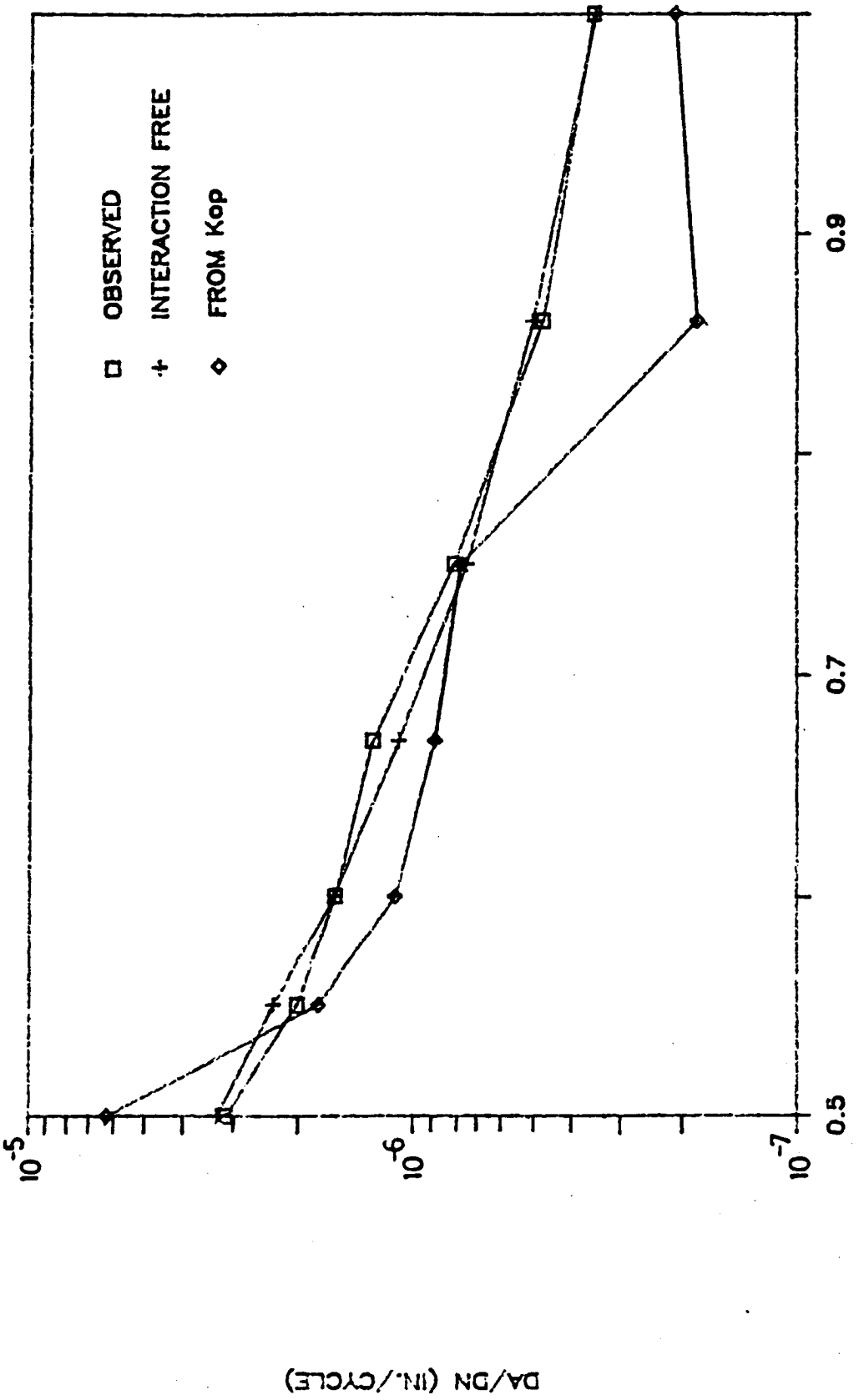

Figure 6.5 Bi-harmonic, plane strain, ascending K_{bmax} rate results.

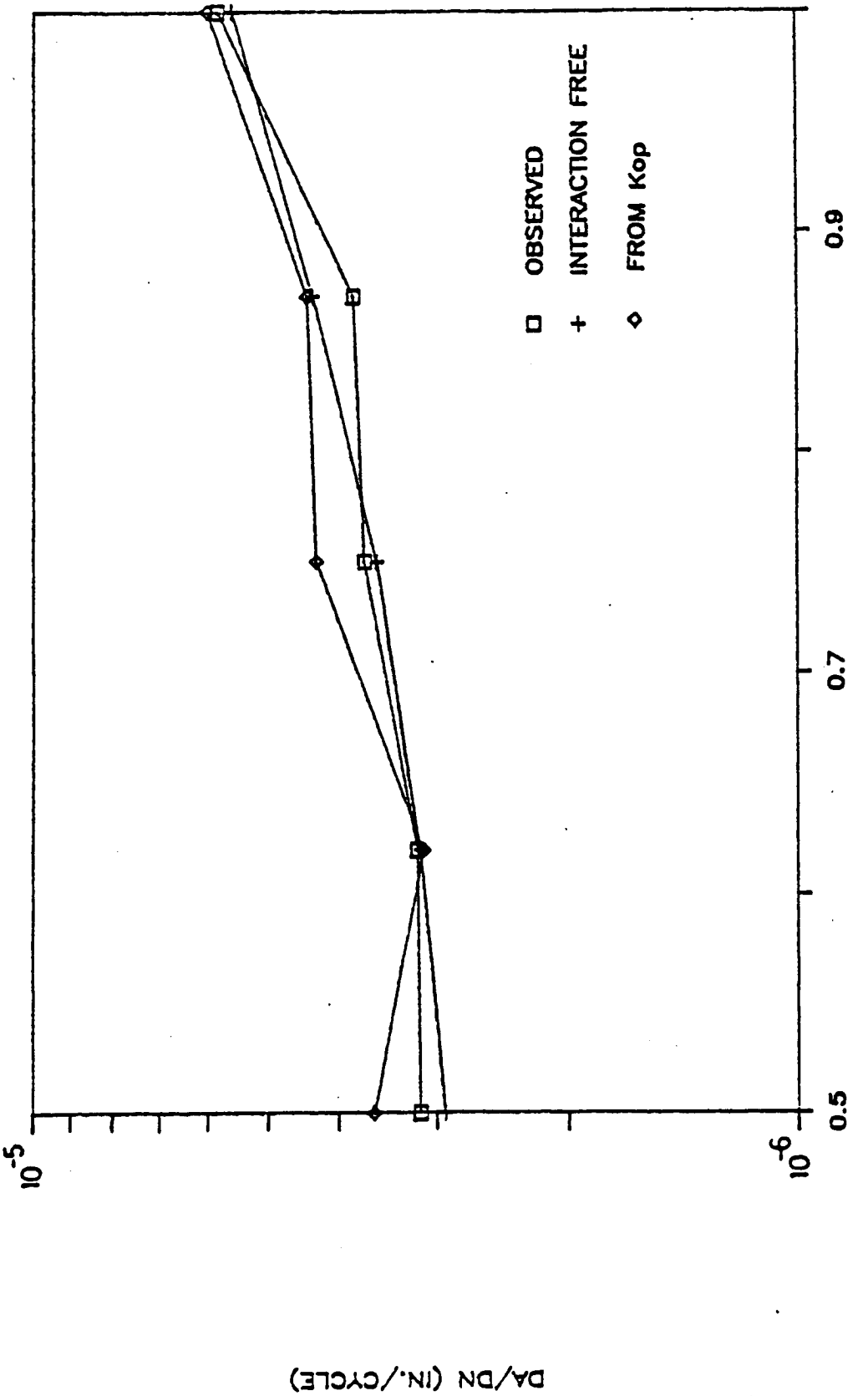

Figure 6.6 Bi-harmonic, plane strain, constant K_{bmax} rate results.

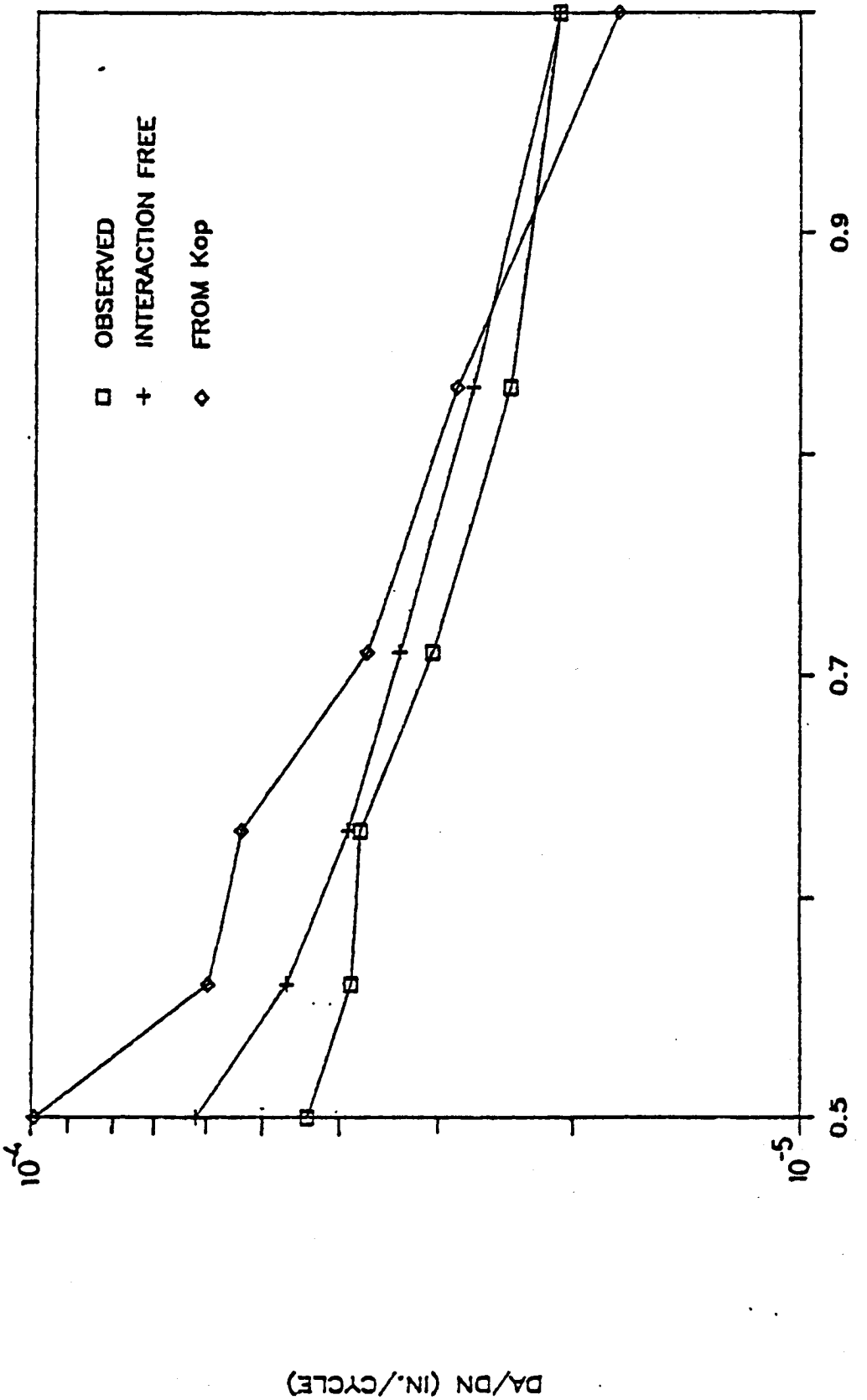

Figure 6.7 Bi-harmonic, mixed mode, ascending K_{bmax} rate results.

6.3 Case III: Variable Fatigue Cycling Test Results

The FCP rate and K_{op} results for mixed mode and plane strain cases of the variable fatigue cycling tests are presented in Tables 6.7 and 6.8. The K_{op} values presented represent the mean of K_{op} values extracted from two data acquisition cycles having K_1 and K_2 as their maximum stress intensity values. In the mixed mode loading case, the K_{op} values taken for the maximum or K_1 cycles were approximately 3 percent higher than their K_2 counterparts. However, observation of all of the data indicate that neither reading varied from the mean by more than five percent. For this reason the mean K_{op} value is used in subsequent calculations of growth rate using the closure based growth rate equation.

6.3.1 Normalized K_{op} Results

As in previous cases, the behavior of K_{op} for this loading condition is best observed when normalized by calculating the quotient of K_{op} and K_{bmax}. For mixed mode data, the mean K_{op} values were divided by 30 ksi$\sqrt{\text{inches}}$. For plane strain data, K_{op} was divided by 7.02 ksi$\sqrt{\text{inches}}$. The results of these calculations plotted against the natural logarithm of N_2 in each loading block are presented in Figures 6.9 and 6.10. These Figures reflect markedly different trends in K_{op} for mixed mode and plane strain data.

In the mixed mode replicates a gradual decrease in the K_{op}/K_{bmax} ratio was observed. Starting at a value of approximately 0.55 at N_2=10 cycles, the ratio fell to nearly 0.38 at N_2 = 1000 cycles. Replicate scatter in the plain strain data does not permit significant observations concerning the behavior of K_{op} to be made. However, there is no indication of the trends observed for the mixed mode data displayed in any of the plane strain replicate data.

6.3.2 Normalized Rate Comparisons: Observed Versus Interaction Free

In order to observe the acceleration or decelerating effects of the various fatigue cycles applied between K_1 cycles, the observed rates were divided by the interaction free rates calculated using constant amplitude data from a previous study [10]. In calculating the interaction free rate, cyclic FCP rate contributions from both the overload and fatigue cycles were considered. The results of these calculations are plotted against the natural logarithm of N_2 in Figures 6.11 and 6.12.

In the mixed mode data displayed in Figure 6.12 a trend in the behavior of the FCP rate ratio is apparent. Starting at a value of 0.39 for N_2 = 10, the ratio falls gradually, reaching a minimum between N_2 = 100 and N_2 = 300 cycles. After reaching the mean minimum value of 0.24, the ratio climbs to a replicate mean value of 0.46.

Replicate scatter in the plane strain rate data prohibits the observation of significant trends in that K_{op} data.

6.3.3 Rate Comparisons Using K_{op}

To examine the correlation between observed K_{op} and FCP rate data, ΔK_{eff} values were used to calculate rates using the closure based growth rate equation. Replicate averages of K_{op} were used to calculate the FCP rates for mixed mode and plane strain stress test data. The resulting rates are plotted with the replicate averages of the observed data in Figures 6.13 and 6.14. In addition, the interaction free rates referred to in the previous discussion are plotted for comparison purposes. In this case, FCP rates calculated under the closure assumption account for the delay observed in the experimental data for both mixed mode and plane strain stress states.

Table 6.7 FCP rate and K_{op} results for plane strain variable fatigue loading. Shown in Figure 3.5, detailed in Appendix A.

Variable Fatigue Cycling: Plane Strain						
T670C	Rep 1		Rep 2		Rep 3	
N_2	da/dN (in./cycle)	K_{op} (ksi$\sqrt{in.}$)	da/dN (in./cycle)	K_{op} (ksi$\sqrt{in.}$)	da/dN (in./cycle)	K_{op} (ksi$\sqrt{in.}$)
10	3.97E-07	2.83	3.86E-07	2.90	3.16E-07	2.56
30	3.01E-07	3.05	3.97E-07	2.14	2.95E-07	2.78
100	2.82E-07	2.85	2.49E-07	2.09	2.97E-07	3.02
300	2.50E-07	2.44	2.44E-07	2.40	2.64E-07	3.21
1000	2.69E-07	2.38	2.35E-07	2.30	2.84E-07	3.64

Table 6.8 FCP rate and K_{op} results for mixed mode variable fatigue loading. Shown in Figure 3.6, detailed in Appendix A.

Variable Fatigue Cycling: Mixed Mode						
	T666C		T667C		T668C	
N_2	da/dN (in./cycle)	K_{op} (ksi$\sqrt{in.}$)	da/dN (in./cycle)	K_{op} (ksi$\sqrt{in.}$)	da/dN (in./cycle)	K_{op} (ksi$\sqrt{in.}$)
10	1.86E-05	15.02	1.86E-05	16.50	1.86E-05	16.31
30	1.38E-05	12.94	1.24E-05	14.44	1.45E-05	15.82
100	9.89E-06	15.69	9.44E-06	15.77	1.20E-05	15.64
300	9.13E-06	10.53	1.23E-05	14.64	1.16E-05	13.90
1000	2.03E-05	13.35	2.40E-05	10.93	1.67E-05	10.95

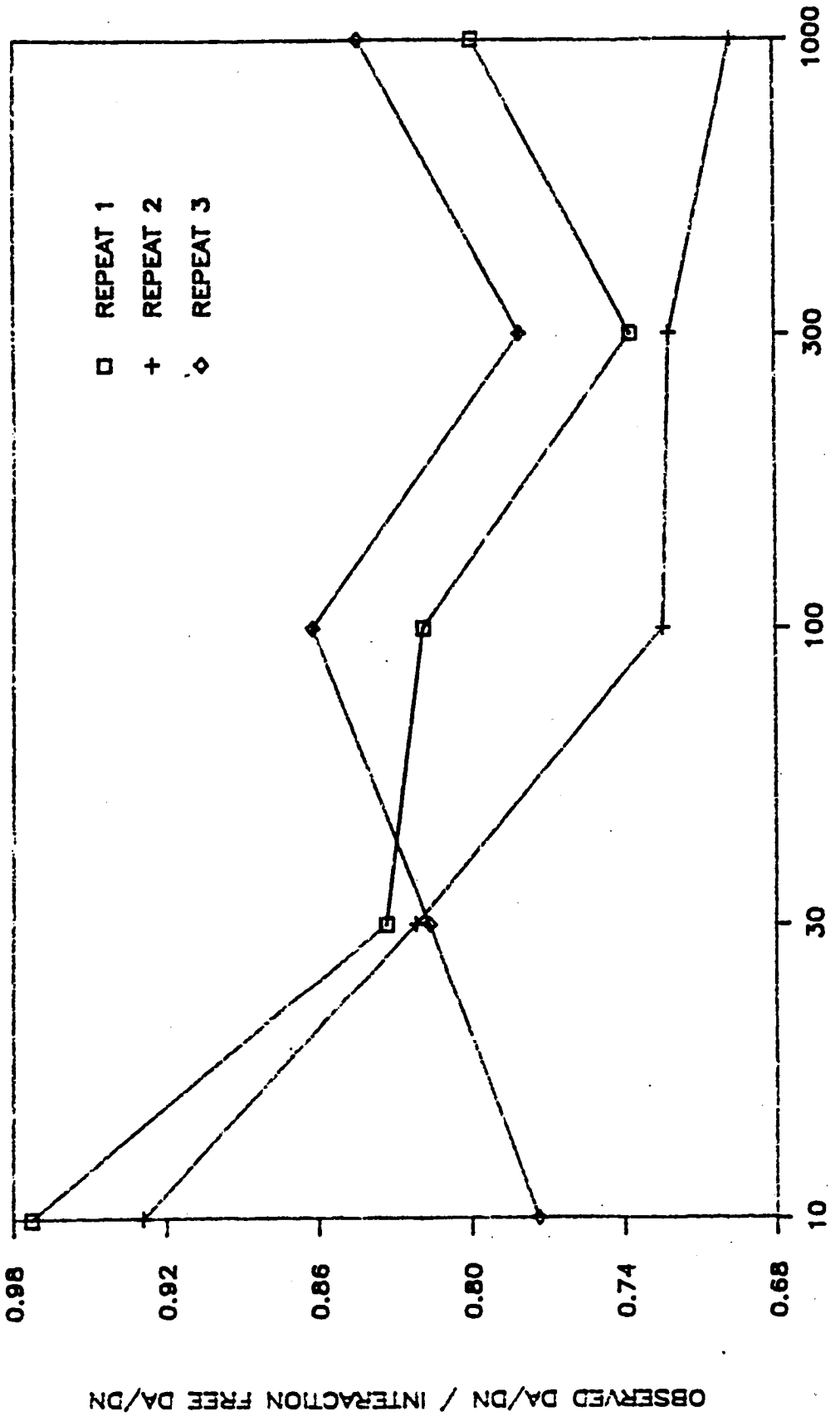

Figure 6.11 Normalized FCP rate results for plane strain variable fatigue loading.

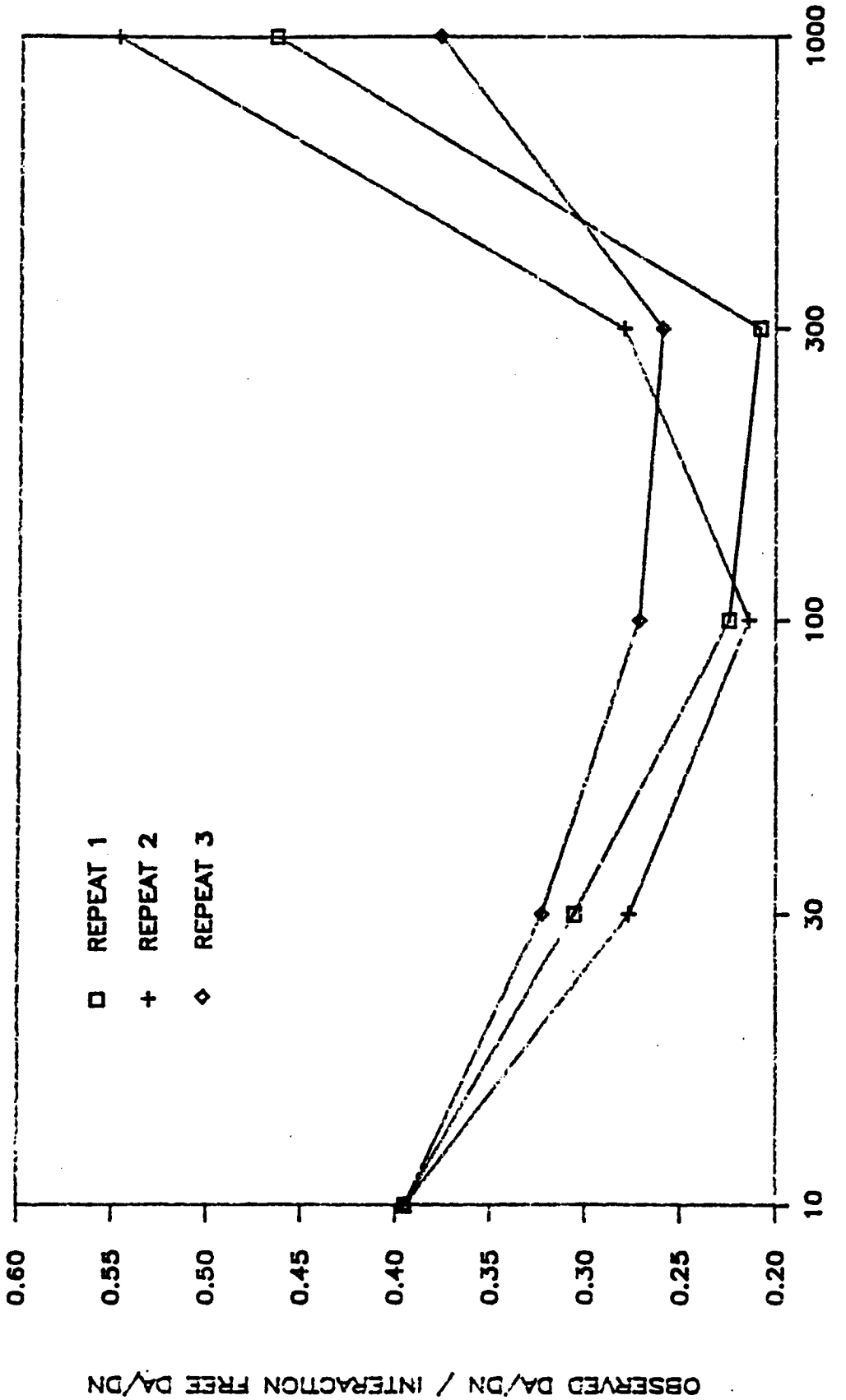

Figure 6.12 Normalized FCP rate results for mixed mode variable fatigue loading.

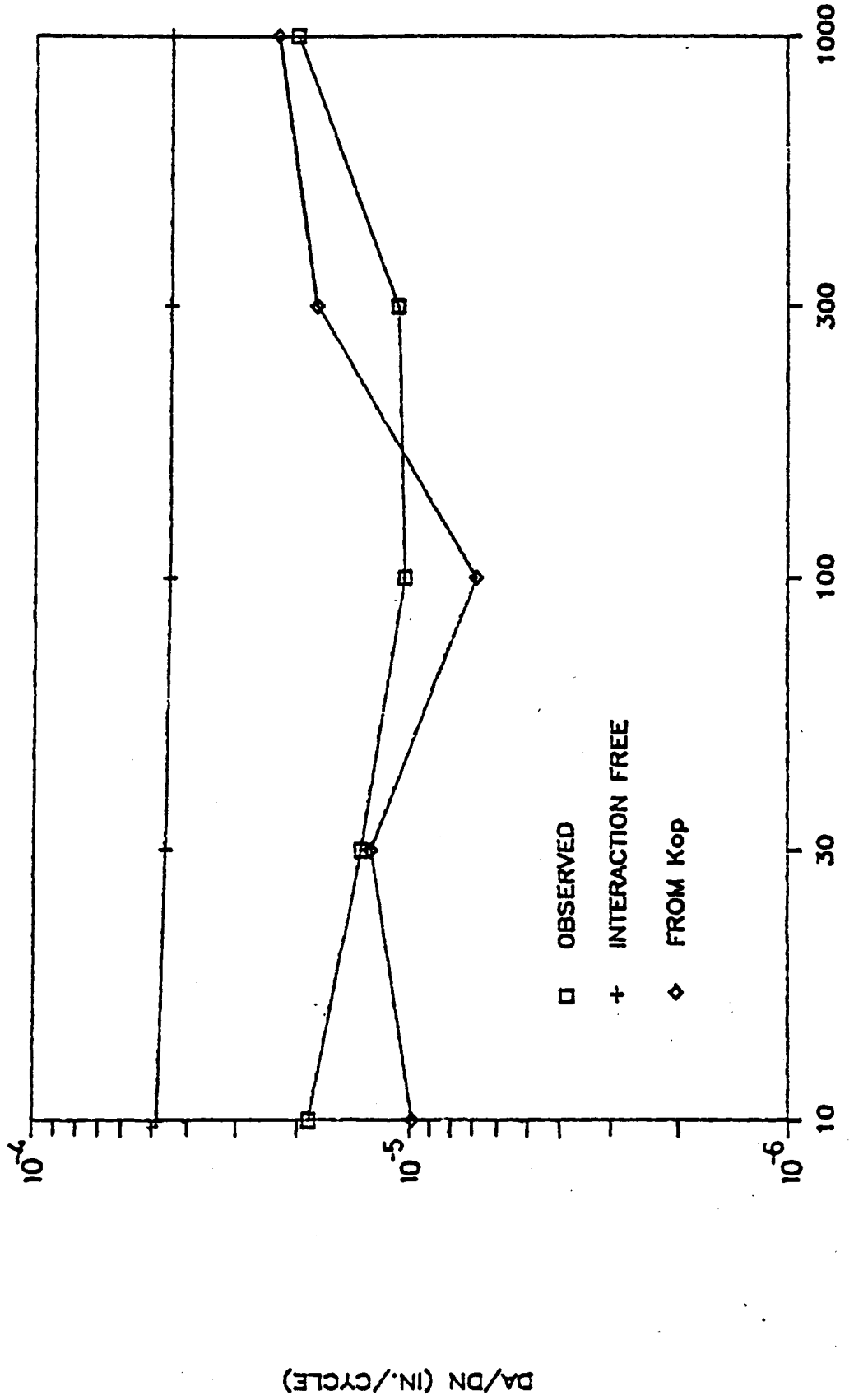

Figure 6.13 FCP rate comparison of observed, interaction free and closure based growth rate relation data for mixed mode variable fatigue loading.

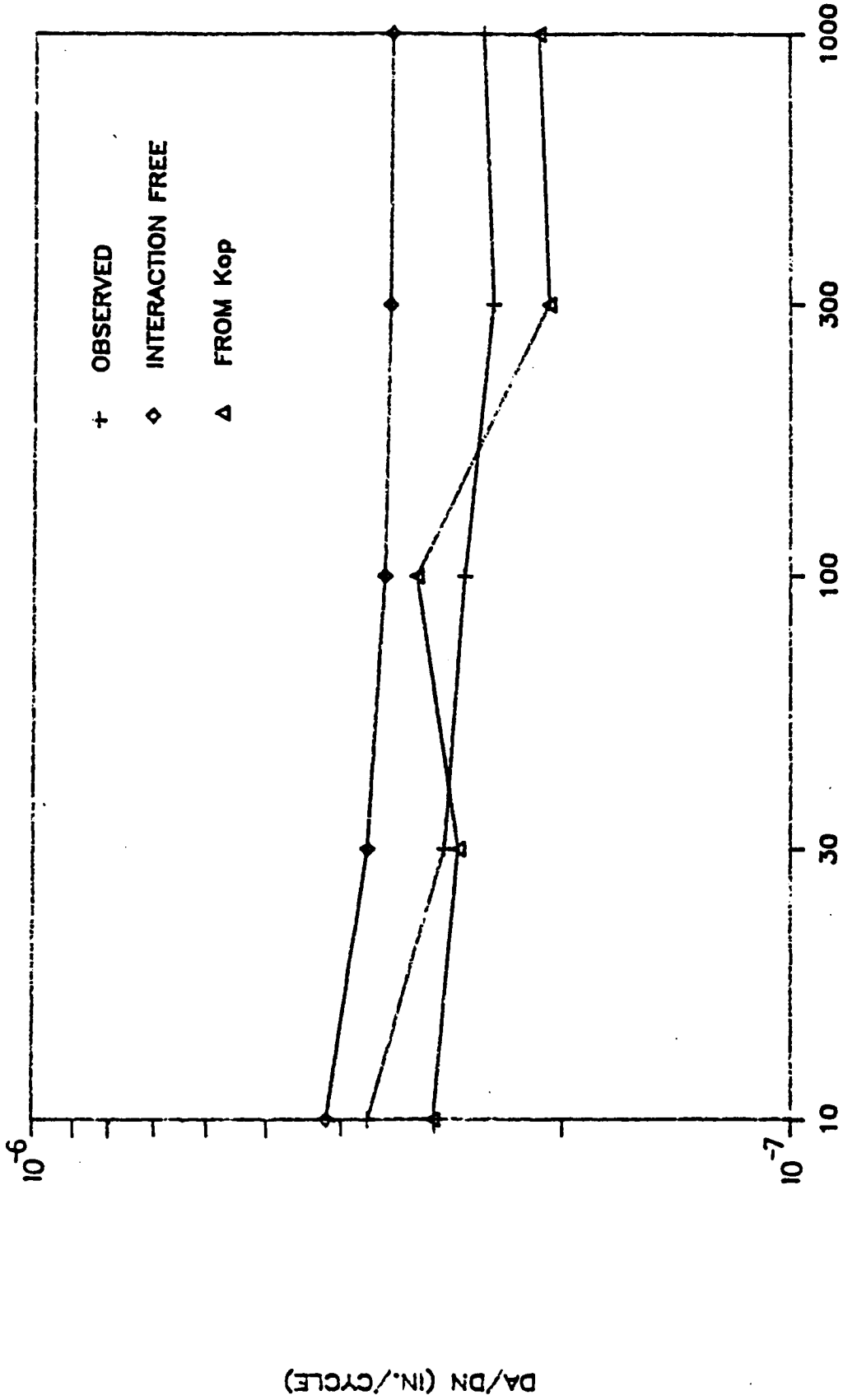

Figure 6.14 FCP rate comparison of observed, interaction free and closure based growth rate relation data for plane strain variable fatigue loading.

6.4 Case IV: High Stress Ratio Overload Results

Fatigue crack propagation calculated for the mixed mode and plane strain high stress ratio tests are presented in Figures 6.15 and 6.16, respectively. Rate data for each individual overload is plotted separately in the figures presented in Appendix D. Several parameters used to describe the retardation following single peak overloads were extracted for each set of overload data using these plots. These parameters include a_{min}, the distance past the overload at which the minimum crack growth rate, $\frac{da}{dN}|_{min}$, occurs. The number of delay cycles associated with overload, N_D, was obtained by determining the number of post overload cycles at which the growth rate returned to its pre overload value, $\frac{da}{dN}|_{ol}$. In addition, N_{min}, the number of post overload cycles at which the minimum FCP rate, $\frac{da}{dN}|_{min}$, was achieved was extracted to facilitate comparisons to K_{op} data which was gathered at fixed-cycle intervals throughout the delay period. A graphic definition of several of these terms is provided in Figure 6.17. The values of these overload parameters for the test data are presented in Tables 6.9 and 6.10. For both plain strain and mixed mode data larger delay periods were associated with larger overloads. An exception to this trend is visible in the post overload data for the mixed mode condition where Q_{ol}=1.37.

6.4.1 Measurements of K_{op} in the Delay Region

Using the wire retaining apparatus described previously, K_{op} measurements were taken at fixed-cycle intervals prior to and following the application of each overload. These readings were taken from the crack tip in the center cracked tensile specimen which was not being used for rate data observations. Once in place, the CTOD extensometer was not moved for the duration of the delay period. Simultaneous rate and K_{op} data were gathered in this manner for each overload.

The load versus CTOD profiles and their associated K_{op} values are not presented in the following text for two reasons. First, the post overload load versus CTOD profiles numbered nearly 200, making their inclusion in this text prohibitive. Also, the sole benefit from their inclusion may be stated in the single, significant observation that $K_{op} = K_{min}$ throughout the post overload delay region.

The non-linear regression algorithm clearly indicated that the relationship between load and CTOD is linear over the entire span of the R=0.7 data acquisition cycle in nearly two thirds of the data taken during post overload delays. The remaining data showing K_{op} larger than K_{min} were scattered in a sporadic fashion throughout the pre and post overload data. These load versus CTOD profiles were characterized by a subtle non-linearity in the region near

K_{min}. The numerical data reduction algorithm readily recognized this non-linearity which is not obvious to the casual observer.

To investigate the implications of this non-linearity in light of the picture presented by all of the data, sequential compilations of pre and post overload load versus CTOD profiles were examined. One such compilation is presented in the plots in Appendix E. The overload data presented is from a mixed mode test where Q_{ol} =1.5. This overload is of particular interest since all of the pre and post overload data display the non-linearity which is observed only sporadically in the much of the remaining data. Visual comparisons of the non-linearity in pre and post overload profiles reveals a similarity which suggest that the same mechanism is the cause in both cases. However, numerous observations by Carman[34] using identical material and equipment, with the exception of the CTOD retainer assembly, indicate that closure is not present in fatigue cycles above a stress ratio of 0.45. These observations lead the author to believe that the subtle non-linearity witnessed in parts of the data is the result of error introduced by unrecognized shortcomings in the wire CTOD gage retainer assembly. Given the experimental procedure used to gather the overload data, it is entirely possible that force imbalances in the retainer resulted in subtle, non-linearities which remained unnoticed.

Compliance values taken from the data presented in Appendix E may be used to substantiate the absence of full crack closure as a mechanism in the delay observed. Assuming that the slope of the linear portion of the load versus CTOD profiles may be related to crack length if the CTOD extensometer remains fixed, compliance values are plotted against post overload cycles in Figure 6.18 to show the growth of the crack following the overload. This analysis indicated that crack growth measured by compliance is completely halted until 8000 cycles after the overload, at which time crack growth resumes. Theoretical predictions of delay based on full crack closure concepts are not characterized by this type of post overload crack growth behavior.

Table 6.9 Results from high stress ratio overload tests; mixed mode, R=0.7. Shown in Figure 3.7, detailed in Appendix A.

Observed Overload Parameters: Mixed Mode						
Specimen Identification: T191C						
Q_{ol}	a_{min} (in.)	a_{ol} (in.)	$\frac{da}{dN}\|_{min}$ (in./cycle)	$\frac{da}{dN}\|_{ol}$ (in./cycle)	N_D (cycles)	N_{min} (cycles)
1.23	0.051	0.381	1.91E-06	2.96E-06	6613	1089
1.30	0.020	0.279	4.97E-07	2.64E-06	7628	1529
1.37	0.200	0.152	1.15E-06	2.62E-06	4035	1008
1.43	0.051	0.508	1.53E-07	2.70E-06	16798	6524
1.50	0.025	0.229	1.47E-07	2.40E-06	15064	5028

Table 6.10 Results from high stress ratio overload tests; plane strain, R=0.7. Shown in Figure 3.7, detailed in Appendix A.

Observed Overload Parameters: Plane Strain						
Specimen Identification: T314C						
Q_{ol}	a_{min} (in.)	a_{ol} (in.)	$\frac{da}{dN}\|_{min}$ (in./cycle)	$\frac{da}{dN}\|_{ol}$ (in./cycle)	N_D (cycles)	N_{min} (cycles)
1.23	0.001	.003	1.31E-06	4.08E-06	1600	600
1.30	0.004	0.010	1.03E-06	4.16E-06	3088	1054
1.37	0.003	0.010	6.20E-07	4.08E-06	2237	953
1.43	0.001	0.012	5.50E-07	3.81E-06	7280	1987
1.50	0.009	0.017	3.09E-07	4.18E-06	15342	6886

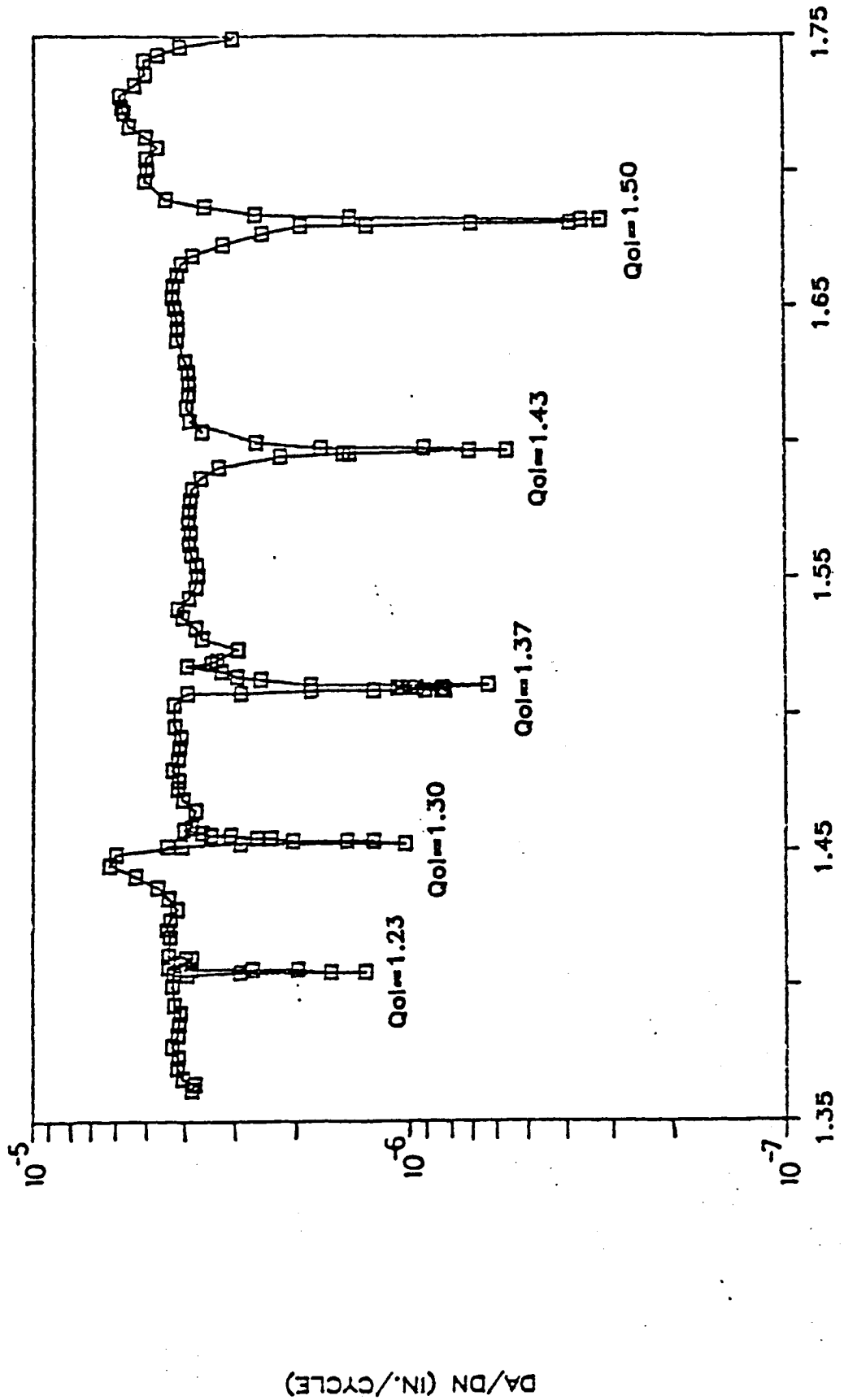

Figure 6.15 Mixed mode high stress ratio overload results: Q_{o1} = 1.23 to 1.50.

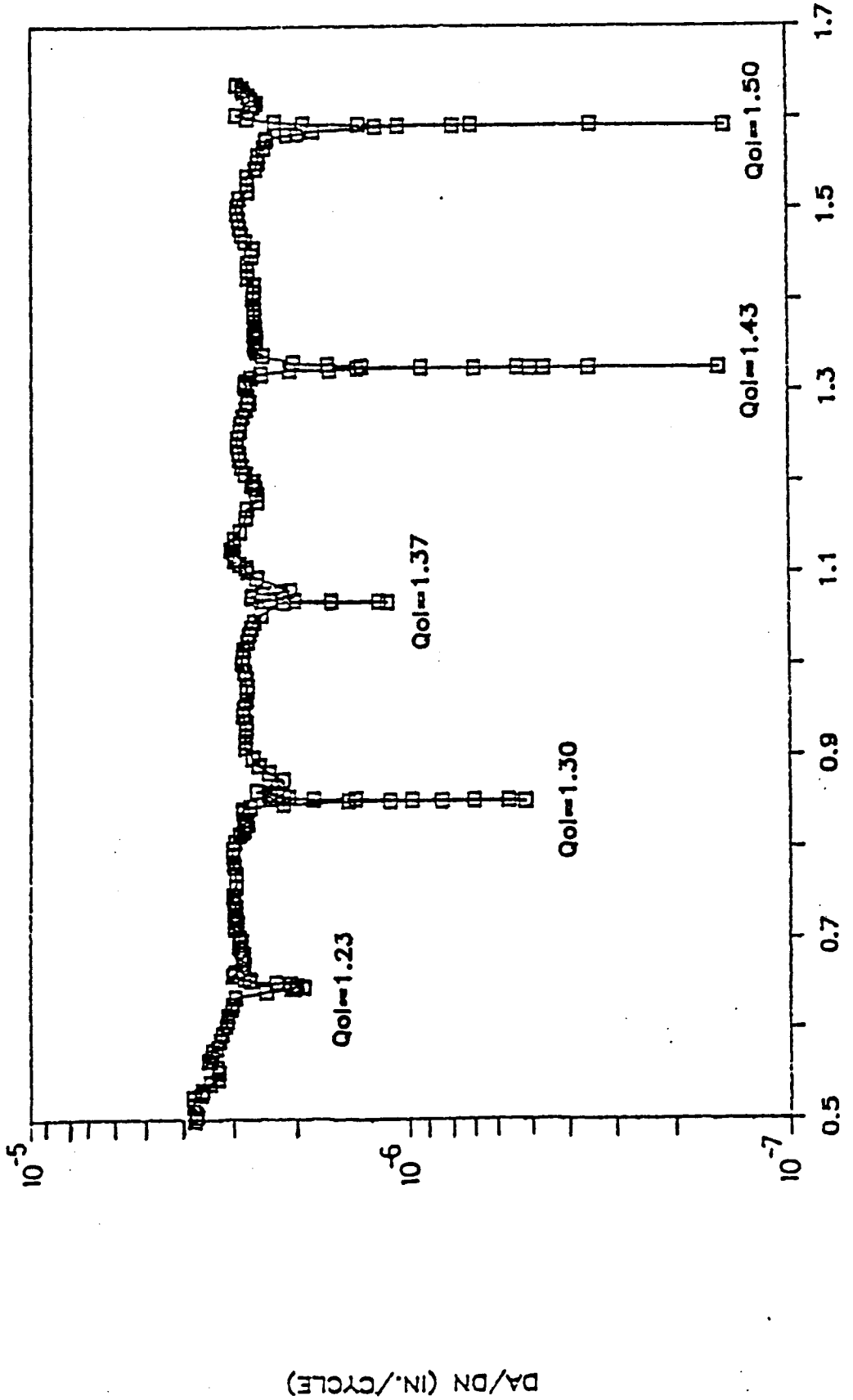

Figure 6.16 Plane strain high stress ratio overload results: Q_{ol} = 1.23 to 1.50.

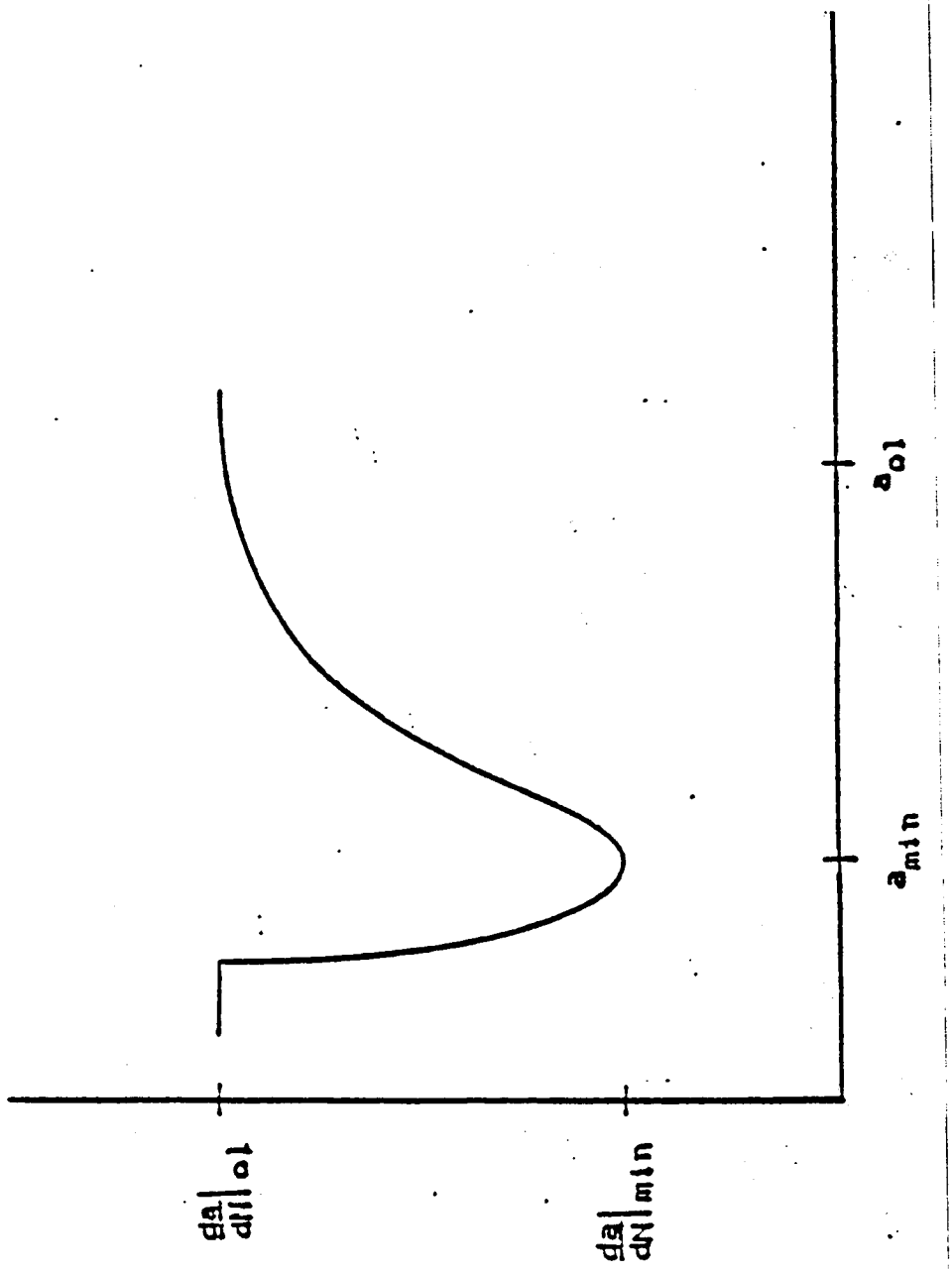

Figure 6.17 Parameters used to define post overload delay.

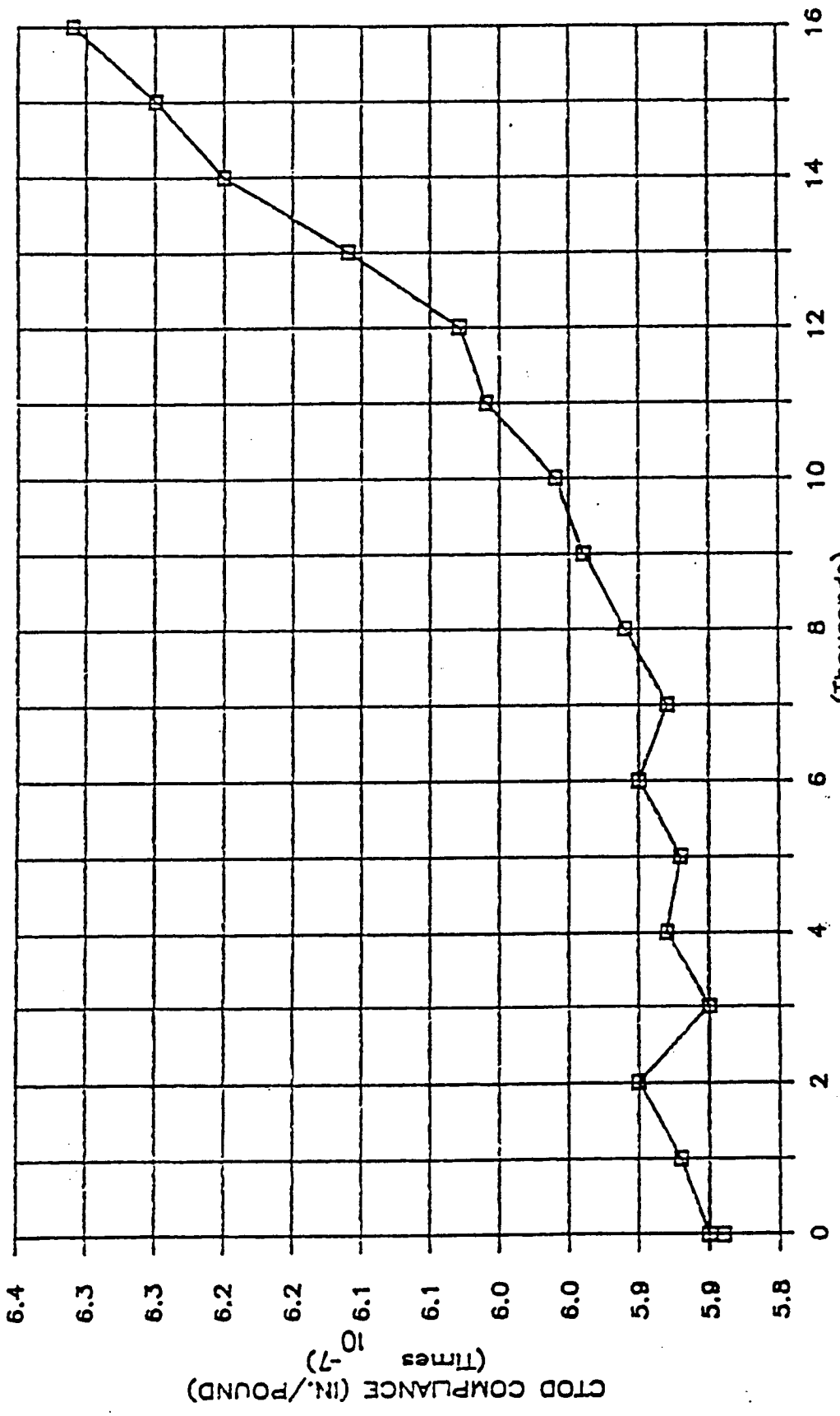

Figure 6.18 CTOD compliance versus cycles past overload results for mixed mode loading Q_{o1}=1.5.

CHAPTER 7 - DISCUSSION OF RESULTS

The results presented for the variable amplitude loading cases examined in this investigation provide valuable insight into the role which closure plays in the load interaction phenomenon. While inherent data scatter among replicate tests was observed, dominant trends in the K_{op} and FCP rate results highlight significant factors in the load interaction process. These trends are discussed in the following pages. In addition, results from the study are analyzed in an attempt to provide a key load interaction parameter for the Multi-Parameter Yield Zone Model [4] developed by Johnson.

7.1 Load Interaction Effects on FCP Rate

When compared to constant amplitude FCP rate data the results from the current series of tests show a marked deceleration effect resulting from load interaction. For multi-step loading cases A and B, direct comparisons to interaction free rate results is inhibited by the diversity in stress ratios at which each of the component cycles in these blocks are executed (Figure 3.8). However, in block

C each component cycle is executed at stress ratios near that of the existing constant amplitude data; R=0.05. This permits a direct comparison of observed, $\frac{da}{dN}$, and interaction free, $\frac{da}{dN}|_{IF}$, rate results. Such a comparison indicates that $\frac{da}{dN}/\frac{da}{dN}|_{IF}$ is approximately 0.8 for all of the replicate data. Given that block C most closely resembles a spectrum loading condition among the loading blocks applied in this test program, it is significant to note the conservative nature of FCP rate predictions based on interaction free rates for this loading case.

The FCP rate results for the bi-harmonic loading series indicate minimal effects of load interaction resulting from the repeated high cycle-low cycle loading blocks. Figures 7.1 through 7.4 reflect the small differences between the interaction free and observed FCP rate data for each of the loading conditions in the bi-harmonic test matrix. In the graphs, $\frac{da}{dN}$ is normalized by the interaction free FCP rate data for the high cycle, $\frac{da}{dN}|_{1IF}$. Using yield zone delay arguments, Johnson anticipates the normalized rate data from this series to approach the $K_2 / K_1 = 0.5$ boundary along an asymptote at $\frac{da}{dN}/\frac{da}{dN}|_{1IF} = 0.5$. The K_2 / K_1 ratio at which the rate contribution of the lower cycle is negligible may be considered as the "B" parameter in the MPYZ model. Using this parameter on a cycle by cycle basis, the MPYZ algorithm determines whether or not crack propagation should occur for a given loading cycle.

Johnson [4] suggests the use of single peak overload tests in determining the "B" parameter, implying that post overload delay data extracted from such tests is applicable to the variable amplitude fatigue situation. However, in the bi-harmonic loading series the effects of load interaction on rate were not observed. Therefore, a value for the "B" parameter could not be extracted from these results.

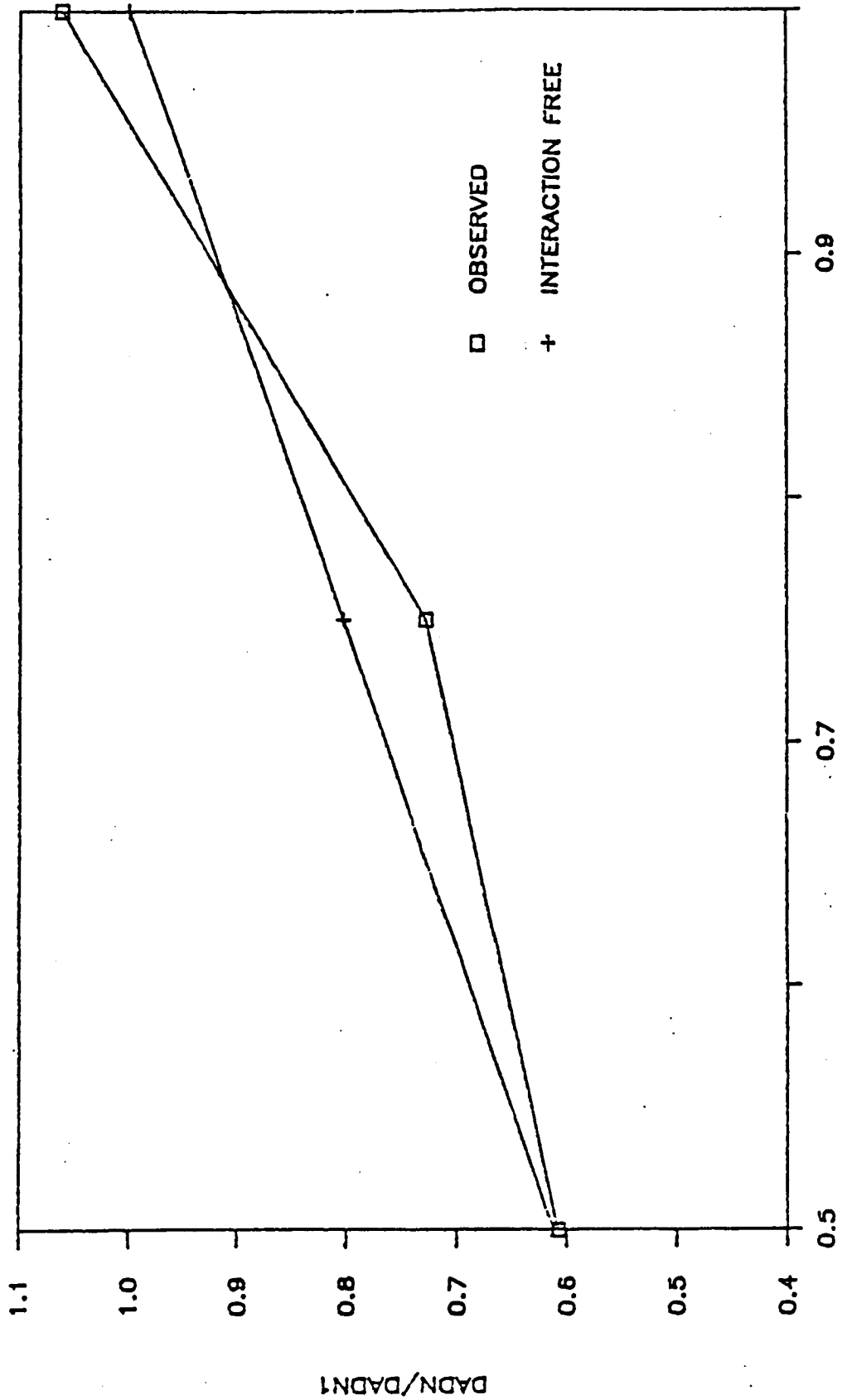

Figure 7.1 Normalized K_{bmax} versus K_2/K_1 results for mixed mode, constant K_{bmax} bi-harmonic loading.

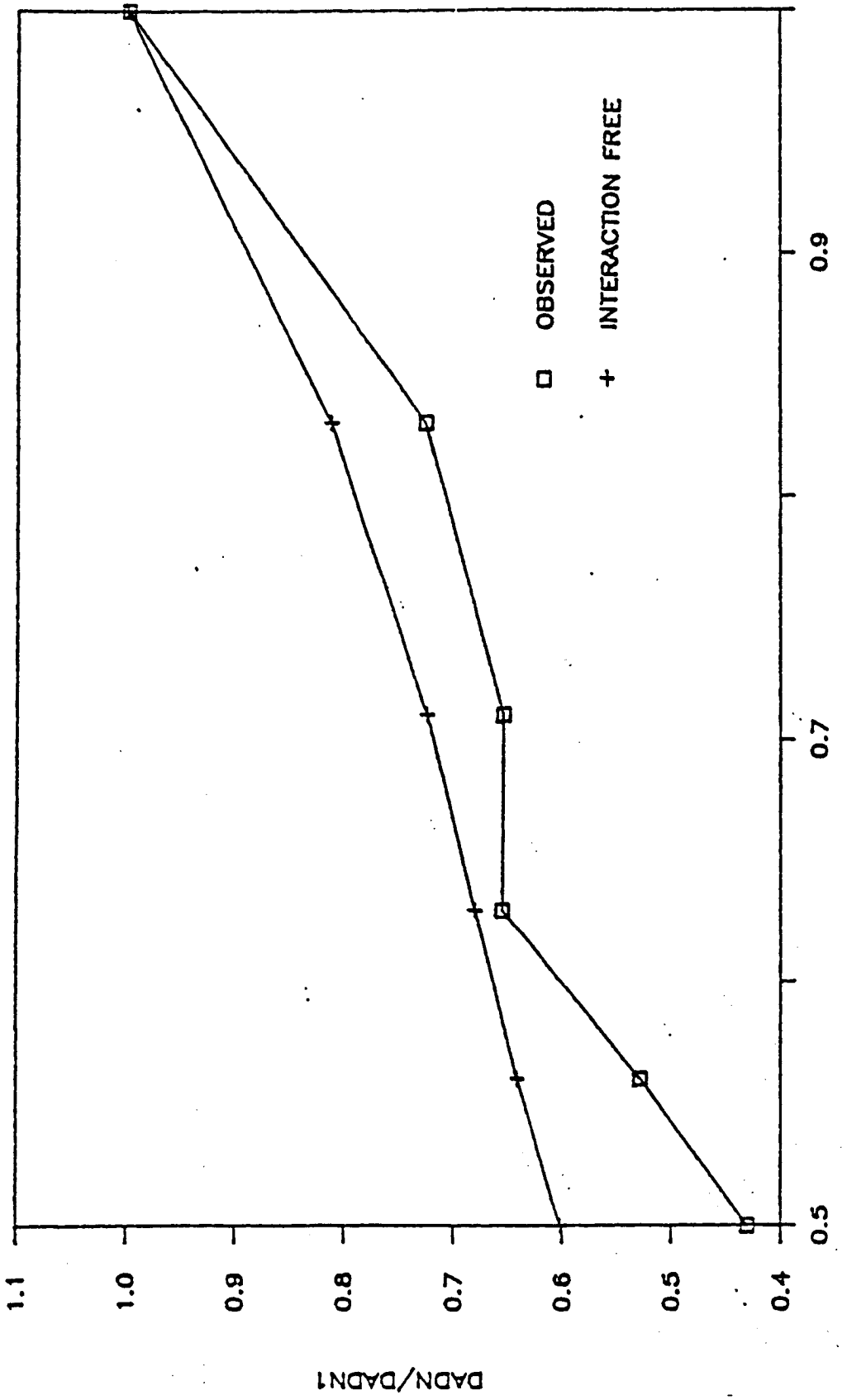

Figure 7.2 Normalized K_{bmax} versus K_2/K_1 results for mixed mode, ascending bi-harmonic loading.

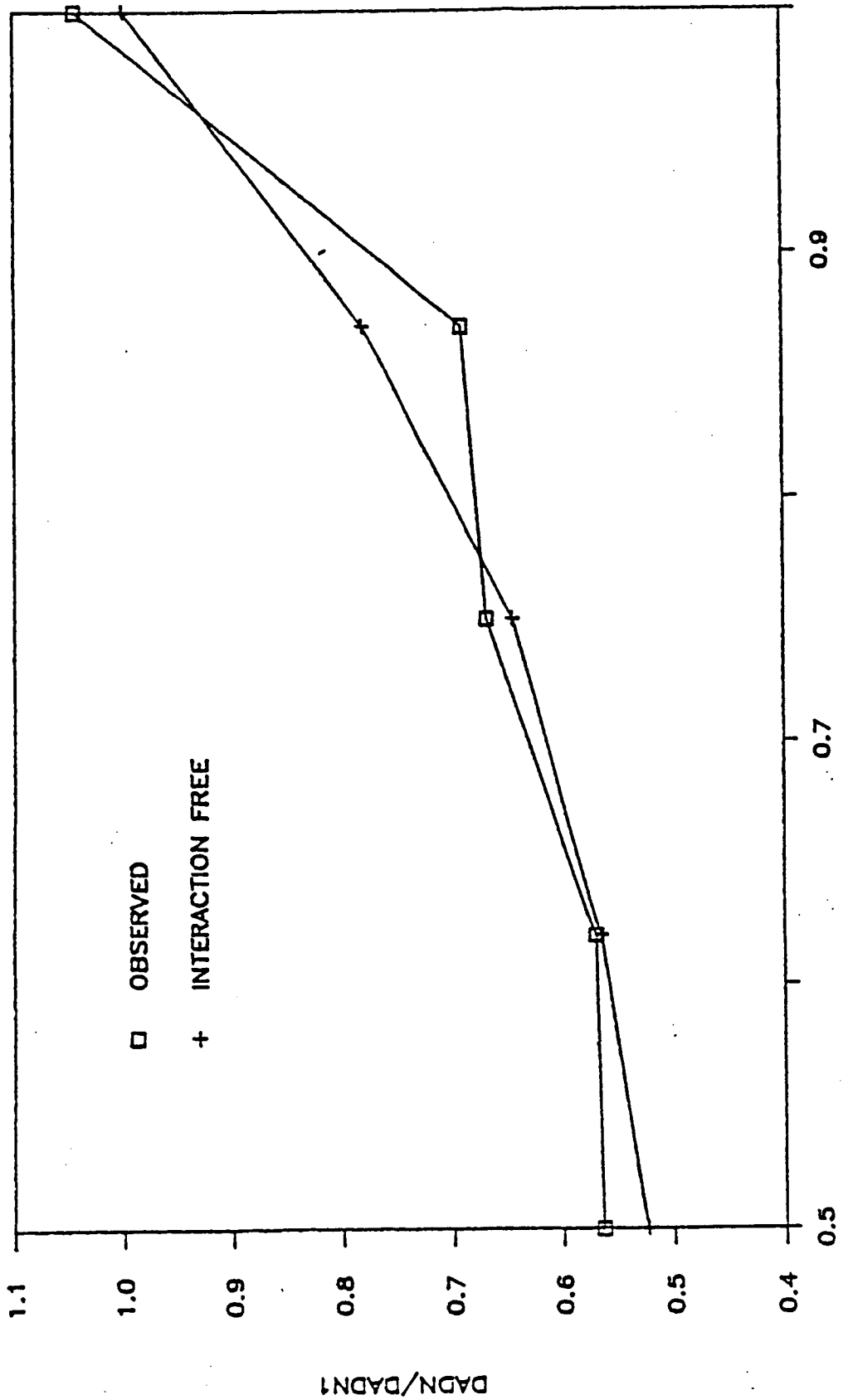

Figure 7.3 Normalized K_{bmax} versus K_2/K_1 results for plane strain, constant bi-harmonic loading.

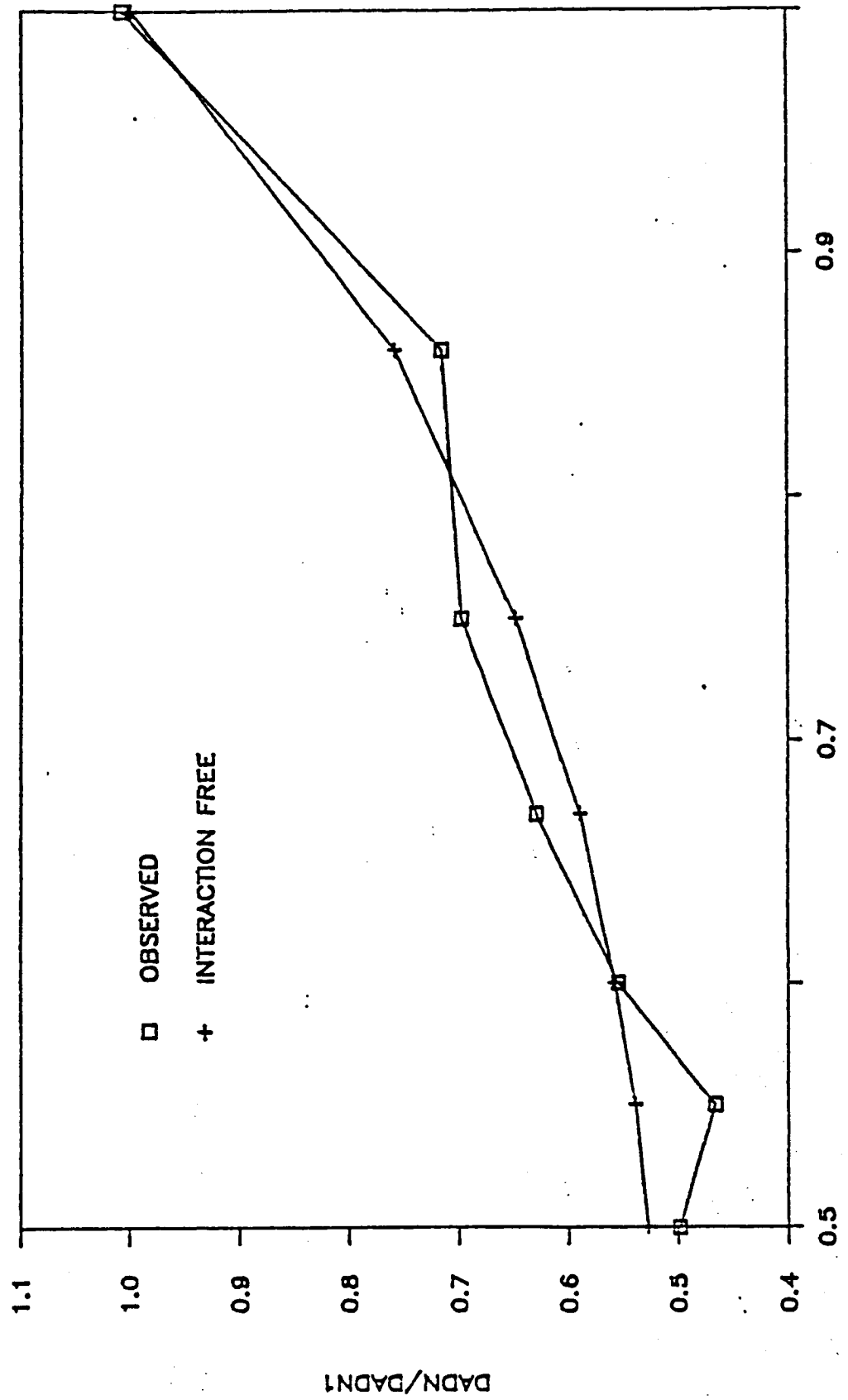

Figure 7.4 Normalized K_{bmax} versus K_2/K_1 results for plane strain, ascending bi-harmonic loading.

This observation raises questions concerning the use of load interaction models based on empirical data extracted from single peak overload test results. Daiuto [10] observed delay in fatigue cycles following single peak overloads at stress ratios of 0.05 and Q_{o1} = 2.0. These loading conditions correspond to a K_2/K_1 = 0.5 fo the bi-harmonic series at which no delay was observed. This indicates that post overload delay in fatigue cycles is likely a function of the number of fatigue cycles between overloads.

This fatigue cycling effect was observed for various numbers of fatigue cycles in the third loading case of the test program. Results for the variable amplitude fatigue cycling tests were combined with the K_2/K_1 = 0.75 test results from the bi-harmonic series to present a complete picture of the interaction effect on fatigue cycles between overloads for this load ratio. These results indicate that the delay effect was greatest when N_2=200. Expected acceleration effects were not present in the steady state FCP rate results obtained for values of N_2 between 1 and 1000 cycles. Based on the load interaction effects observed by Elber [3] immediately following single peak overloads, the results shown in Figure 7.5 would be expected for the variable amplitude loading case. These results show a brief period of acceleration for low values of N_2 followed by a significant delay period at larger N_2

values. The discrepancy between load interaction test data and results anticipated based on single peak overloads indicates the potential deficiencies of load interaction models which predict FCP rate behavior based on empirical results from single peak overload results. This suggests the need for an understanding of the basic mechanism of delay which is provided by the observations of K_{op} which accompany the rate data in this study.

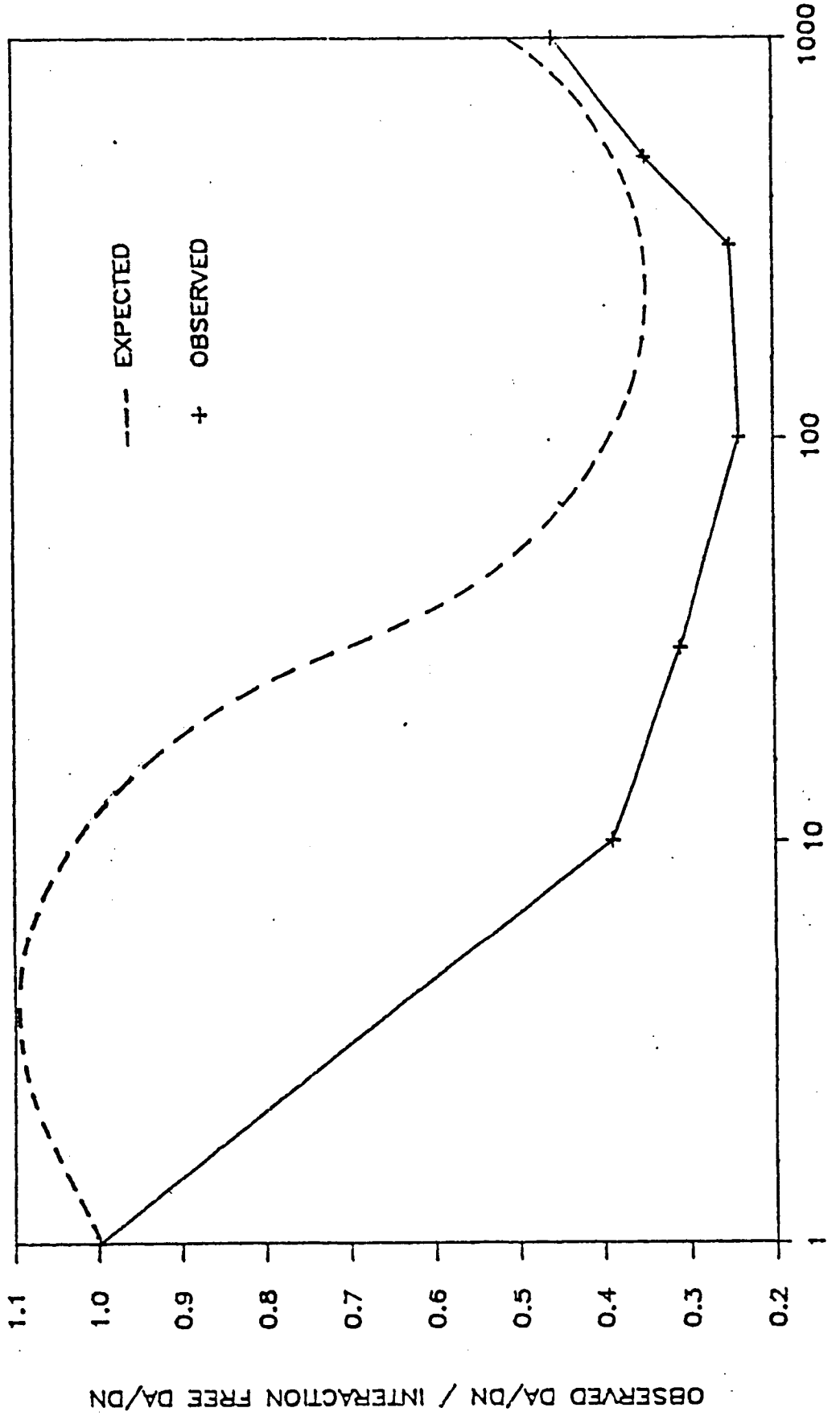

Figure 7.5 Anticipated and observed behavior of FCP rate in variable fatigue loading.

7.2 K_{op} Behavior and the Role of Closure in Interaction

Several noteworthy aspects of K_{op} behavior were observed in this investigation. The cyclic stability of crack opening load in a given repeated loading block was significant. Detailed observations of this stability were enabled by the data acquisition and reduction techniques which were employed in this study. Graphics illustrating this stability are presented in Figures 7.6 and 7.7, showing the actual CTOD versus load data taken for high and low cycles in the bi-harmonic loading block. In these Figures, the quality of the load and CTOD data are typical of the data obtained throughout the study. The broken line on each plot represents the optimized model data calculated for each load profile by the non-linear regression algorithm. The optimized coordinates of the crack opening load is encircled on each graph. This pair of data sets indicate identical crack opening loads. Typical optimized crack opening load levels for a given loading block differed by no more than five percent. These results imply that K_{op} in variable amplitude loading conditions is not a cyclically dynamic quantity. The data indicates that the stable K_{op} value observed for each loading block is a product of the cycles preceding it. This strongly suggests that closure and, by virtue of the rate correlations presented herein, load interaction is a plastic wake phenomenon. Since the cycles preceding each K_{op}

measurement in this study are well defined, several significant observations concerning the factors affecting K_{op} may be made.

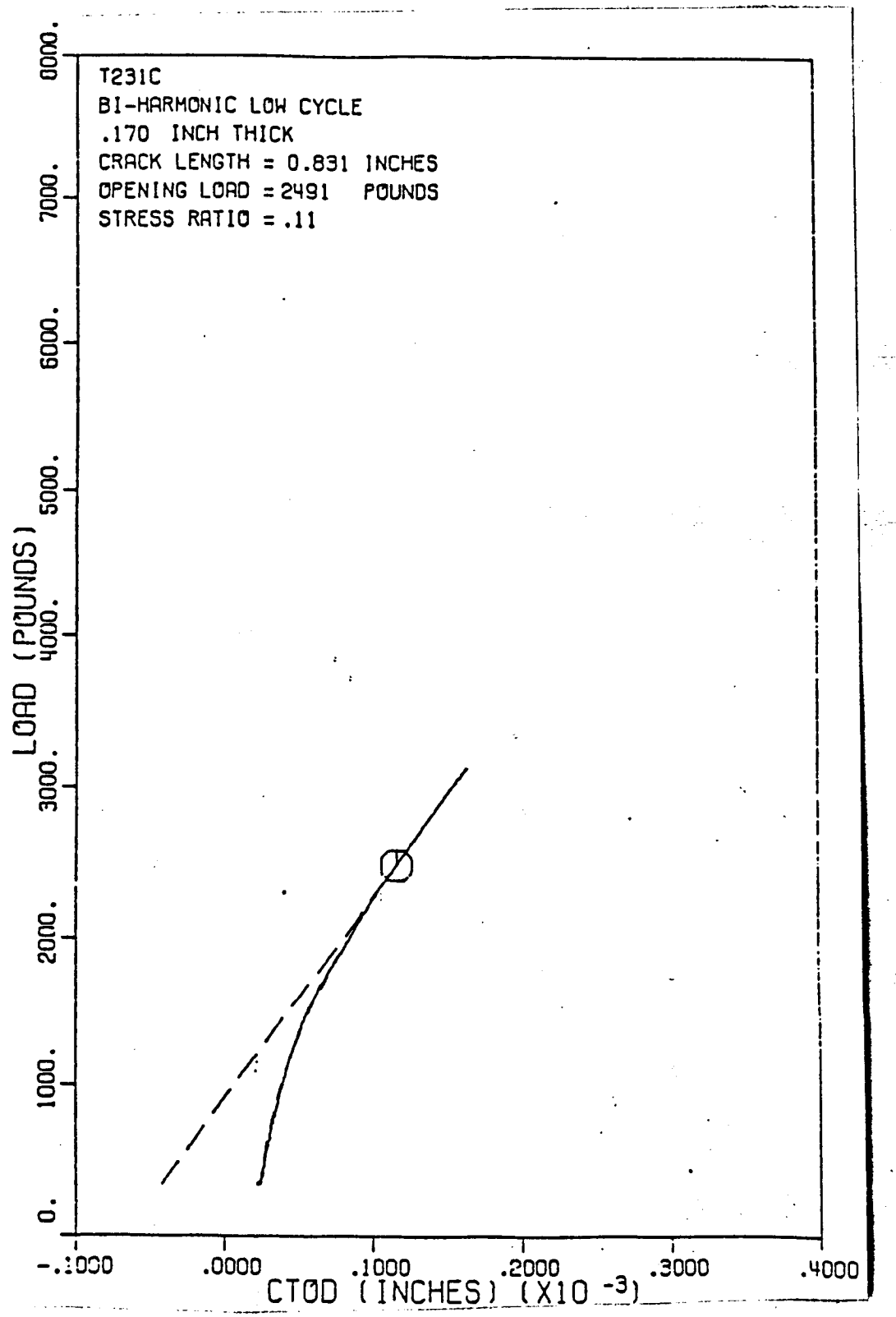

Figure 7.7 Typical bi-harmonic low cycle load versus CTOD profile and associated non-linear regression results.

By correlating the characteristics of each loading block to observed K_{op} behavior, the first order factors effecting K_{op} were highlighted. The most significant factor effecting K_{op} in the bi-harmonic test series, where the effects of K_{min} and stress ratio was essentially eliminated, is K_{bmax}; the maximum stress intensity value in the repeated loading block. The K_{op}/K_{bmax} results for this test series presented in Figure 6.4 clearly show K_{op} is a direct proportion of K_{bmax}. These results are observed for both constant and ascending K_{bmax} testing series in both mixed mode and plane strain. This is strong experimental evidence in support of plasticity induced closure in plane strain and plane stress.

The role of K_{bmin} and K_{min} on the behavior of K_{op} is displayed in the results of the multi-step loading tests. These results, presented in Figure 6.2, show the subtle influence of K_{min} on K_{op}. These changes in the K_{op} level are reflected in the FCP rate results presented in Figure 6.3. This figure also illustrates how these slight changes in K_{op} may be used in the closure based growth rate expression to account for the observed change in FCP rate. The close agreement between observed and calculated FCP rates was not seen in FCP data calculated under the assumption that K_{op} maintained the same constant value for all three

loading blocks in the multi-step loading case.

The role which the number of fatigue cycles between overloads played in the value of K_{op} appears to be dependent on stress state. Considering the results of the biharmonic and variable fatigue cycling tests, a comprehensive picture of the effect of N_2 on K_{op} is formed. For mixed mode cases, K_{op}/K_{bmax} starts at a value dictated by K_{bmax} and rises as N_2 increases to 10 cycles. This rise in K_{op} relative to K_{bmax} was an unexpected phenomenon which must be attributed to load interaction in some form. For the mixed mode loading conditions, the subsequent fall in K_{op}/K_{bmax} values at large N_2 values may be attributed to the increasing effect of the fatigue cycles in establishing K_{op}. Plane strain data indicate that K_{op}/K_{bmax} remains at a constant value of approximately 0.4 for all values of N_2. Both mixed mode and plane strain K_{op} data correlate well with the observed FCP rate results using the closure based crack growth expression, indicating that closure is the primary mechanism of the load interaction results observed for variable fatigue cycling tests. Lack of marked interaction effects in the plane strain loading tests is supportive of plasticity induced closure theory which would predict less interaction with smaller plastic zones.

Fatigue crack closure theory did not explain the delays observed in the high stress ratio overload tests.

Measures of the CTOD following overload indicate that the crack tip was fully open following the application of overloads under mixed mode and plane strain conditions. These observations suggests that another mechanism is responsible for the delay observed at stress ratios above R_{cut}. The post overload CTOD compliance data in Figure 6.18 shows little or no change in compliance until approximately 8000 cycles after the overload, thus indicating that crack growth was virtually halted during this period. This method of observing post overload crack growth behavior is inherently more refined than rates calculated by the seven point polynomial method applied to optical crack length measurements. The growth evidence resulting from these more refined measures of growth suggest a blunting mechanism of delay rather than closure.

CHAPTER 8 - CONCLUSIONS AND RECOMMENDATIONS

The objective of this investigation was to accurately measure and observe $\frac{da}{dN}$ and K_{op} under variable amplitude loading conditions. In order to attain this objective, considerable effort on the part of the author was expended in the development of testing equipment and techniques which permit the application of variable amplitude loads and provide accurate measurements of K_{op}. The data provided in this thesis is a direct result of this effort. Based on an intrinsic understanding and confidence in the testing techniques, observations of the experimental data, and correlations of observed and predicted FCP rates, the following conclusions and recommendations are presented.

8.1 Conclusions

[1] Repeated variable amplitude loading blocks may be used to induce load interaction effects resulting in FCP rates which are measurably different than corresponding interaction free rates.

[2] In cases where load interaction effects are observed, measured ΔK_{eff} may be used to calculate FCP rates with the closure based growth rate equation to account for these effects.

[3] A CTOD extensometer placed at a distance of 1.5 plastic zones behind the crack tip may be used to provide accurate , bulk crack tip opening displacement data which may be used to calculate K_{op}.

[4] Digital load versus CTOD data may be numerically processed using a non-linear regression algorithm to optimize the value for load at which crack opening, as defined by Elber, occurs.

[5] K_{op} remains at a constant value throughout each cycle of a repeated variable amplitude loading block.

[6] The maximum stress intensity in a repeated loading block, K_{bmax} , effects the level of K_{op} most directly in tests conducted at a constant stress ratio of 0.05.

[7] Plasticity induced closure appears to be the mechanism of delay in both mixed mode and plane strain stress state loading conditions at stress ratios of 0.05.

[8] Closure is not the mechanism of delay in single peak overloads performed at high stress ratios.

8.2 Recommendations

[1] Development of the microprocessor fatigue testing equipment should be continued toward the goal of complete automation of growth rate data acquisition. This may be accomplished by correlating CMOD compliance measurements to observed crack length data. This would also facilitate computer controlled constant ΔK tests. Care should be taken to insure that motion of the specimen and CMOD gage are properly restrained.

[2] Using the refined experimental equipment and current data reduction techniques, a series of constant K growth tests conducted at different stress ratios would provide valuable information on the behavior of K_{op} when all of the first order influences on it are held constant.

[3] Finally, further high and low stress ratio overload tests should be performed with an improved technique for simultaneous collection of rate and K_{op} data. Refinements in the CTOD retainer assembly or a completely new design will be required. Compliance data from subsequent measurements using the refined device should yield valuable insight into the mechanism of post overload delay at high stress ratios.

LIST OF REFERENCES

LIST OF REFERENCES

[1] Paris, P.C., Gomez, M.P., and Anderson, W.F., A Rational Analytic Theory of Fatigue, The Trend in Engineering, 13(1961) pp. 9-14.

[2] Elber,W., "The Significance of Fatigue Crack Closure", Damage Tolerance in Aircraft Structures, ASTM STP 486, American Society for Testing and Materials,1970.

[3] Elber, W., "Fatigue Crack Closure Under Cyclic Tension", Engineering Fracture Mechanics, Vol 2, 1970, pp. 37-45.

[4] Johnson, W.S., "Multi-Parameter Yield Zone Model for Prediction Of Fatigue Crack Growth", Methods and Models for Predicting Fatigue Crack Growth Under Random Loading, ASTM STP 748, American Society for Testing and Materials, Philadelphia, 1981, pp. 85-102.

[5] Katcher, M. and Kaplan M., "Effects of R-Factor and Crack Closure on Fatigue Crack Growth for Aluminum and Titanium Alloys", Fracture Toughness and Slow-Stable Cracking, ASTM STP 559, American Society for Testing and Materials, 1974, pp. 264-282.

[6] McEvily, A.J., "On the Quantitative Analysis of Fatigue Crack Propagation", Fatigue Mechanisms: Advances in Quantitative Measurement of Physical Damage, ASTM STP 811, J. Lankford, D.L. Davidson, W.L. Morris, and R.P. Wei, Eds., American Society for Testing and Materials, 1983, pp. 283-312.

[7] Yu, M.T., Topper, T.H., and Au, P., "The Effects of Stress Ratio, Compressive Load and Underload on the Threshold Behavior of a 2024-T351 Aluminum Alloy", Fatigue 84: Proceedings of the Second International Conference on Fatigue and Fatigue Thresholds, C.J. Beevers, Editor, Engineering Materials Advisory Service, Vol 1, 1984, pp. 179-190.

[8] Lafarie-Frenot, M.C., and Gasc, C., "The Influence of Surface Roughness Induced by Fracture Mechanisms on Fatigue Crack Closure Phenomenon in Vacuum", Fatigue 84: Proceedings of the Second International Conference on Fatigue and Fatigue Thresholds, C.J. Beevers, Editor, Engineering Materials Advisory Service, Vol 2, 1984, pp. 687-696.

[9] Irwin, G.R., and McClintock, F. A., "Plasticity Aspects of Fracture Mechanics, ASTM STP 381, 1965, pp. 84-113.

[10] Daiuto, R.A. and Hillberry, B.M., "Effects of Thickness on Fatigue Crack Propagation in 7475-T731 Aluminum Alloy Sheet, NASA contract report 172367, National Aeronautics and Space Administration, Langley Research Center, 1984.

[11] Lindley, T.C., and Richards, C.E., "The Relevance of Crack Closure to Fatigue Crack Propagation", Materials Science and Engineering, 14 (1974), pp. 281-293.

[12] Shaw, W.J.P., and LeMay, I., "Crack Closure During Fatigue Crack Propagation", Fracture Mechanics, ASTM STP 677, C.W. Smith, Ed., American Society for Testing and Materials, 1979, pp. 233-246.

[13] Fleck, N.A., An Investigation of Fatigue Crack Closure, P.H.D. Thesis, Cambridge University, May, 1984.

[14] Vasquez, J.A., Morrone, A., and Gasco, J.C.,"A Comparative Experimental Study on the Fatigue Crack Closure Behavior Under Cyclic Loading for Steels and Aluminum Alloys",
Fracture Mechanics, ASTM STP 677, C.W. Smith, Ed., American Society for Testing and Materials, 1979, pp. 187-197.

[15] Probst, E.P. and Hillberry, B.M., "Fatigue Crack Delay and Arrest Due to Single Peak Overloads", AIAA Paper No. 73-325, 1973.

[16] Himmelein, M.K. and Hillberry, B.M., "Effect of Stress Ratio and overload ratio on fatigue crack delay and arrest behavior Due to Single Peak Overloads", ASTM STP 590, American Society for Testing and Materials, 1976, pp. 321-330.

[17] Alzos, P. W. X., Skat, A.C., Jr., and Hillberry, B.M., "Effect of Single Overload/Underload Cycles on Fatigue Crack Propagation", ASTM STP 595, American Society for Testing and Materials, pp. 41-60.

[18] Crandall. G.M., "Residual Stress Intensity Parameters for Prediction of Delay in Fatigue Crack Propagation", M.S. Thesis, Purdue University, December 1975.

[19] Chehimi, C., et al, "Influence of Multiple Overloads on the Propagation of Fatigue Cracks, Fatigue 84: Proceedings of the Second International Conference on Fatigue and Fatigue Thresholds, C.J. Beevers, Editor, Engineering Materials Advisory Service, Vol 2, 1984, pp. 915-925.

[20] Trebules, V.W., Roberts,R., and Hertzberg, "Effects of Multiple Overloads on Fatigue Crack Propagation in 2024-T3 aluminum alloy, Progress in Flow Growth and Fracture Toughness Testing, ASTM STP 536, American Society for Testing and Materials, 1973, pp. 115-146.

[21] LeMay, I., and Cheung, S.K.P., "Crack Closure Effects for Short Cracks and Variable Amplitude Loading, Fatigue 84: Proceedings of the Second International Conference on Fatigue and Fatigue Thresholds, C.J. Beevers, Editor, Engineering Materials Advisory Service, Vol II, 1984, pp. 677-686.

[22] Topper, T.H., Yu, M.T., "The Effect of Overloads on Threshold and Crack Closure", International Journal of Fatigue, No. 5 (1985), pp. 159-164.

[23] Newman, J.C., Jr., "A Crack Closure Model for Predicting Fatigue Crack Growth Under Aircraft Spectrum Loading", Methods and Models for Predicting Fatigue Crack Growth Under Random Loading, ASTM STP 748, American Society for Testing and Materials, Philadelphia, 1981, pp. 53-84.

[24] Saff, C.R., "Crack Growth Retardation and Acceleration Models", Damage Tolerance of Metallic Structures: Analysis Methods and Applications, ASTM STP 842, J.B. Chang and J.L. Rudd, Eds. American Society for Testing and Materials, 1984, pp. 36-49.

[25] DeKoning, A.U., "A Simple Crack Closure Model for Prediction of Fatigue Crack Grwoth Rates Under Variable Amplitude Loading", NLF MP-80006U, National Aerospace Laboratory NLR, Amsterdam, Netherlands, Jan. 1980.

[26] Marissen, R., Trautmann, K.H., Nowack, H., "The Influence of Compression Loads and of dK/da on the Crack Propagation Under Variable Amplitude Loading", Fracture Mechanics, No. 5, Vol 19, 1984, pp. 863-879.

[27] Microprocessor and Peripheral Handbook, Intel Corporation, Santa Clara, 1984.

[28] Reuping, J.E., "Fatigue Crack Closure Behavior: A Comparative Study", M.S. Thesis, Purdue University, August 1976.

[29] 1981 Annual Book of ASTM Standards, Part 10, Metals-Mechanical, Fracture, and Corrosion Testing; Fatigue: Erosion and Wear; Effect of Temperature, ASTM, Philadelphia, 1981.

[30] Fedderson, C.E., Discussion, ASTM STP 410, 1967, pp. 77-79.

[31] McCabe, G.S., Personal Communication, Professor of Statistics and Head Statistical Consultant, Purdue University, January 13, 1986.

[32] Ray, S., "Three-Dimensional Crack Closure Measurements in Polycarbonate", M.S. Thesis, School of Aeronautics and Astronautics, Purdue University, December 1984.

[33] Hooke, R. and Jeeves, T.A., "Direct Search Solution of Numerical and Statistical Problems," Journal of the Association of Computing Machinery, Volume 8, 1961, pp. 212-229.

[34] Broek, D., Elementary Engineering and Fracture Mechanics , 3rd ed., Martinus Nijhoff, 1982, p.88.

[35] Carman, C.D., "Fatigue Crack Closure Behavior" M.S. Thesis, Purdue University, May 1986.

APPENDICES

Appendix A: Test Program Loading Details

CASE 1 THICKNESS= 0.17

	Rep 1			Rep 2			Rep 3			Rep 4		
Crack Length	0.350 8.890	0.450 11.430	0.583 14.799	0.715 18.169	0.848 21.538	0.981 24.908	1.113 28.277	1.246 31.647	1.379 35.016	1.511 38.386	1.644 41.755	1.777 45.125
K0 (KSI-SQRT.IN)	0.50	0.50	0.50	0.50	0.50	0.50	0.50	0.50	0.50	0.50	0.50	0.50
K1 (KSI-SQRT.IN)	8.00	8.00	8.00	8.00	8.00	8.00	8.00	8.00	8.00	8.00	8.00	8.00
K2 (KSI-SQRT.IN)	4.00	2.00	0.50	4.00	2.00	0.50	4.00	2.00	0.50	4.00	2.00	0.50
K3 (KSI-SQRT.IN)	12.00	12.00	12.00	12.00	12.00	12.00	12.00	12.00	12.00	12.00	12.00	12.00
K4 (KSI-SQRT.IN)	8.00	4.00	0.50	8.00	4.00	0.50	8.00	4.00	0.50	8.00	4.00	0.50
K5 (KSI-SQRT.IN)	16.00	16.00	16.00	16.00	16.00	16.00	16.00	16.00	16.00	16.00	16.00	16.00
K6 (KSI-SQRT.IN)	12.00	6.00	0.50	12.00	6.00	0.50	12.00	6.00	0.50	12.00	6.00	0.50
K7 (KSI-SQRT.IN)	20.00	20.00	20.00	20.00	20.00	20.00	20.00	20.00	20.00	20.00	20.00	20.00
Load 0 (KIPS)	0.470	0.412	0.358	0.319	0.289	0.263	0.242	0.223	0.205	0.189	0.174	0.160
Load 1 (KIPS)	7.520	6.593	5.736	5.110	4.619	4.215	3.868	3.562	3.285	3.029	2.790	2.561
Load 2 (KIPS)	3.760	1.648	0.358	2.555	1.155	0.263	1.934	0.890	0.205	1.515	0.697	0.160
Load 3 (KIPS)	11.280	9.890	8.604	7.665	6.929	6.322	5.801	5.342	4.927	4.544	4.185	3.842
Load 4 (KIPS)	7.520	3.297	0.358	5.110	2.310	0.263	3.868	1.781	0.205	3.029	1.395	0.160
Load 5 (KIPS)	15.040	13.187	11.472	10.220	9.239	8.429	7.735	7.123	6.569	6.059	5.579	5.122
Load 6 (KIPS)	11.280	4.945	0.358	7.665	3.465	0.263	5.801	2.671	0.205	4.544	2.092	0.160
Load 7 (KIPS)	18.800	16.484	14.340	12.776	11.549	10.536	9.669	8.904	8.212	7.573	6.974	6.403
R01	0.06	0.06	0.06	0.06	0.06	0.06	0.06	0.06	0.06	0.06	0.06	0.06
R07	0.03	0.03	0.03	0.03	0.03	0.03	0.03	0.03	0.03	0.03	0.03	0.03
Pl.Stress K7 Pls. Zone (Thousandths)	19.59	19.59	19.59	19.59	19.59	19.59	19.59	19.59	19.59	19.59	19.59	19.59
Pl.Strain K7 Pls. Zone (Thousandths)	6.53	6.53	6.53	6.53	6.53	6.53	6.53	6.53	6.53	6.53	6.53	6.53
Data Rang	0.350 0.450	0.483 0.583	0.615 0.715	0.748 0.848	0.881 0.981	1.013 1.113	1.146 1.246	1.279 1.379	1.411 1.511	1.544 1.644	1.677 1.777	1.809 1.909

CASE II R2=.05 THICKNESS= 0.17

Crack Length	0.300 7.620	0.400 10.160	0.502 12.757	0.605 15.376	0.709 18.018	0.814 20.687	0.921 23.387	1.028 26.120	1.137 28.890	1.256 31.897	1.382 35.109	1.518 38.563	1.665 42.291
K2 (KSI-SQRT.IN)	5.26	5.26	5.26	5.26	5.26	5.26	5.26	15.00	15.00	15.00	15.00	15.00	15.0
K1 (KSI-SQRT.IN)	5.26	6.14	7.02	7.90	8.78	9.65	10.53	15.00	18.00	21.00	24.00	27.00	30.0
Kein (KSI-SQRT.IN)	0.26	0.26	0.26	0.26	0.26	0.26	0.26	0.75	0.75	0.75	0.75	0.75	0.7
Load 2 (KIPS)	5.356	4.615	4.091	3.695	3.378	3.114	2.887	7.658	7.143	6.638	6.145	5.656	5.16
Load 1 (KIPS)	5.356	5.385	5.456	5.544	5.633	5.713	5.778	7.658	8.571	9.293	9.832	10.180	10.32
Load ein (KIPS)	0.268	0.231	0.204	0.185	0.169	0.156	0.144	0.383	0.357	0.332	0.307	0.283	0.25
K2/K1	1.00	0.86	0.75	0.67	0.60	0.55	0.50	1.00	0.83	0.71	0.63	0.56	0.5
e1	0.05	0.04	0.04	0.03	0.03	0.03	0.02	0.05	0.04	0.04	0.03	0.03	0.(
e2	0.05	0.05	0.05	0.05	0.05	0.05	0.05	0.05	0.05	0.05	0.05	0.05	0.(
Fi.Stress Fis. Zone r1/r2 (Thousandths)	1.36 1.36	1.85 1.36	2.41 1.36	3.06 1.36	3.77 1.36	4.57 1.36	5.43 1.36	11.02 11.02	15.87 11.02	21.60 11.02	28.22 11.02	35.71 11.02	44. 11.(
Fi.Strain Fis. Zone r1/r2 (Thousandths)	0.45 0.45	0.62 0.45	0.80 0.45	1.02 0.45	1.26 0.45	1.52 0.45	1.81 0.45	3.67 3.67	5.29 3.67	7.20 3.67	9.41 3.67	11.90 3.67	14. 3.
Data Rang	0.300 0.400	0.402 0.502	0.505 0.605	0.609 0.709	0.714 0.814	0.821 0.921	0.928 1.028	1.037 1.137	1.156 1.256	1.282 1.382	1.418 1.518	1.565 1.665	1.7 1.8

CASE II R2=.05 THICKNESS= 0.17

Crack Length	0.300 7.620	0.400 10.160	0.509 12.930	0.618 15.700	0.727 18.470	0.836 21.240	0.945 24.010	1.266 32.149
K2 - (KSI-SQRT.IN)	10.53	10.53	10.53	10.53	10.53	30.00	30.00	30.00
K1 (KSI-SQRT.IN)	10.53	9.21	7.90	6.58	5.26	30.00	22.50	15.00
Kain (KSI-SQRT.IN)	0.53	0.53	0.53	0.53	0.53	1.50	1.50	1.50
Load 2 (KIPS)	10.717	9.234	8.126	7.307	6.663	17.471	16.185	13.195
Load 1 (KIPS)	10.717	8.078	6.092	4.564	3.328	17.471	12.139	6.597
Load ain (KIPS)	0.536	0.462	0.406	0.365	0.333	0.874	0.809	0.660
K2/K1	1.00	1.14	1.33	1.60	2.00	1.00	1.33	2.00
K1/K2	1.00	0.87	0.75	0.62	0.50	1.00	0.75	0.50
R1	0.05	0.06	0.07	0.08	0.10	0.05	0.07	0.10
R2	0.05	0.05	0.05	0.05	0.05	0.05	0.05	0.05
Pl.Stress Pls. Zone r1/r2 (Thousandths)	5.43 5.43	4.16 5.43	3.05 5.43	2.12 5.43	1.36 5.43	44.09 44.09	24.80 44.09	11.02 44.09
Pl.Strain Pls. Zone r1/r2 (Thousandths)	1.81 1.81	1.39 1.81	1.02 1.81	0.71 1.81	0.45 1.81	14.70 14.70	8.27 14.70	3.67 14.70
Data Rang	0.300 0.400	0.409 0.509	0.518 0.618	0.627 0.727	0.736 0.836	0.845 0.945	1.166 1.266	1.486 1.586

CASE IX R2=0.7 THICKNESS= 0.08

Crack Length	0.300 7.620	0.461 11.719	0.643 16.329	0.846 21.482	1.071 27.207	1.320 33.534	1.594 40.493
K2 (KSI-SQRT.IN)	16.50	16.50	16.50	16.50	16.50	16.50	16.50
K1 (KSI-SQRT.IN)	18.15	19.25	20.35	21.45	22.55	23.65	24.75
Kein (KSI-SQRT.IN)	11.55	11.55	11.55	11.55	11.55	11.55	11.55
Load 2 (KIPS)	7.902	6.315	5.271	4.491	3.856	3.303	2.793
Load 1 (KIPS)	8.693	7.368	6.501	5.638	5.270	4.735	4.190
Load min (KIPS)	5.532	4.421	3.690	3.144	2.699	2.312	1.955
Bol	1.10	1.17	1.23	1.30	1.37	1.43	1.50
P1	0.64	0.60	0.57	0.54	0.51	0.49	0.47
P2	0.70	0.70	0.70	0.70	0.70	0.70	0.70
Pl.Stress	16.14	18.15	20.29	22.54	24.91	27.40	30.01
Pls. Zone r1/r2 (Thousandths)	13.34	13.34	13.34	13.34	13.34	13.34	13.34
Pl.Strain	5.38	6.05	6.76	7.51	8.30	9.13	10.00
Pls. Zone r1/r2 (Thousandths)	4.45	4.45	4.45	4.45	4.45	4.45	4.45
Data Rang	0.300 0.461	0.461 0.643	0.643 0.846	0.846 1.071	1.071 1.320	1.320 1.594	1.594 1.894

CASE IV R2=0.7 THICKNESS= 0.248

Crack Length	1.000 25.400	1.054 26.766	1.114 28.303	1.182 30.021	1.257 31.929	1.340 34.038	1.431 36.358
K2 (KSI-SQRT.IN)	16.50	16.50	16.50	16.50	16.50	16.50	16.50
K1 (KSI-SQRT.IN)	18.15	19.25	20.35	21.45	22.55	23.65	24.75
Kain (KSI-SQRT.IN)	11.55	11.55	11.55	11.55	11.55	11.55	11.55
Load 2 (KIPS)	12.519	12.088	11.630	11.148	10.643	10.117	9.571
Load 1 (KIPS)	13.771	14.102	14.343	14.492	14.546	14.502	14.356
Load ain (KIPS)	8.763	8.461	8.141	7.803	7.450	7.082	6.699
Beta	1.10	1.17	1.23	1.30	1.37	1.43	1.50
P1	0.64	0.60	0.57	0.54	0.51	0.49	0.47
P2	0.70	0.70	0.70	0.70	0.70	0.70	0.70
Pl.Stress Pls. Zone r1/r2 (Thousandths)	16.14 13.34	18.15 13.34	20.29 13.34	22.54 13.34	24.91 13.34	27.40 13.34	30.01 13.34
Pl.Strain Pls. Zone r1/r2 (Thousandths)	5.38 4.45	6.05 4.45	6.76 4.45	7.51 4.45	8.30 4.45	9.13 4.45	10.00 4.45
Data Rang	1.000 1.054	1.054 1.114	1.114 1.182	1.182 1.257	1.257 1.340	1.340 1.431	1.431 1.531

Appendix B: Multi-step Rate Calculations

CASE 1 THICKNESS= 0.17

K0 (KSI-SQRT.IN)	0.50	0.50	0.50
K1 (KSI-SQRT.IN)	8.00	8.00	8.00
K2 (KSI-SQRT.IN)	4.00	2.00	0.50
K3 (KSI-SQRT.IN)	12.00	12.00	12.00
K4 (KSI-SQRT.IN)	8.00	4.00	0.50
K5 (KSI-SQRT.IN)	16.00	16.00	16.00
K6 (KSI-SQRT.IN)	12.00	6.00	0.50
K7 (KSI-SQRT.IN)	20.00	20.00	20.00

From Daiuto R=0.75, t=0.17" Constant Amplitude data

Paris Exp	4.4929	3.205	3.205
C-act	2.5E-09	1.6E-08	1.6E-08

	Block Identification A	B	C
DA/DN01	2.1E-05	1.8E-12	2.5E-09
DA/DN12	1.2E-06	1.8E-12	2.5E-09
DA/DN23	7.8E-07	1.6E-06	2.8E-06
DA/DN34	7.8E-07	1.6E-06	2.8E-06
DA/DN45	2.2E-05	1.3E-05	1.8E-05
DA/DN56	1.2E-06	1.3E-05	1.8E-05
DA/DN67	2.8E-05	4.8E-05	5.9E-05
Kop Rate	7.6E-06	1.1E-05	1.4E-05
Kop avg.	8.4	7.8	7.0
Exp. Rate	6.5E-06	9.5E-06	1.2E-05

	Block Identification A	B	C
DKeff01	0.0	0.2	1.0
DKeff12	0.0	0.2	1.0
DKeff23	3.6	4.2	5.0
DKeff34	3.6	4.2	5.0
DKeff45	7.6	8.2	9.0
DKeff56	4.0	8.2	9.0
DKeff67	8.0	12.2	13.0

Appendix C: Bi-harmonic Rate Calculations

CASE 11 K2=.05 THICKNESS=. 0.17 Ascending Kbmax

K2 (KSI-SQRT.IN)	5.26	5.26	5.26	5.26	5.26	5.26	5.26	15.00	15.00	15.00	15.00	15.00
K1 (KSI-SQRT.IN)	5.26	6.14	7.02	7.90	8.78	9.65	10.53	15.00	18.00	21.00	24.00	27.00
Kmin (KSI-SQRT.IN)	0.26	0.26	0.26	0.26	0.26	0.26	0.26	0.75	0.75	0.75	0.75	0.75
K2/K1	1.00	0.86	0.75	0.67	0.60	0.55	0.50	1.00	0.83	0.71	0.63	0.56
K1/K2	1.00	1.17	1.33	1.50	1.67	1.83	2.00	1.00	1.20	1.40	1.60	1.80
From Daiuto Constant Amplitude Crack Growth Tests: R=0.75, t=0.17												
m-eff	4.49	4.49	4.49	4.49	4.49	4.49	4.49	3.205	3.205	3.205	3.205	3.205
C-eff	2.5E-09	2.5E-09	2.5E-09	2.5E-09	2.5E-09	2.5E-09	2.5E-09	1.6E-08	1.6E-08	1.6E-08	1.6E-08	1.6E-08
Observed Kop/Kmax												
T252C	0.48	0.51	0.38	0.42	0.42	0.45	0.36	0.39	0.32	0.38	0.34	0.39
T271C	0.50	0.54	0.46	0.50	0.59	0.51	0.37	0.43	0.40	0.35	0.38	0.42
Observed Kop												
T252C	2.52	3.13	2.67	3.32	3.69	4.34	3.79	5.85	5.76	7.98	8.16	10.53
T271C	2.63	3.32	3.23	3.95	5.18	4.92	3.90	6.45	7.20	7.35	9.12	11.34
Calculated DKeff												
T252C1	2.74	3.01	4.35	4.58	5.09	5.31	6.74	9.15	12.24	13.02	15.84	16.47
T252C2	2.74	2.13	2.59	1.94	1.57	0.92	1.47	9.15	9.24	7.02	6.84	4.47
T271C1	2.63	2.82	3.79	3.95	3.60	4.73	6.63	8.55	10.80	13.65	14.88	15.66
T271C2	2.63	1.94	2.03	1.31	0.08	0.34	1.36	8.55	7.80	7.65	5.88	3.66
Calculated Growth Rate Using Closure Based Growth Rate Relation												
T252C	2.26E-07	2.10E-07	9.98E-07	1.17E-06	1.85E-06	2.22E-06	6.48E-06	1.92E-05	3.42E-05	3.38E-05	5.94E-05	6.40E-05
T271C	1.89E-07	1.55E-07	5.19E-07	5.92E-07	3.88E-07	1.32E-06	6.04E-06	1.54E-05	2.20E-05	3.99E-05	4.79E-05	5.41E-05
Mean	2.08E-07	1.82E-07	7.58E-07	8.81E-07	1.12E-06	1.77E-06	6.26E-06	1.73E-05	2.81E-05	3.69E-05	5.36E-05	5.91E-05

CASE II R2=.05 THICKNESS=. 0.17 Constant Kbmax

K2 (KSI-SQRT.IN)	10.53	10.53	10.53	10.53	10.53	30.00	30.00	30.00
K1 (KSI-SQRT.IN)	10.53	9.21	7.90	6.58	5.26	30.00	22.50	15.00
Kmin (KSI-SQRT.IN)	0.53	0.53	0.53	0.53	0.53	1.50	1.50	1.50
K2/K1	1.00	1.14	1.33	1.60	2.00	1.00	1.33	2.00
K1/K2	1.00	0.87	0.75	0.62	0.50	1.00	0.75	0.50

From Daiuto Constant Amplitude Crack Growth Tests: R=0.75, t=0.17

m-eff	3.205	3.205	3.205	3.205	3.205	3.205	3.205	3.205
C-eff	1.6E-08	1.6E-08	1.6E-08	1.6E-08	1.6E-08	1.6E-08	1.6E-08	1.6E-08
Observed Kop/Kmax								
T264C	0.34	0.36	0.33	0.37	0.33	0.41	0.38	0.42
T231C	0.47	0.44	0.40	0.43	0.40	0.58	0.49	0.33
Observed Kop								
T264C	3.58	3.79	3.47	3.90	3.47	12.30	11.40	12.60
T231C	4.95	4.63	4.21	4.53	4.21	17.40	14.70	9.90
Calculated DKeff								
T264C1	6.95	5.42	4.42	2.68	1.79	17.70	11.10	2.40
T264C2	6.95	6.74	7.06	6.63	7.06	17.70	18.60	17.40
T231C1	5.58	4.58	3.68	2.05	1.05	12.60	7.80	5.10
T231C2	5.58	5.90	6.32	6.00	6.32	12.60	15.30	20.10

Calculated Growth Rate Using Closure Based Growth Rate Relation

T264C	7.94E-06	5.39E-06	5.10E-06	3.61E-06	4.22E-06	1.59E-04	1.11E-04	7.53E-05
T231C	3.93E-06	3.39E-06	3.44E-06	2.56E-06	2.93E-06	5.34E-05	5.55E-05	1.21E-04
Mean	5.93E-06	4.39E-06	4.27E-06	3.08E-06	3.57E-06	1.06E-04	8.32E-05	9.81E-05

Appendix D: High Stress Ratio Post Overload Rate Data

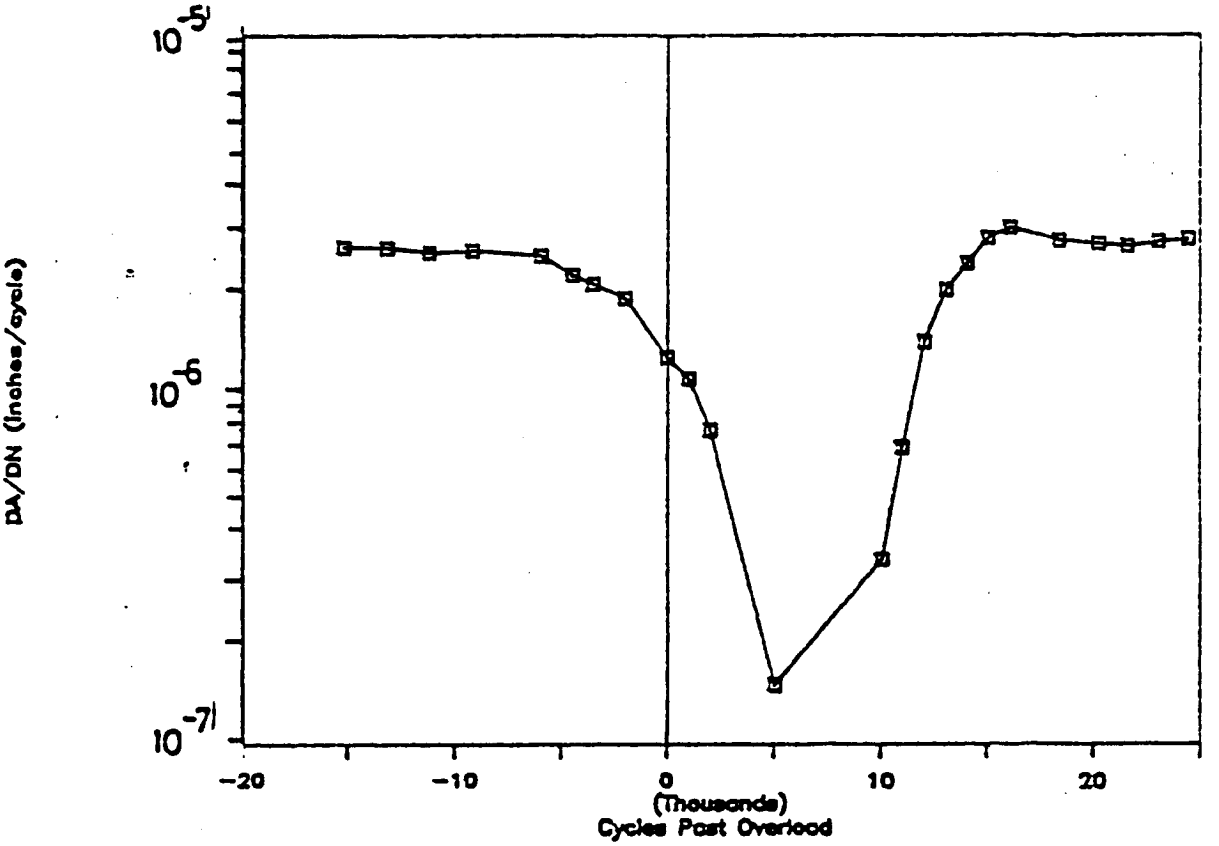

Figure D1. FCP rate versus cycles past overload for plane strain, $Q_{o1} = 1.23$.

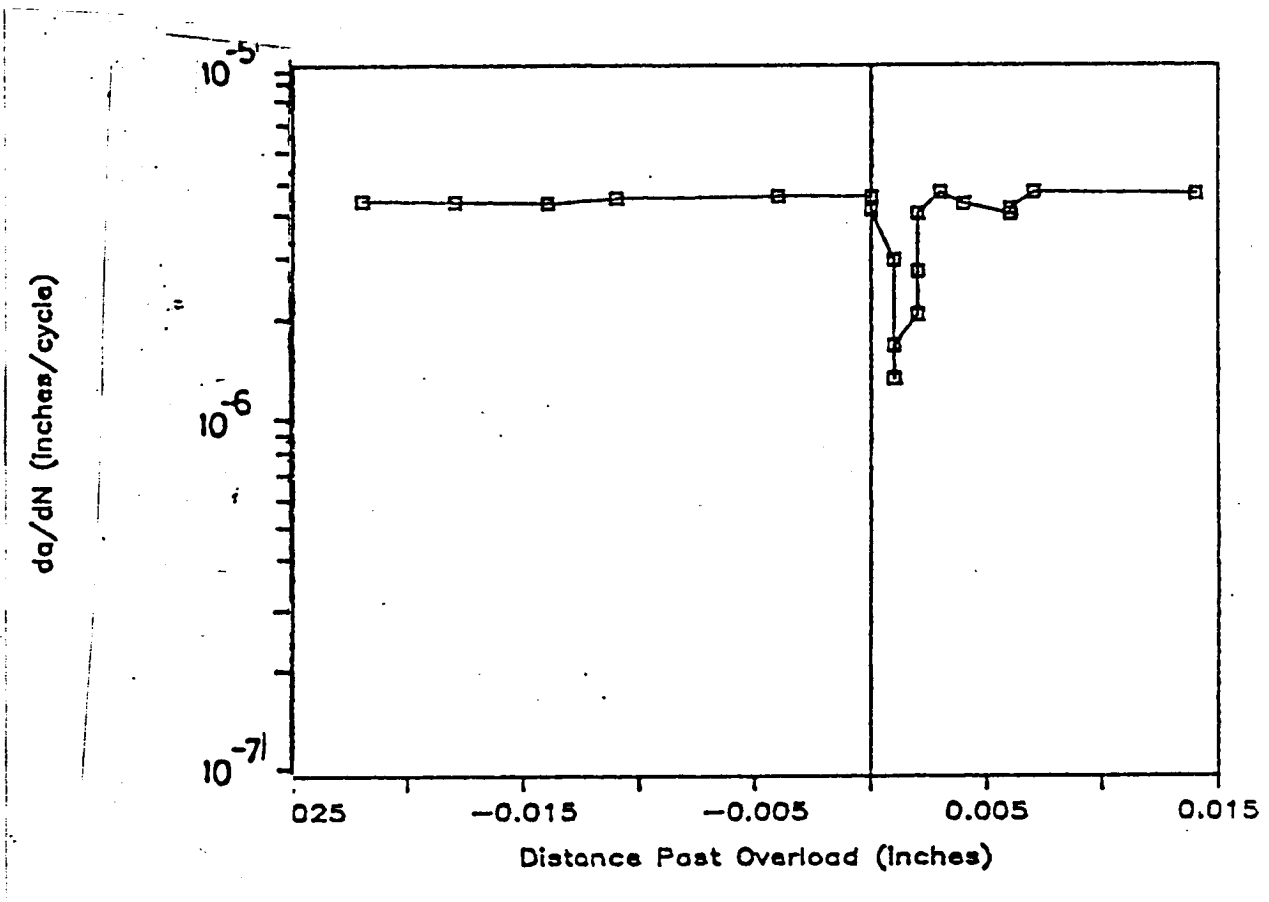

Figure D2. FCP rate versus distance past overload for plane strain, Q_{ol} = 1.23.

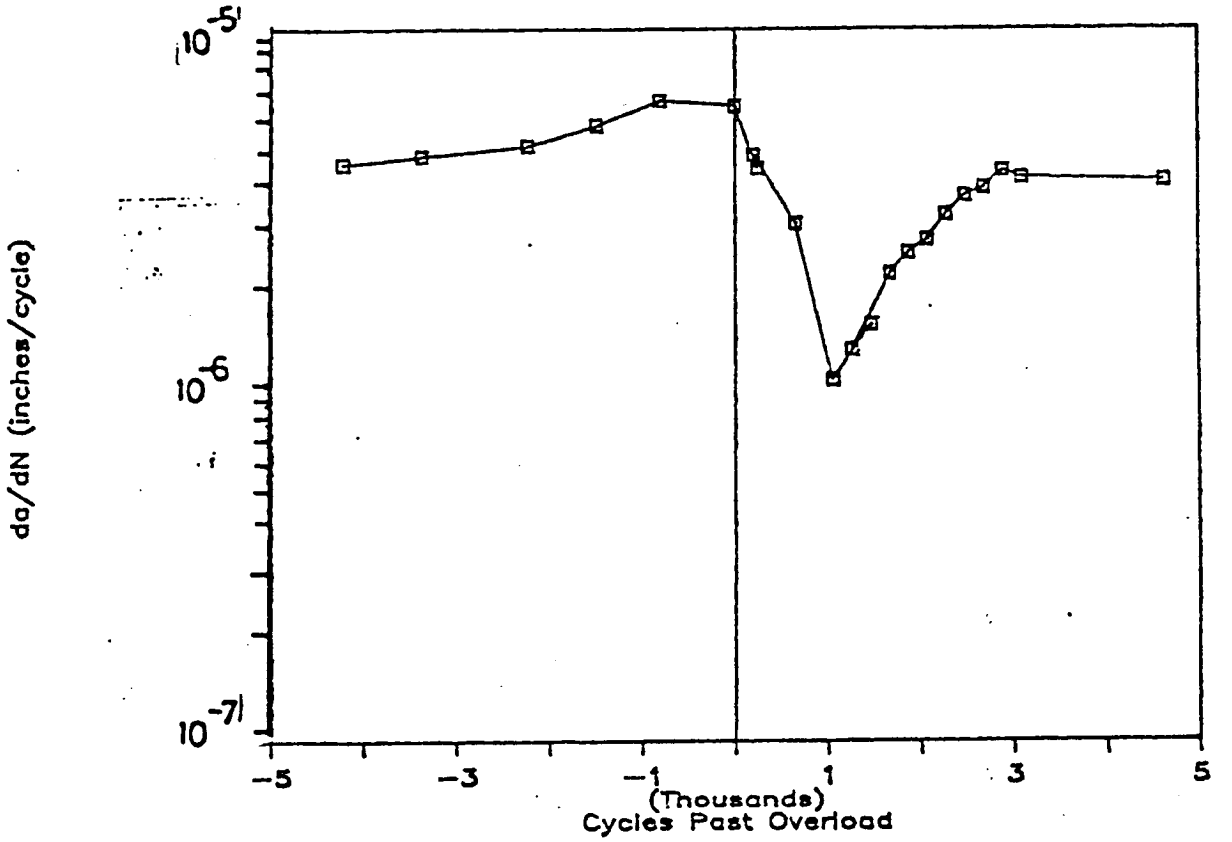

Figure D3. FCP rate versus cycles past overload for plane strain, $Q_{ol} = 1.30$.

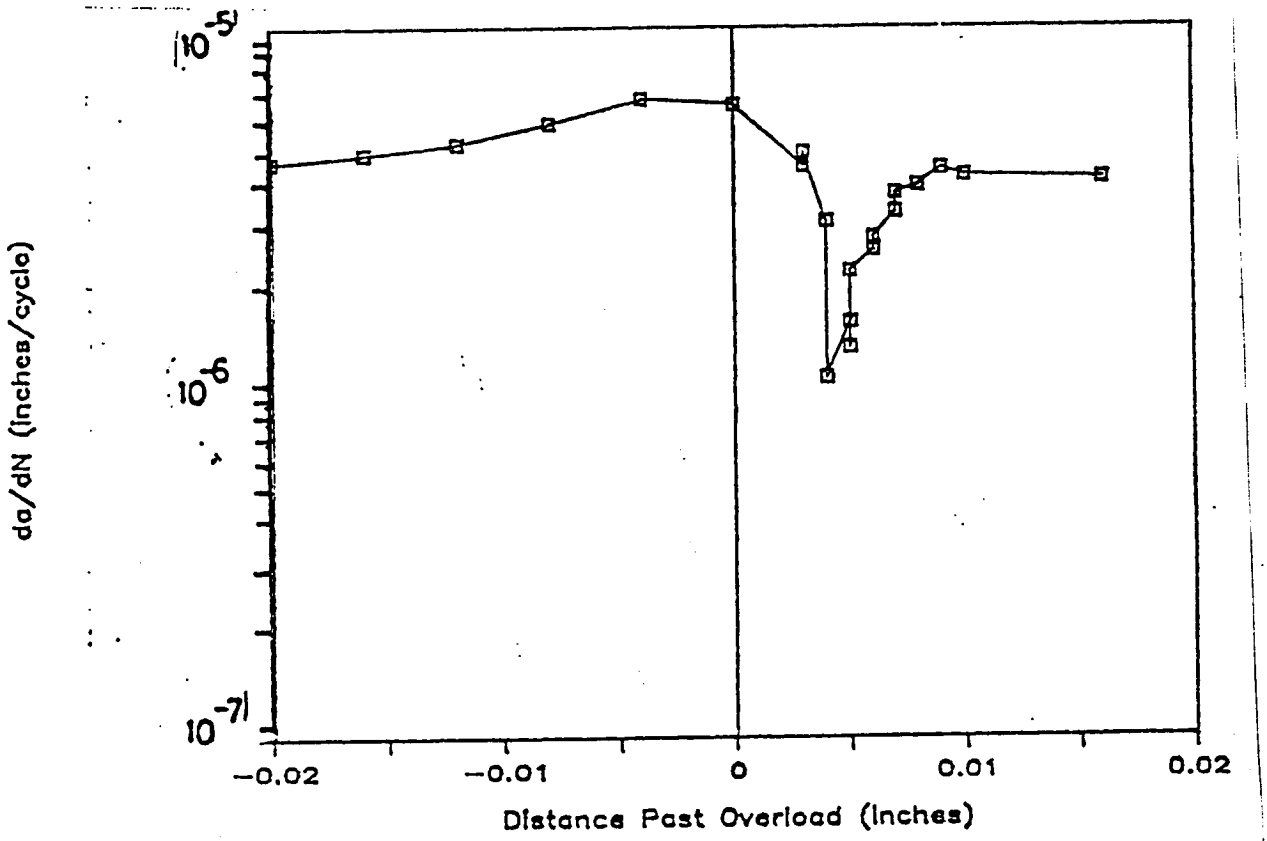

Figure D4. FCP rate versus distance past overload for plane strain, Q_{o1} = 1.30.

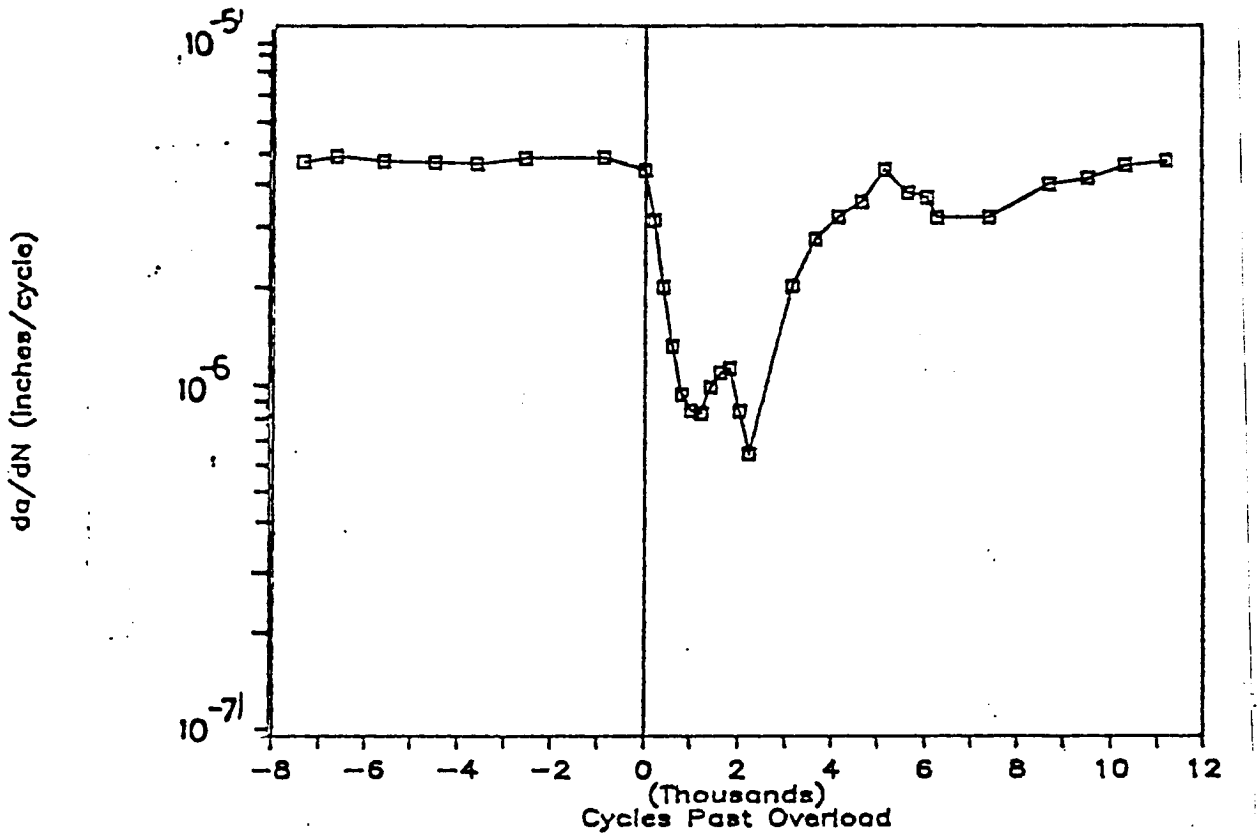

Figure D5. FCP rate versus cycles past overload for plane strain, $Q_{ol} = 1.37$.

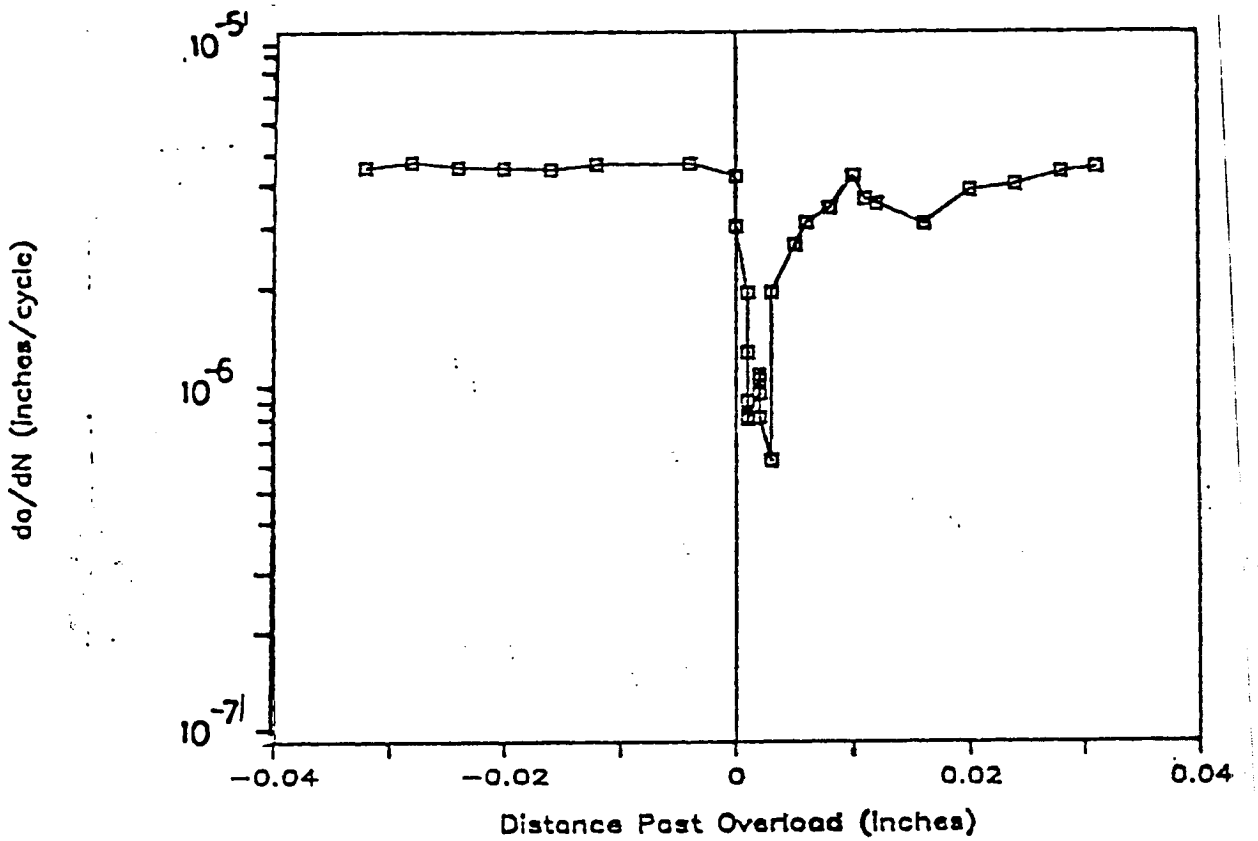

Figure D6. FCP rate versus distance past overload for plane strain, Q_{ol} = 1.37.

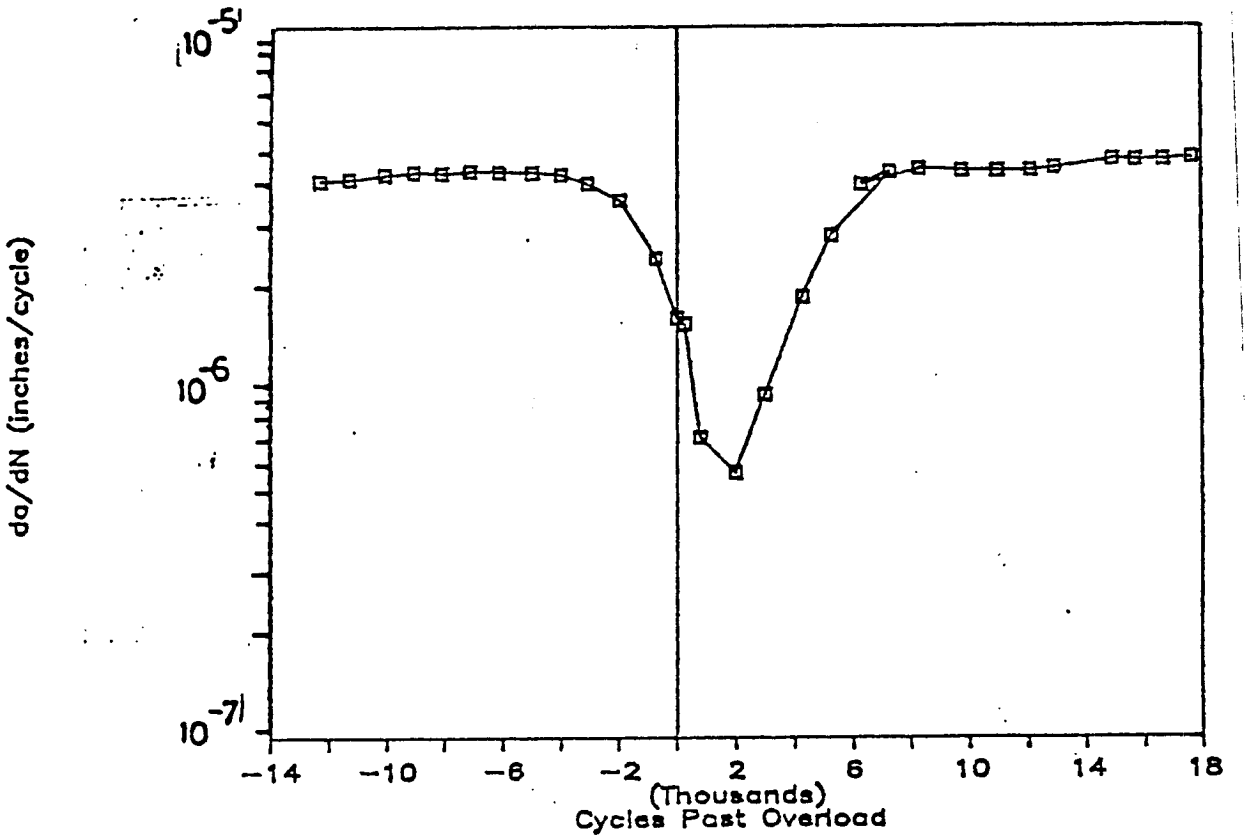

Figure D7. FCP rate versus cycles past overload for plane strain, Q_{ol} = 1.43.

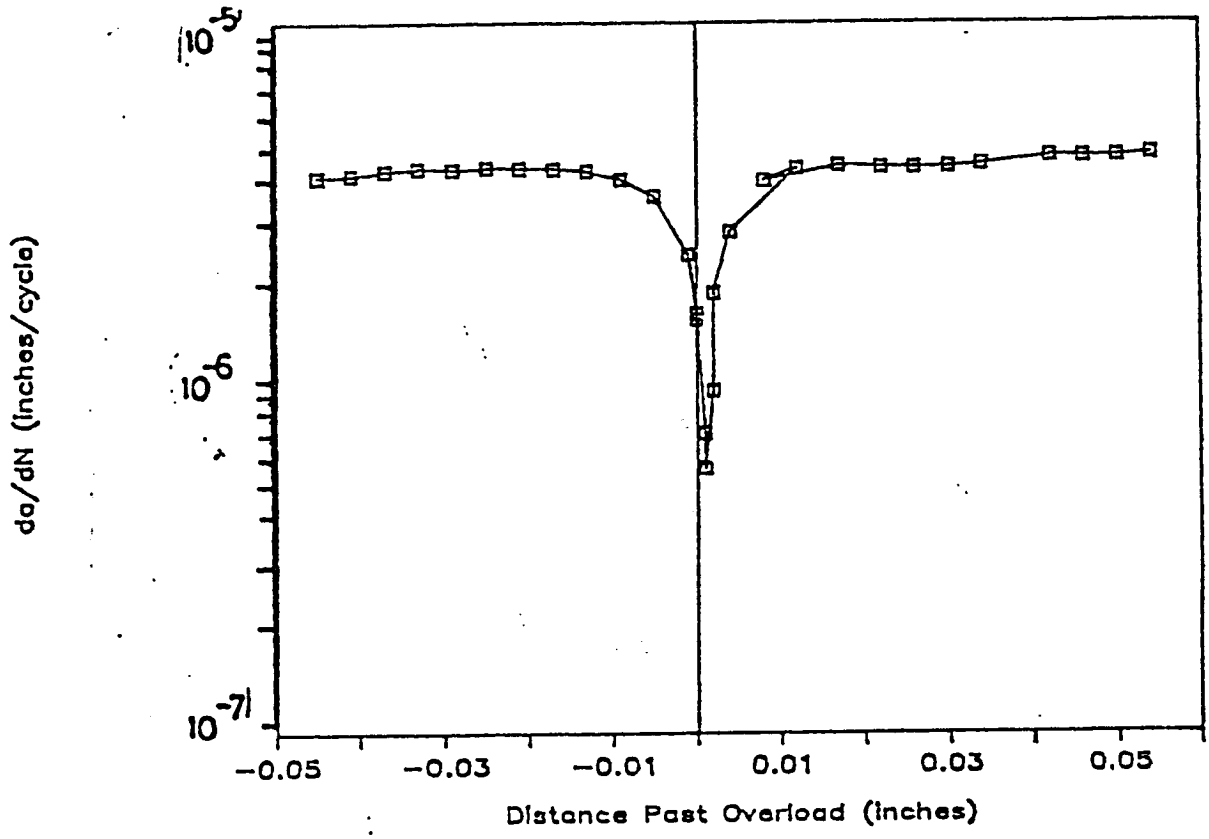

Figure D8. FCP rate versus distance past overload for plane strain, Q_{ol} = 1.43.

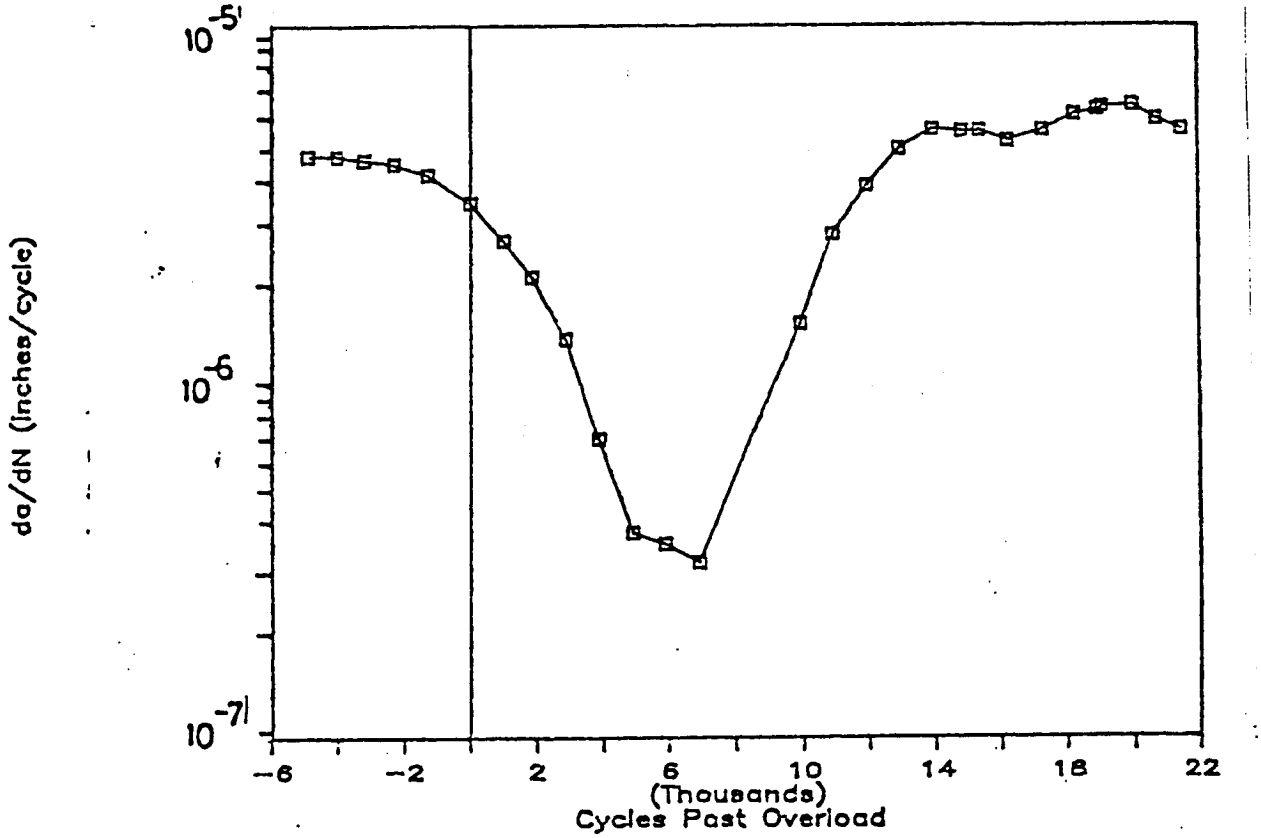

Figure D9. FCP rate versus cycles past overload for plane strain, $Q_{o1} = 1.50$.

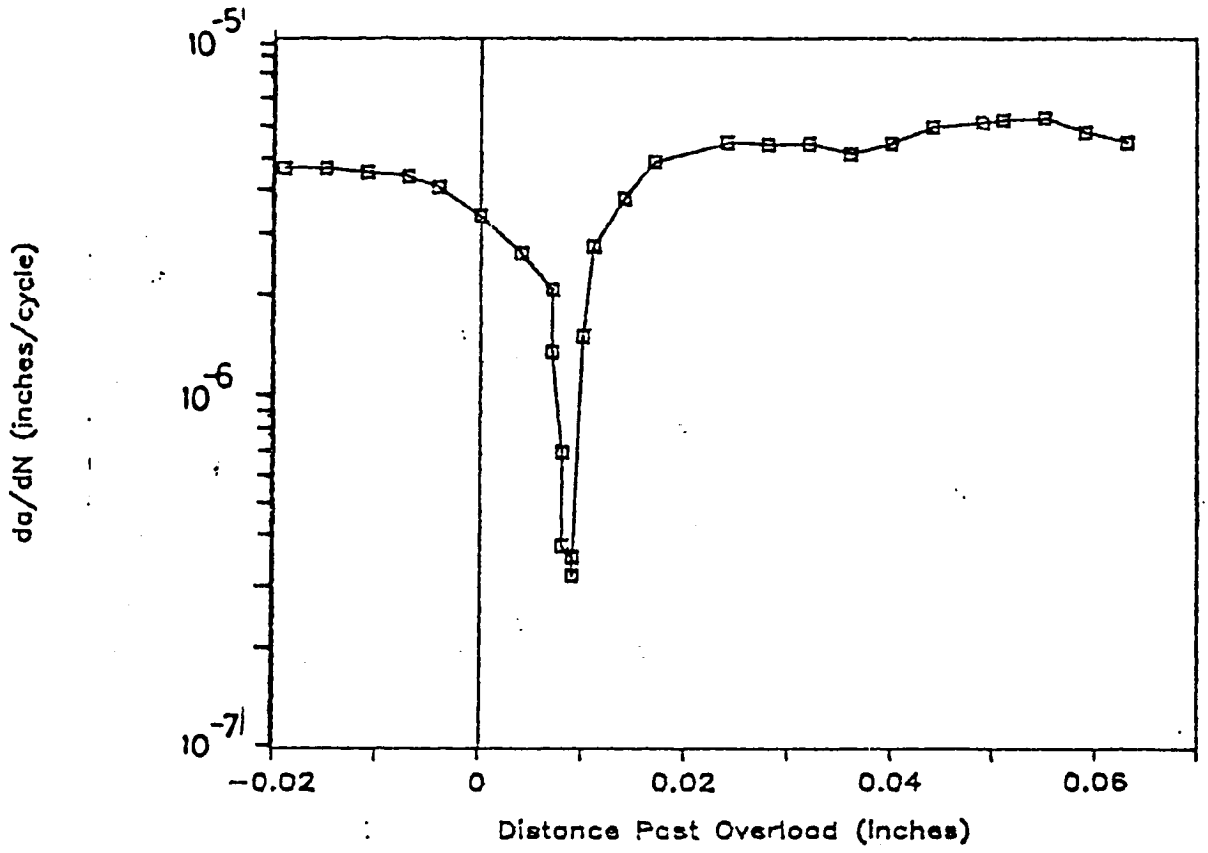

Figure D10. FCP rate versus distance past overload for plane strain, Q_{ol} = 1.50.

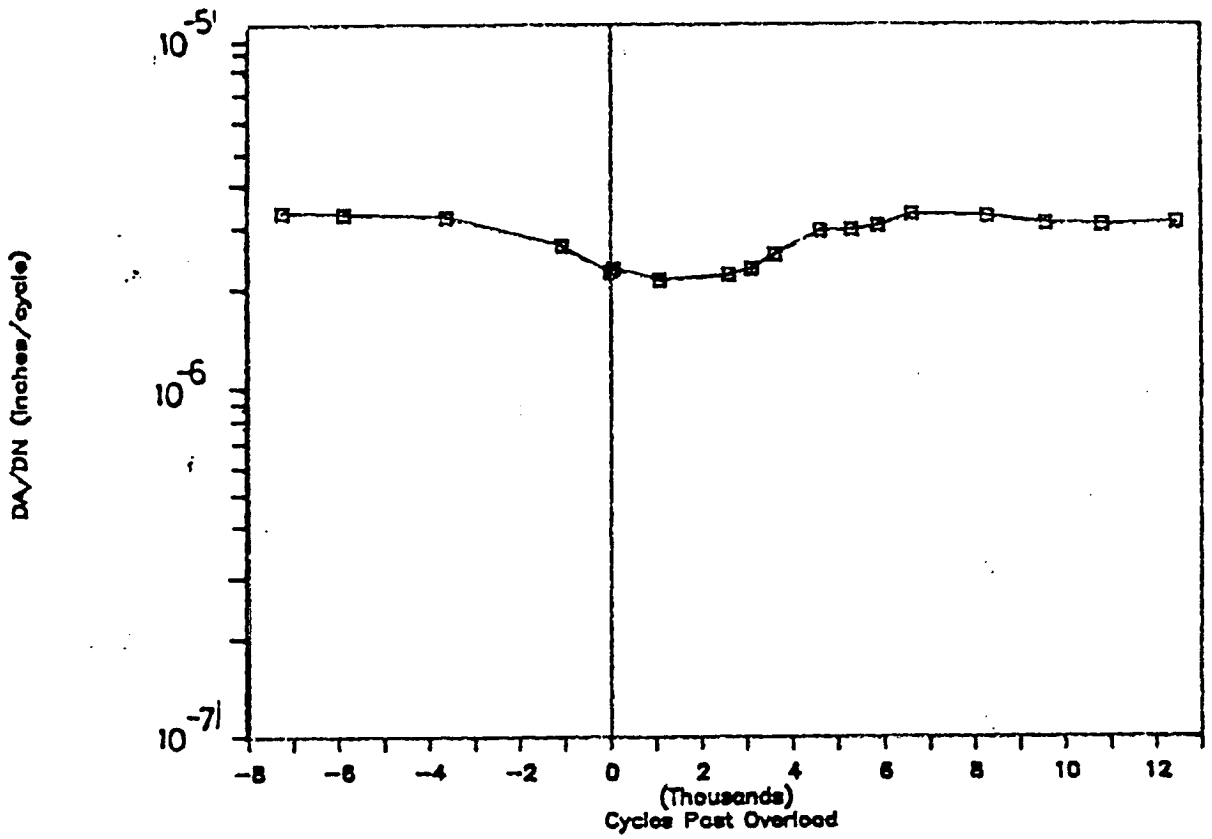

Figure D11. FCP rate versus cycles past overload for mixed mode, Q_{ol} = 1.23.

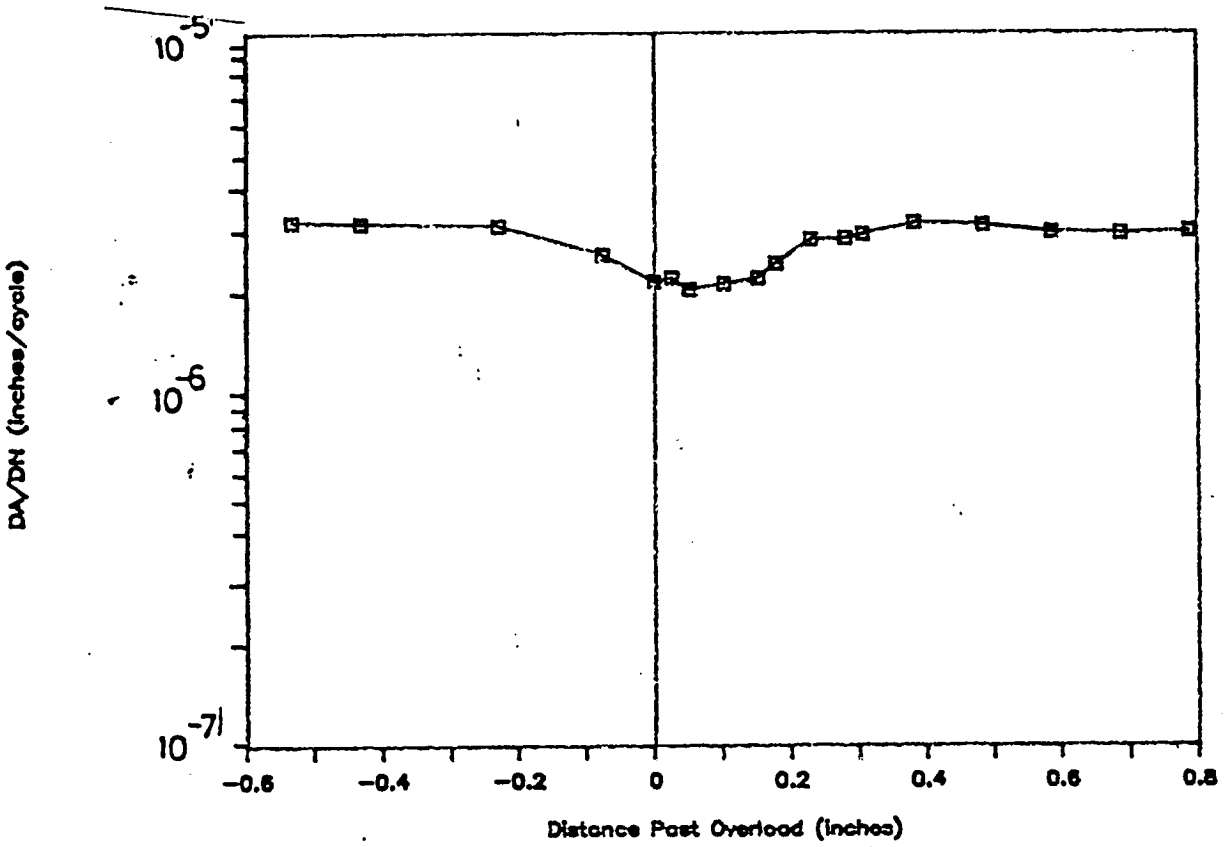

Figure D12. FCP rate versus distance past overload for mixed mode, Q_{ol} = 1.23.

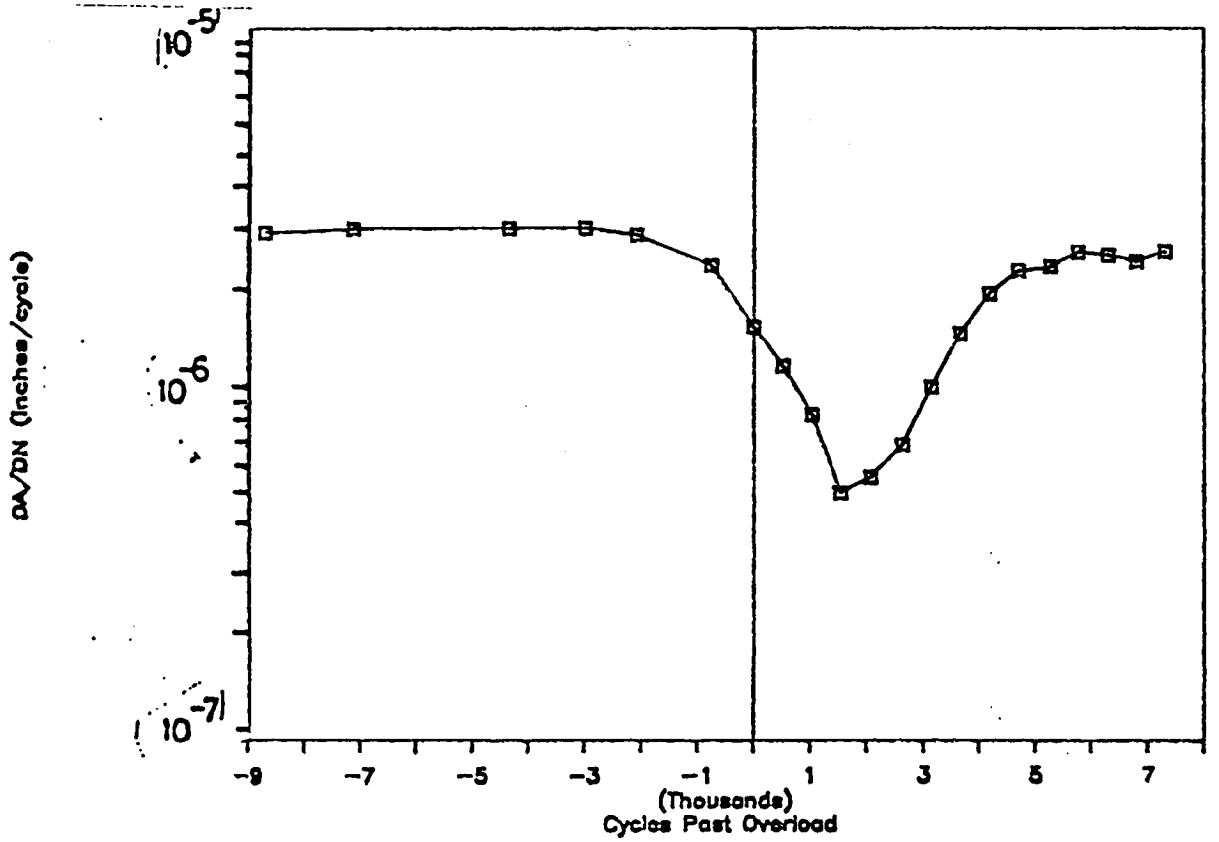

Figure D13. FCP rate versus cycles past overload for mixed mode, Q_{ol} = 1.30.

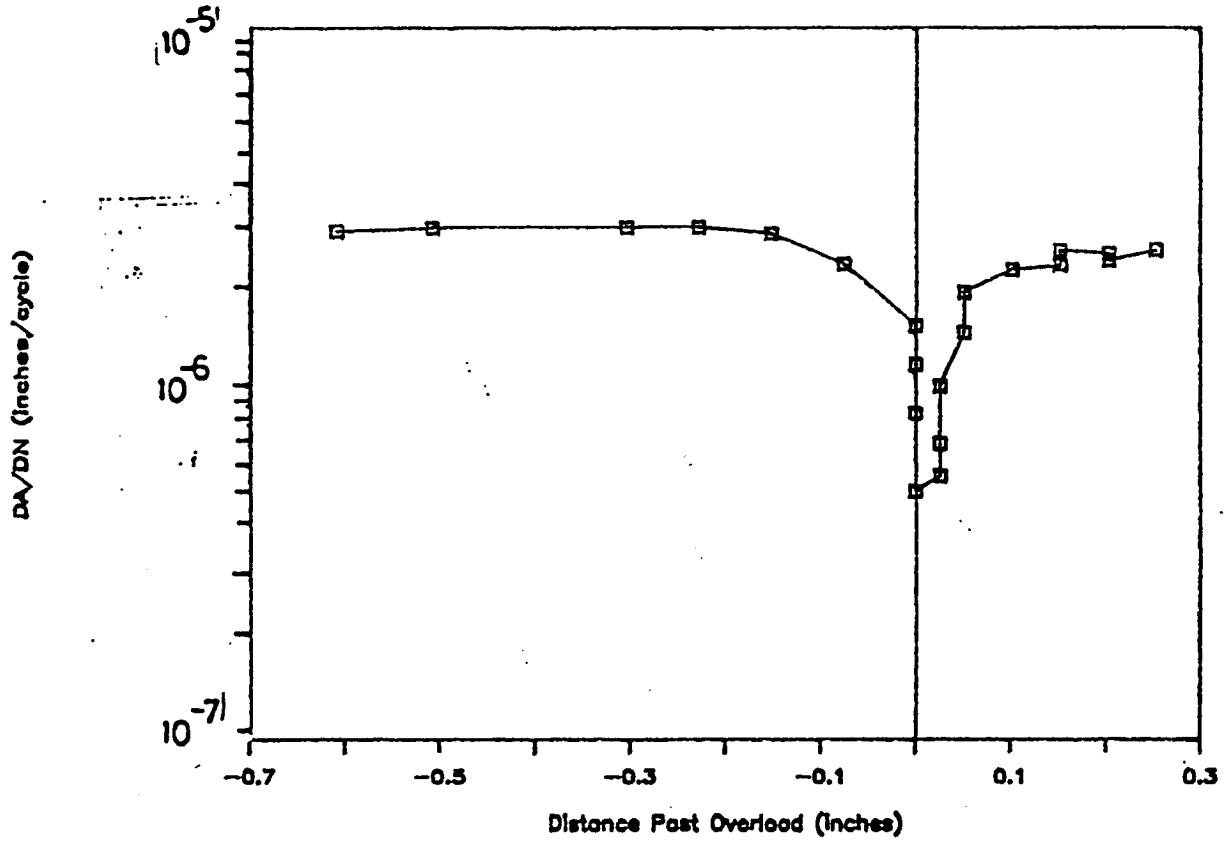

Figure D14. FCP rate versus distance past overload for mixed mode, Q_{ol} = 1.30.

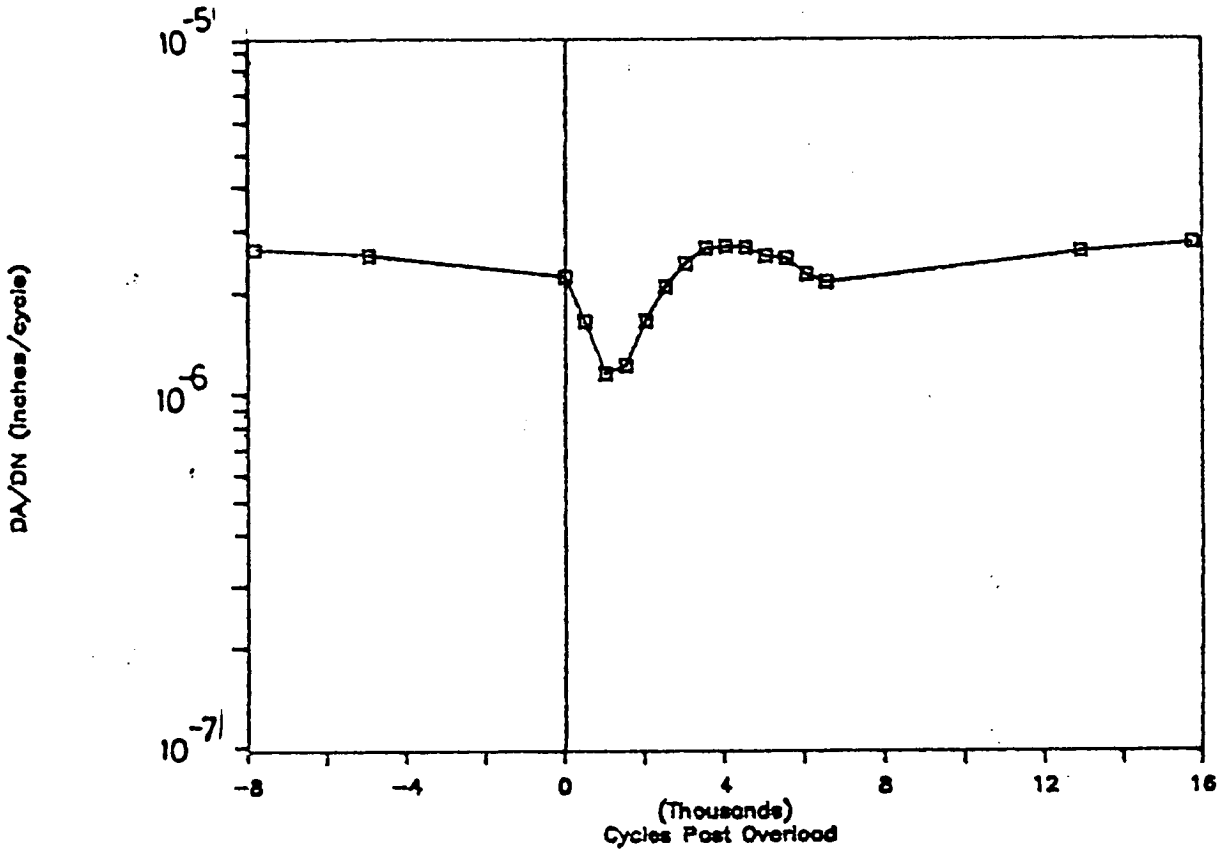

Figure D15. FCP rate versus cycles past overload for mixed mode, Q_{ol} = 1.37.

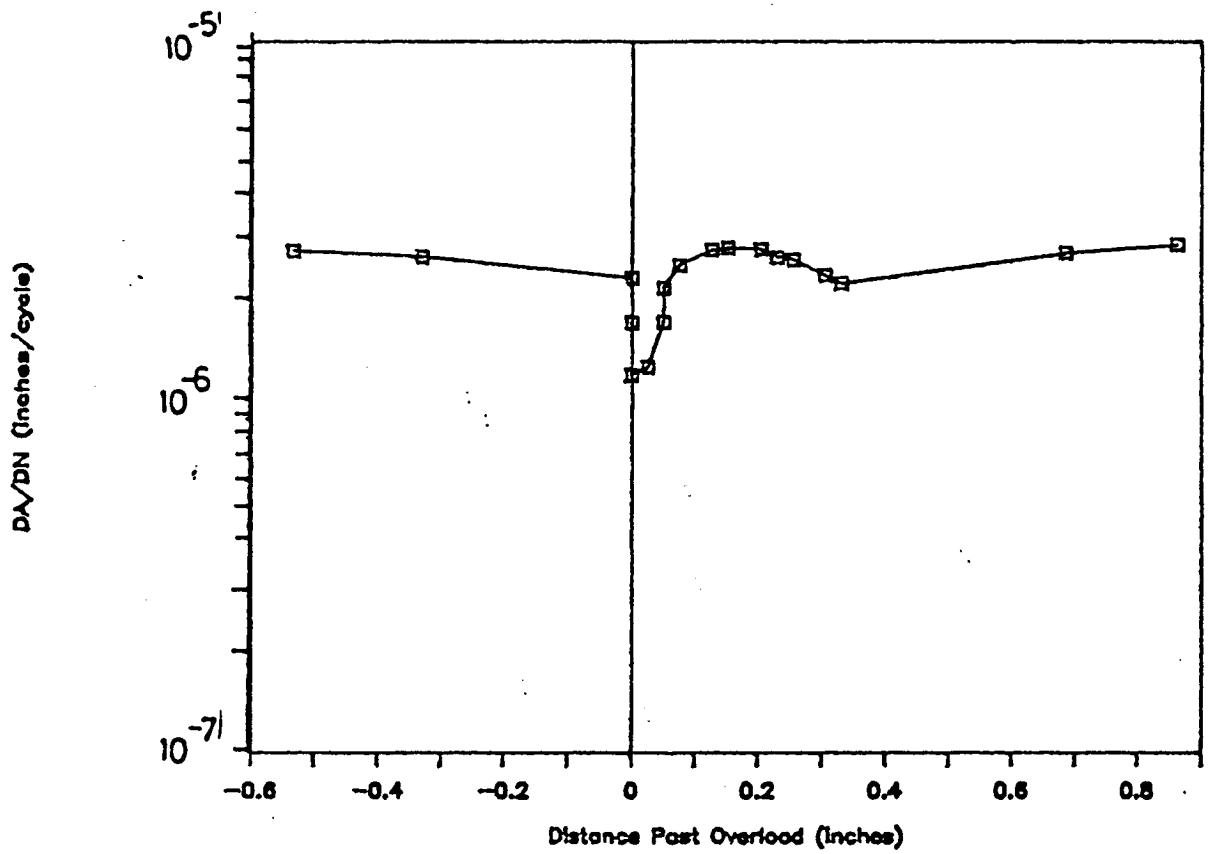

Figure D16. FCP rate versus distance past overload for mixed mode, $Q_{ol} = 1.37$.

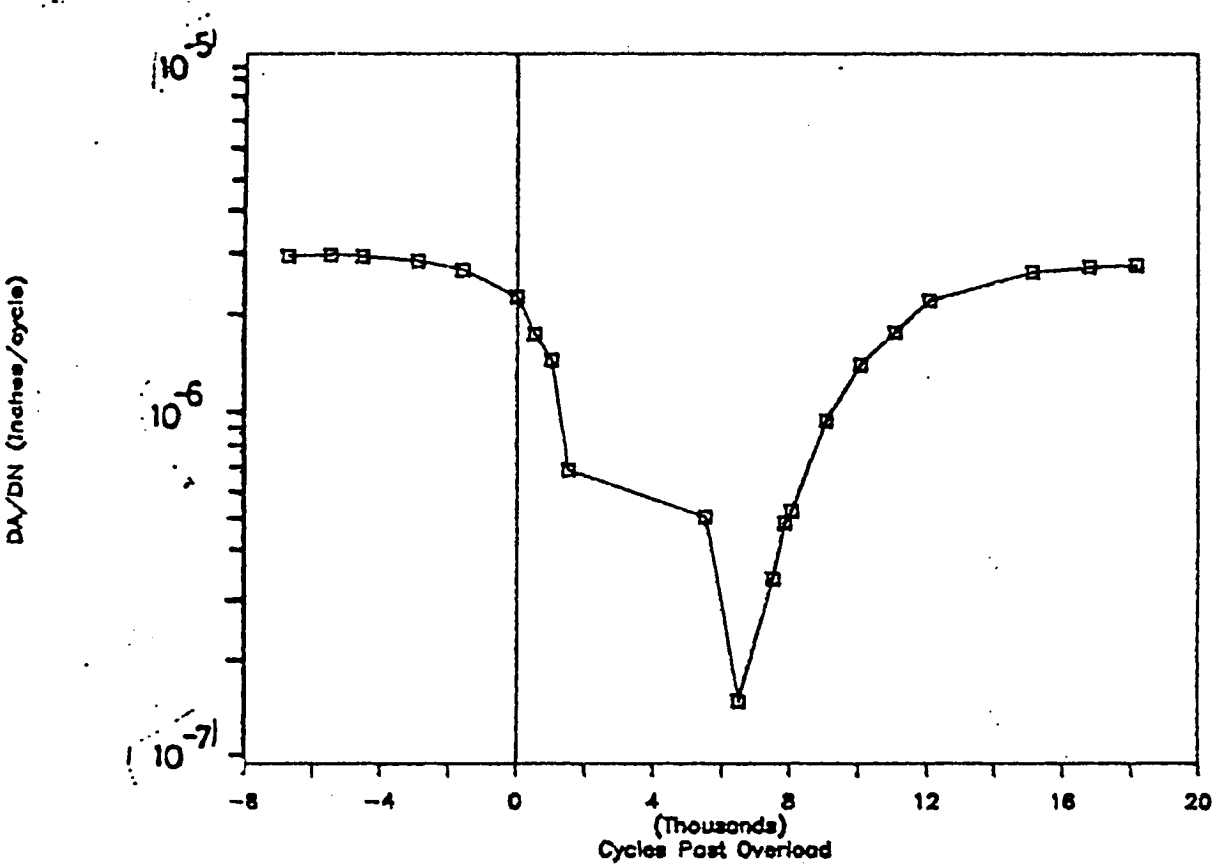

Figure D17. FCP rate versus cycles past overload for mixed mode, Q_{ol} = 1.43.

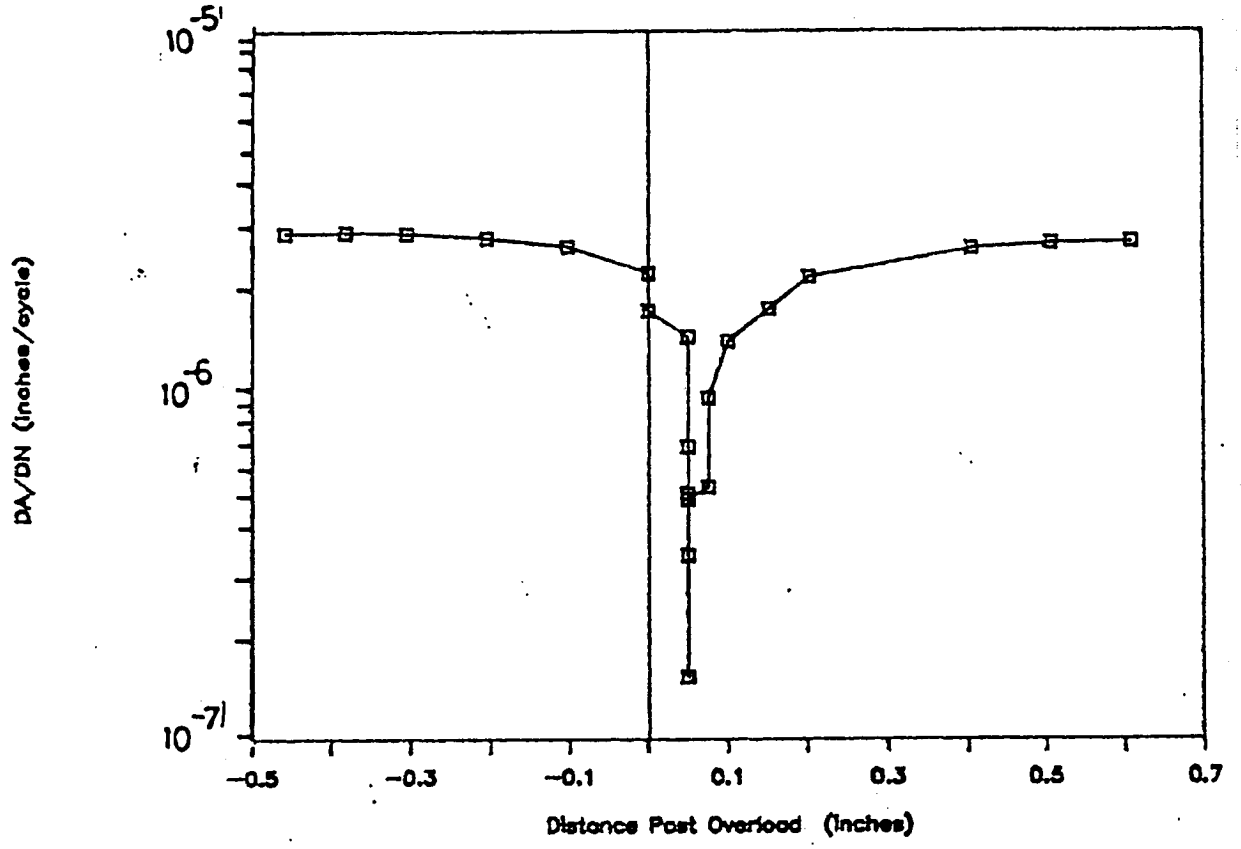

Figure D18. FCP rate versus distance past overload for mixed mode, Q_{o1} = 1.43.

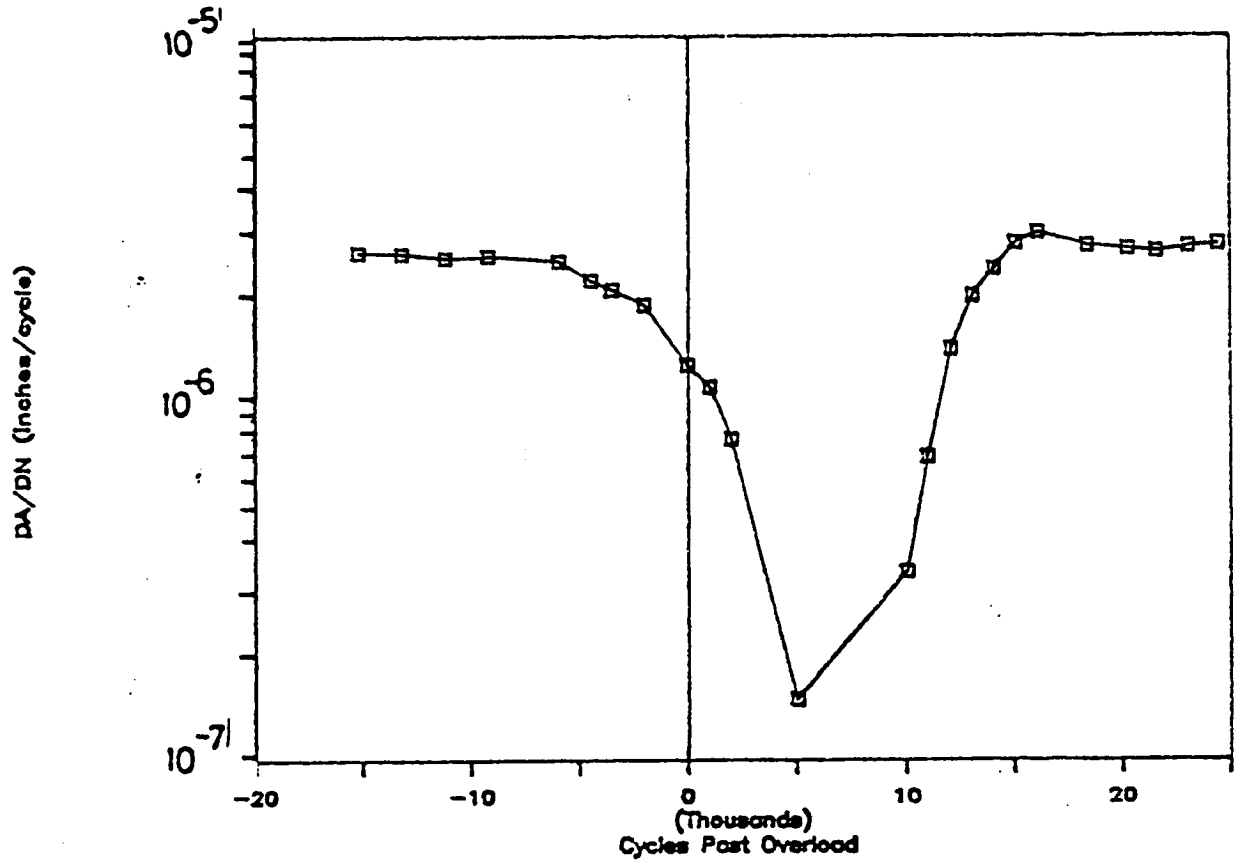

Figure D19. FCP rate versus cycles past overload for mixed mode, Q_{ol} = 1.50.

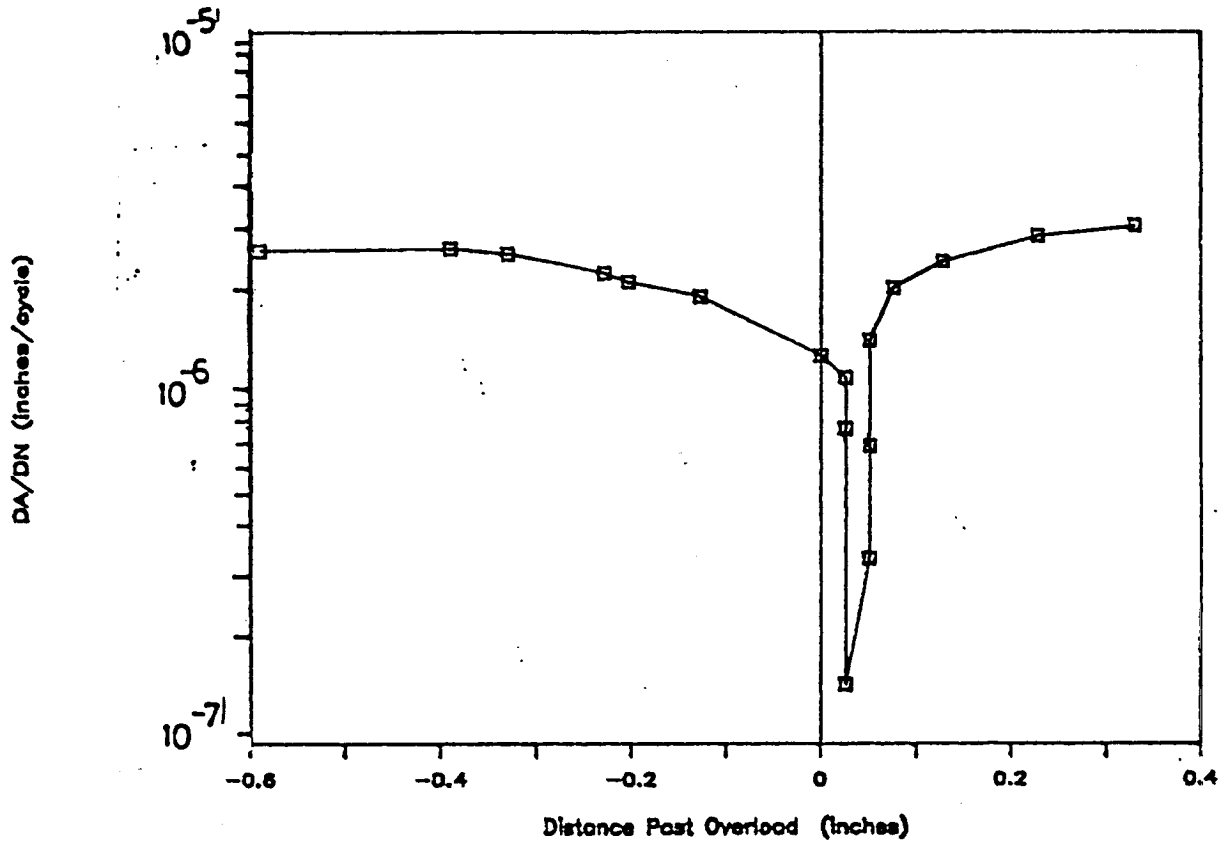

Figure D20. FCP rate versus distance past overload for mixed mode, Q_{ol} = 1.50.

APPENDIX E: Post Overload Compliance Data, Q_{o1} =1.5, R=0.7

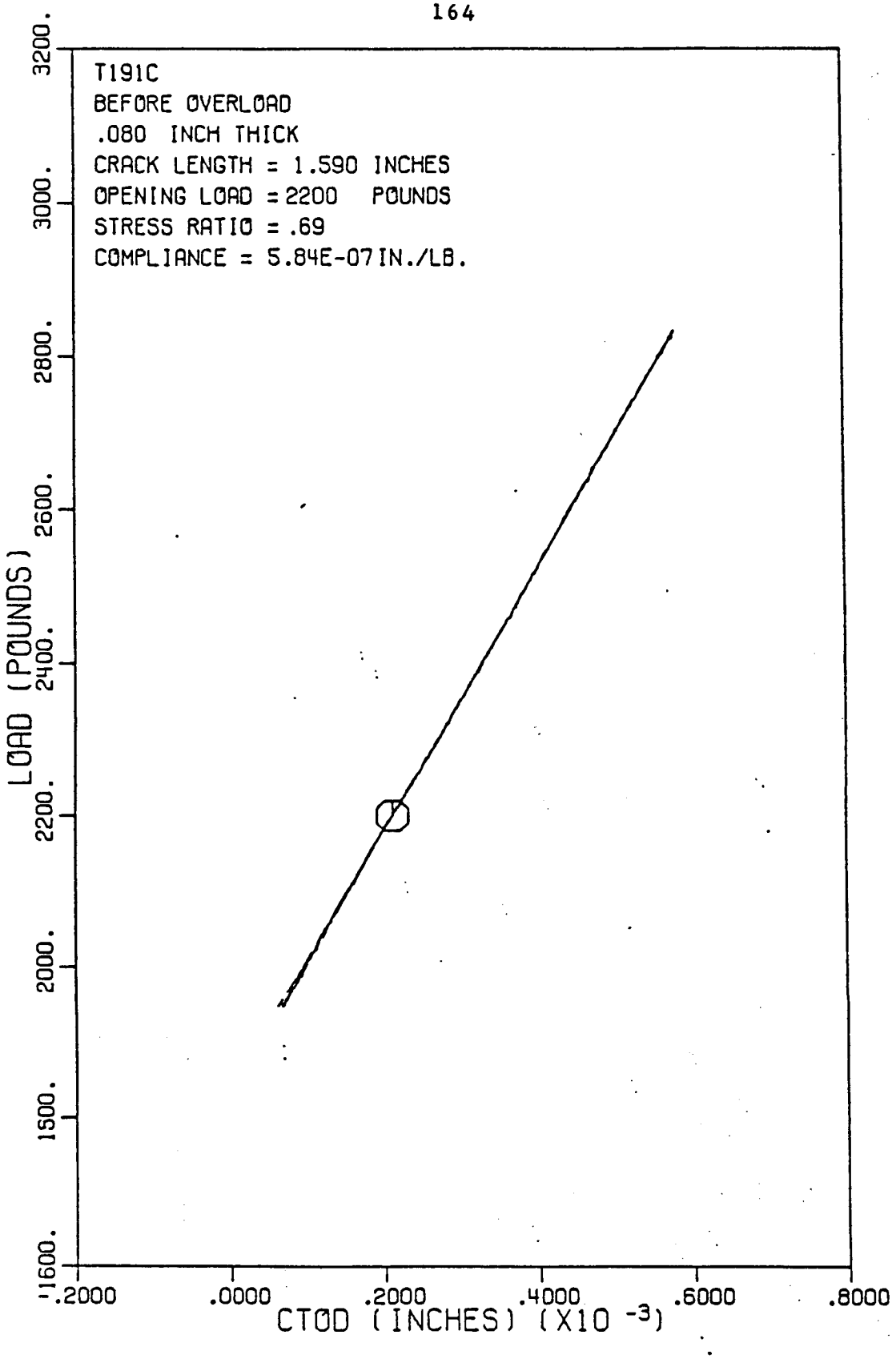

Figure E1. Load versus crack opening displacement before mixed mode overload: $Q_{ol} = 1.50$.

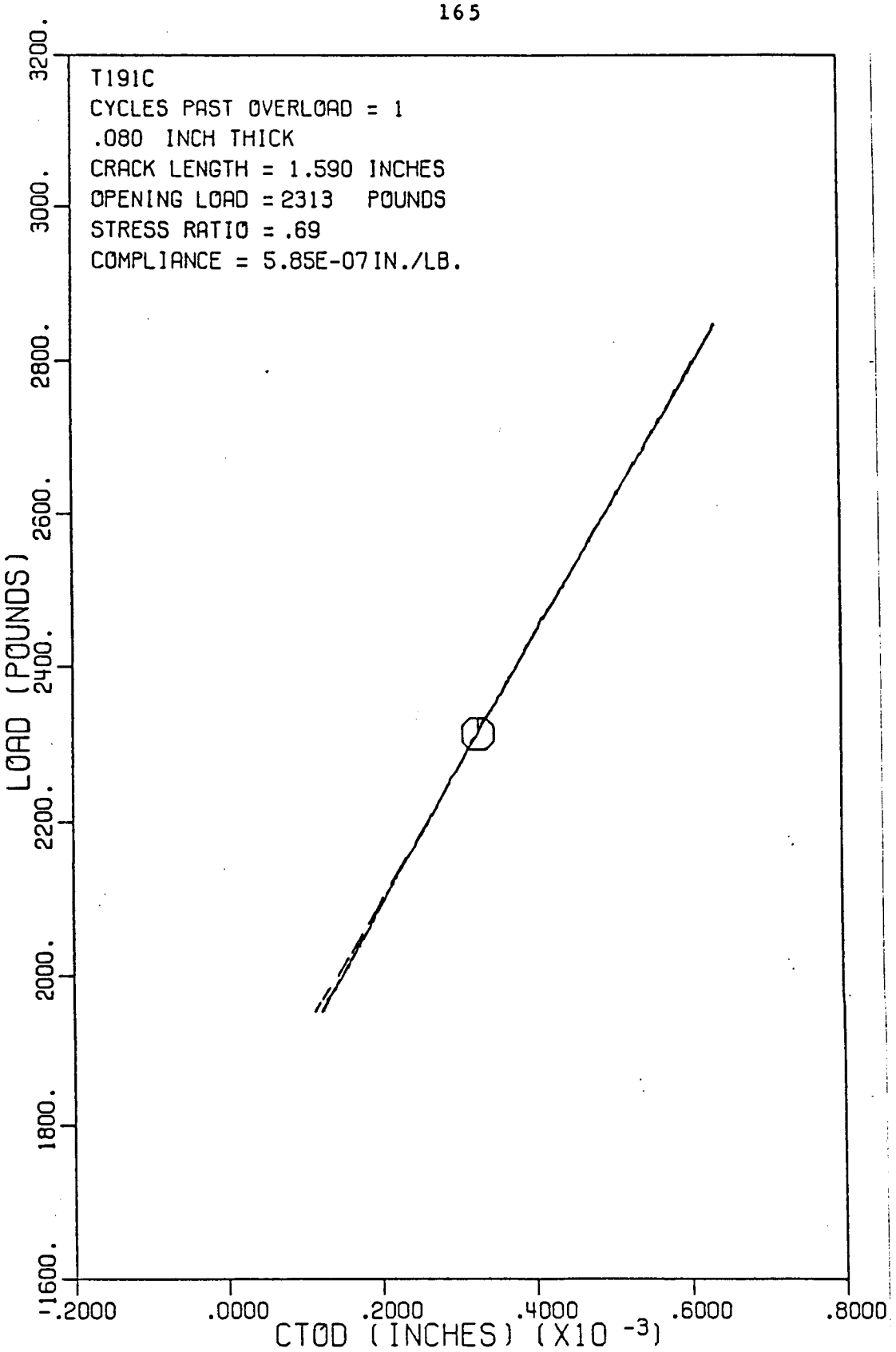

Figure E2. Load versus crack opening displacement 1 cycle after mixed mode overload: $Q_{ol} = 1.50$.

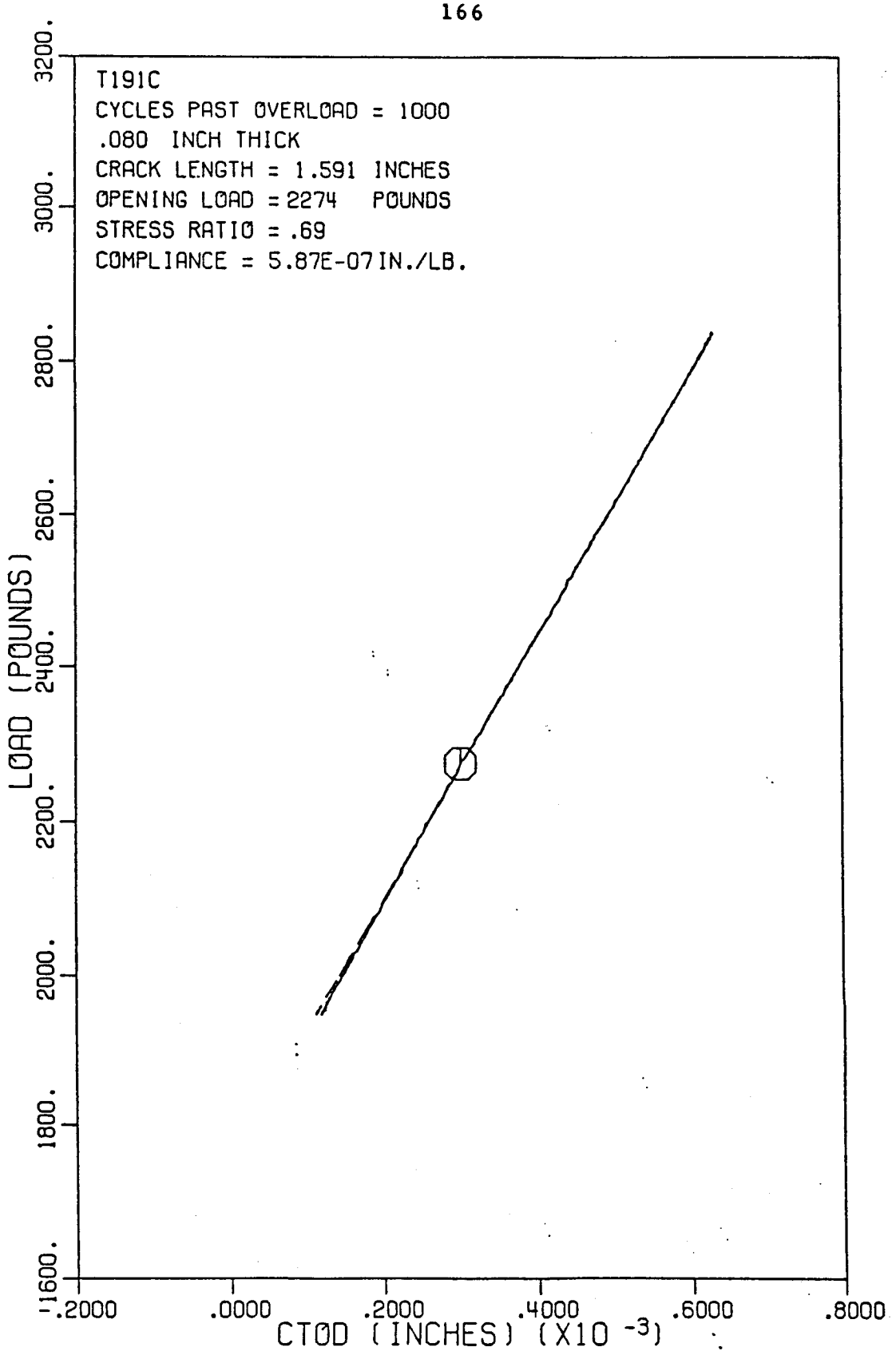

Figure E3. Load versus crack opening displacement 1000 cycles after mixed mode overload: $Q_{ol} = 1.50$.

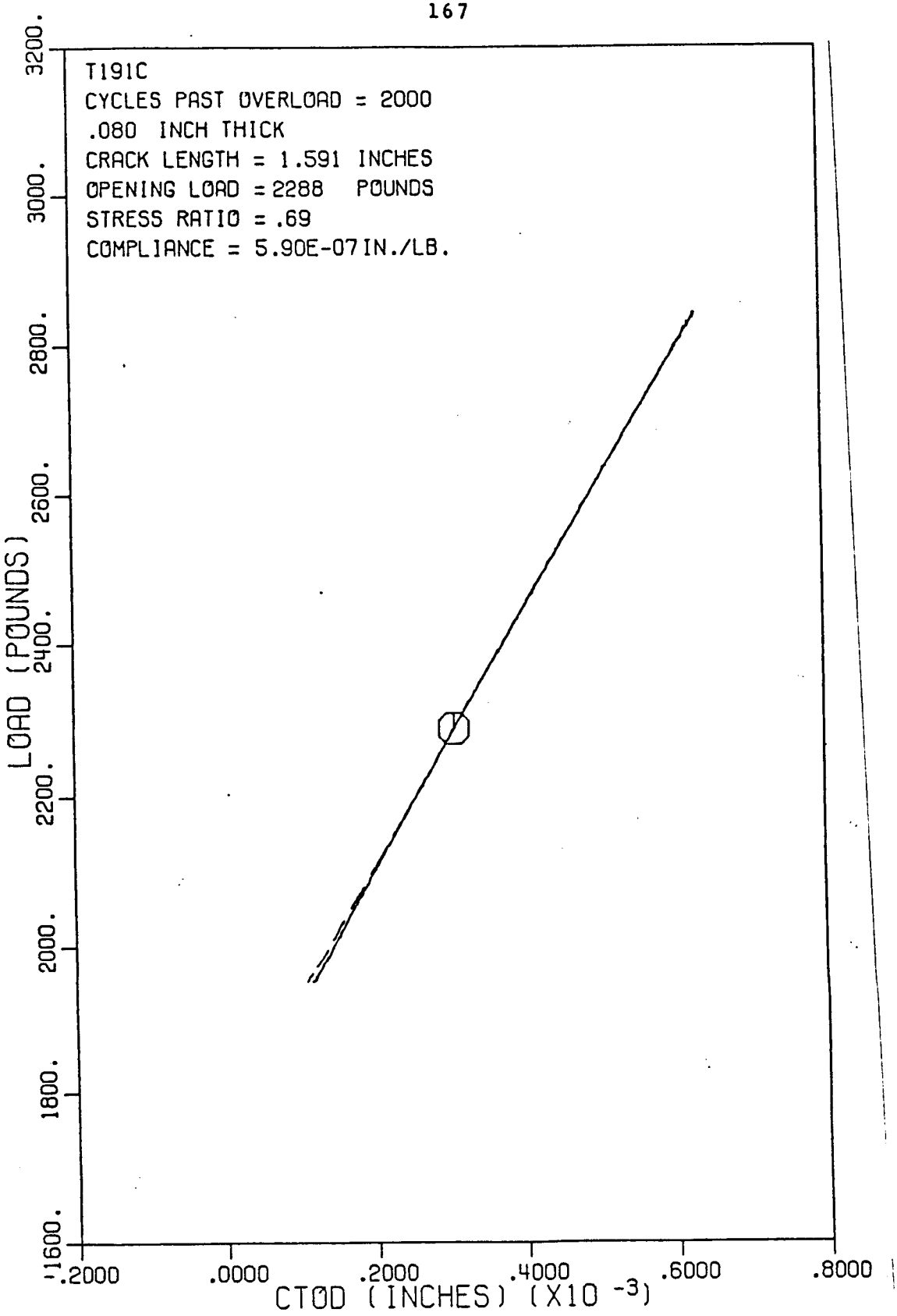

Figure E4. Load versus crack opening displacement 2000 cycles after mixed mode overload: $Q_{ol} = 1.50$.

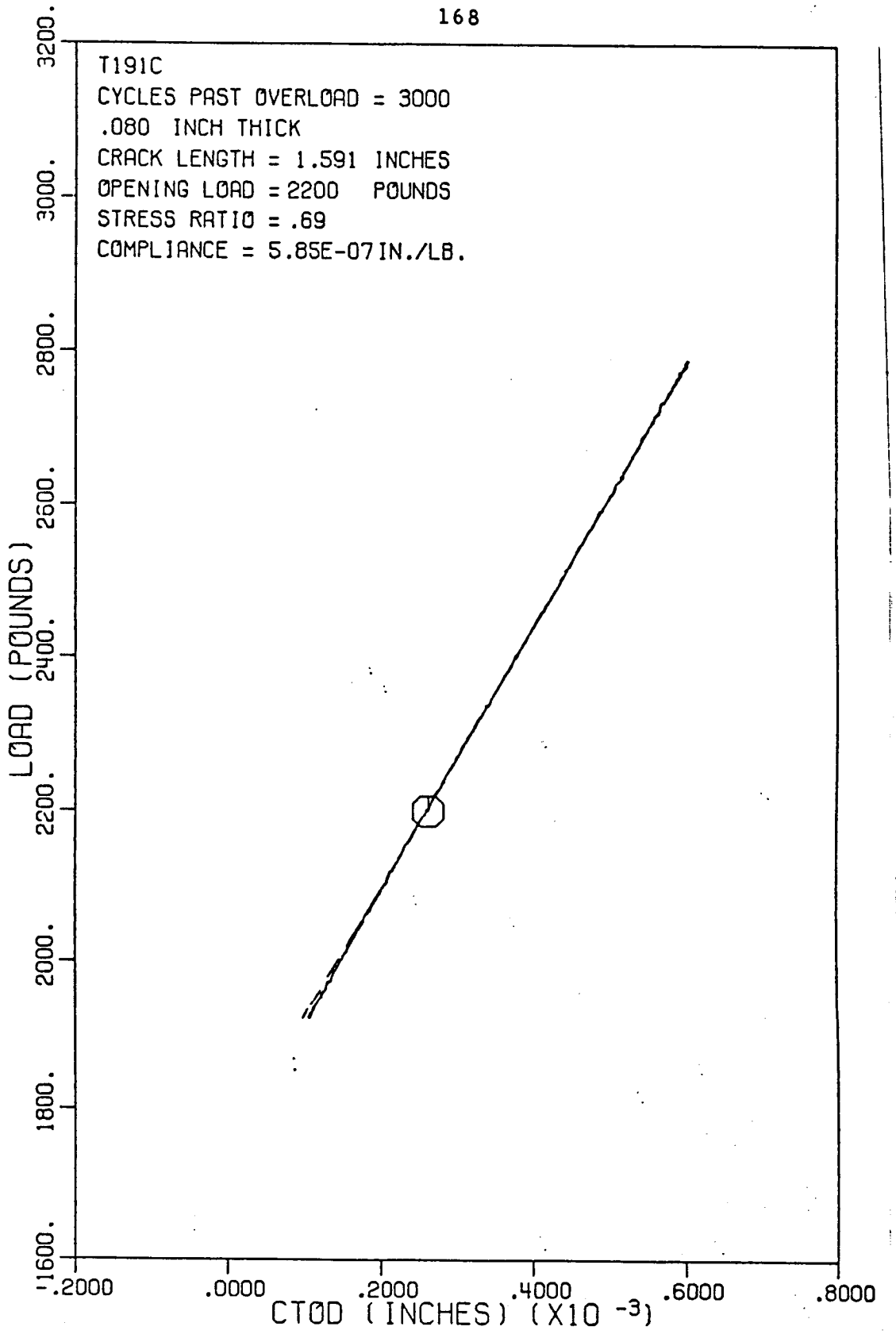

Figure E5. Load versus crack opening displacement 3000 cycles after mixed mode overload: Q_{ol} = 1.50.

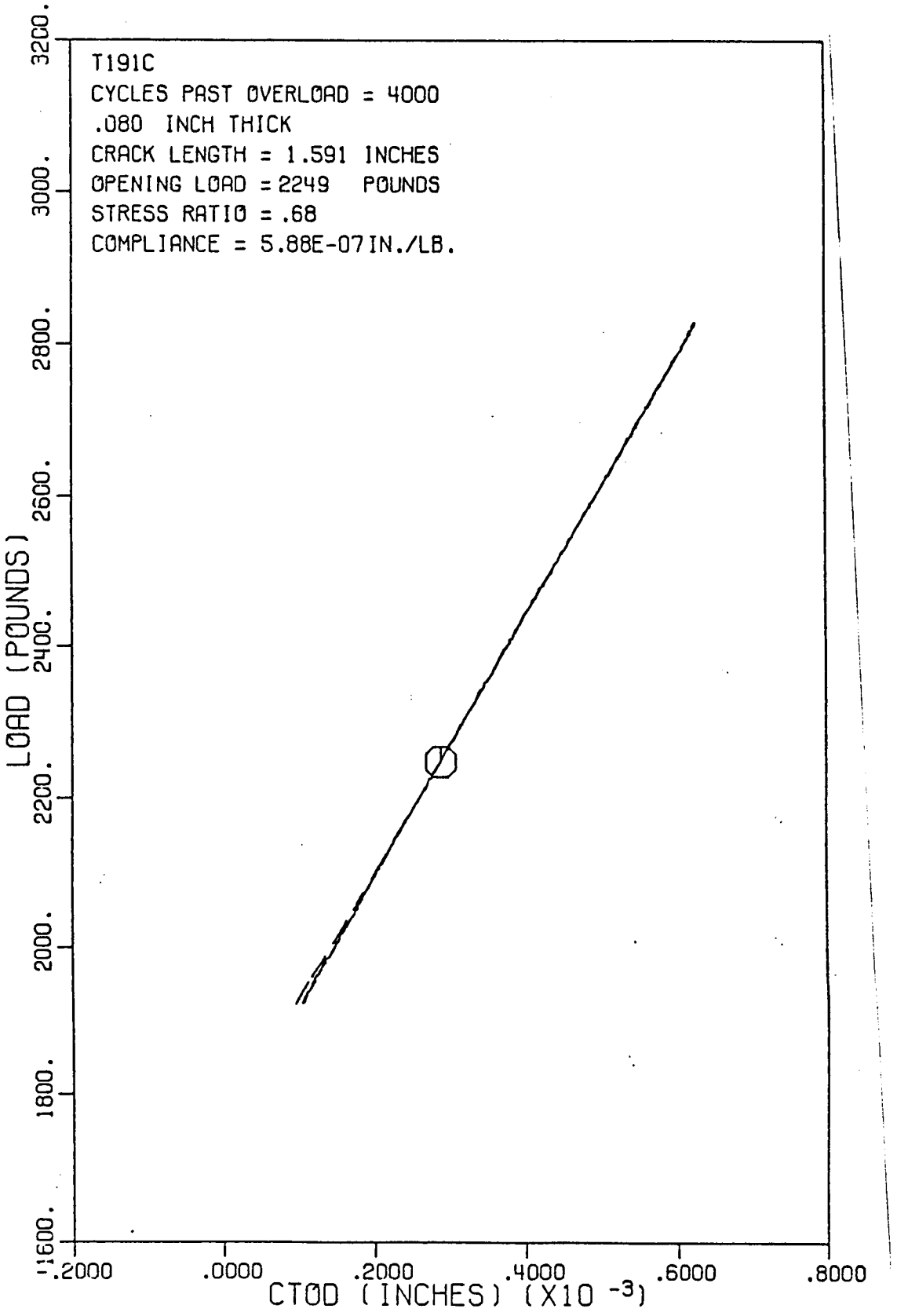

Figure E6. Load versus crack opening displacement 4000 cycles after mixed mode overload: Q_{ol} = 1.50.

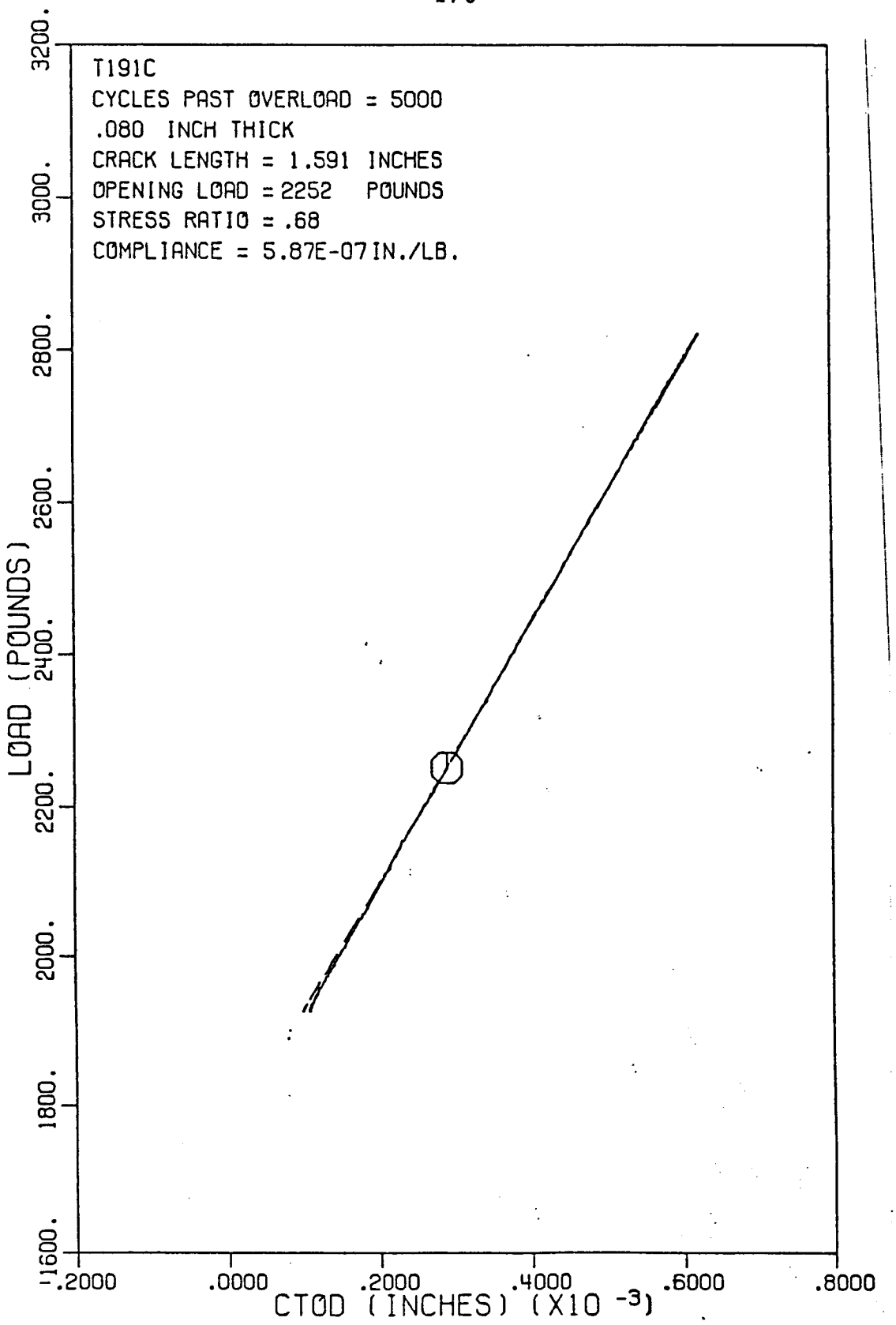

Figure E7. Load versus crack opening displacement 5000 cycles after mixed mode overload: Q_{ol} = 1.50.

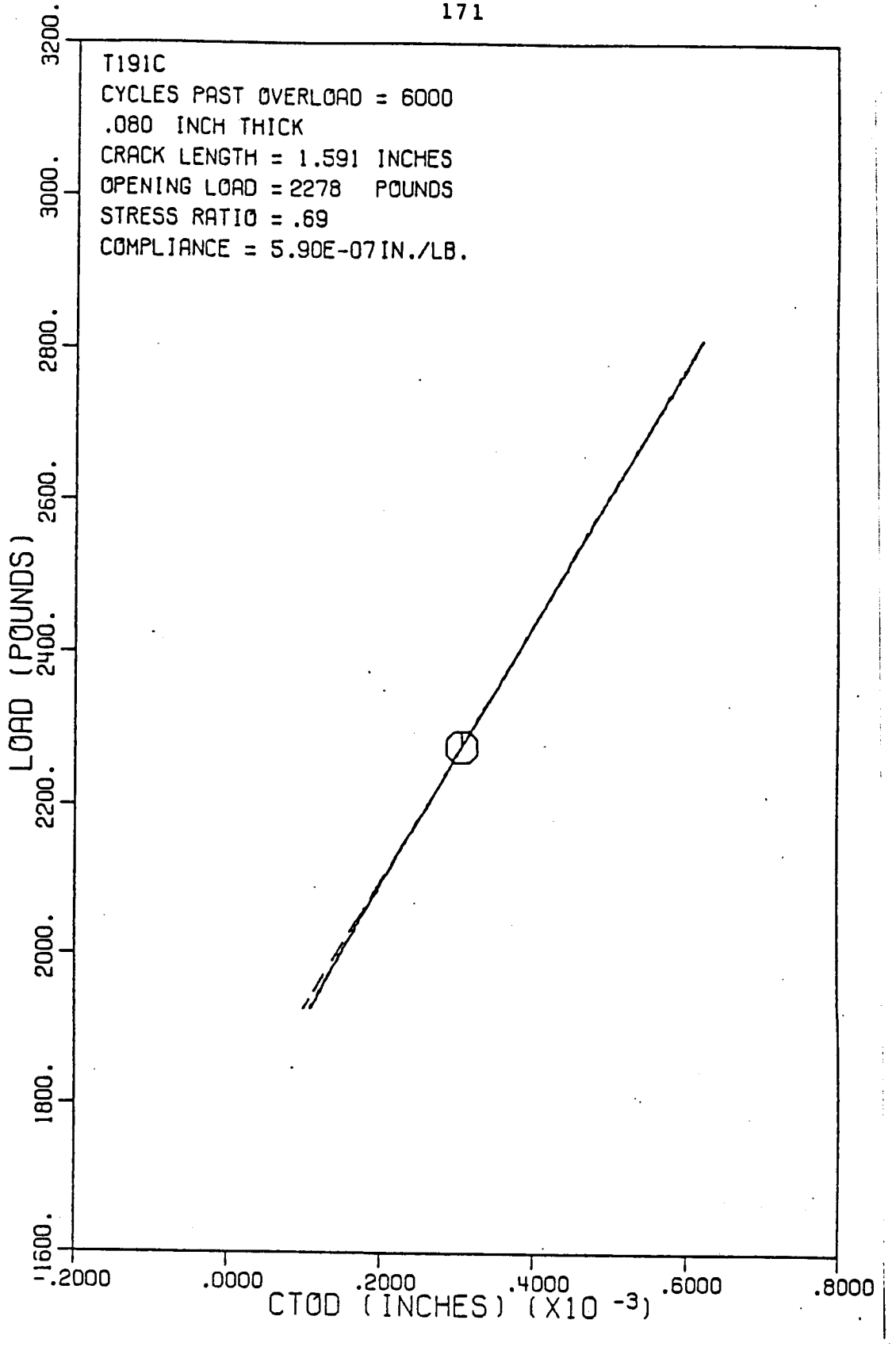

Figure E8. Load versus crack opening displacement 6000 cycles after mixed mode overload: $Q_{ol} = 1.50$.

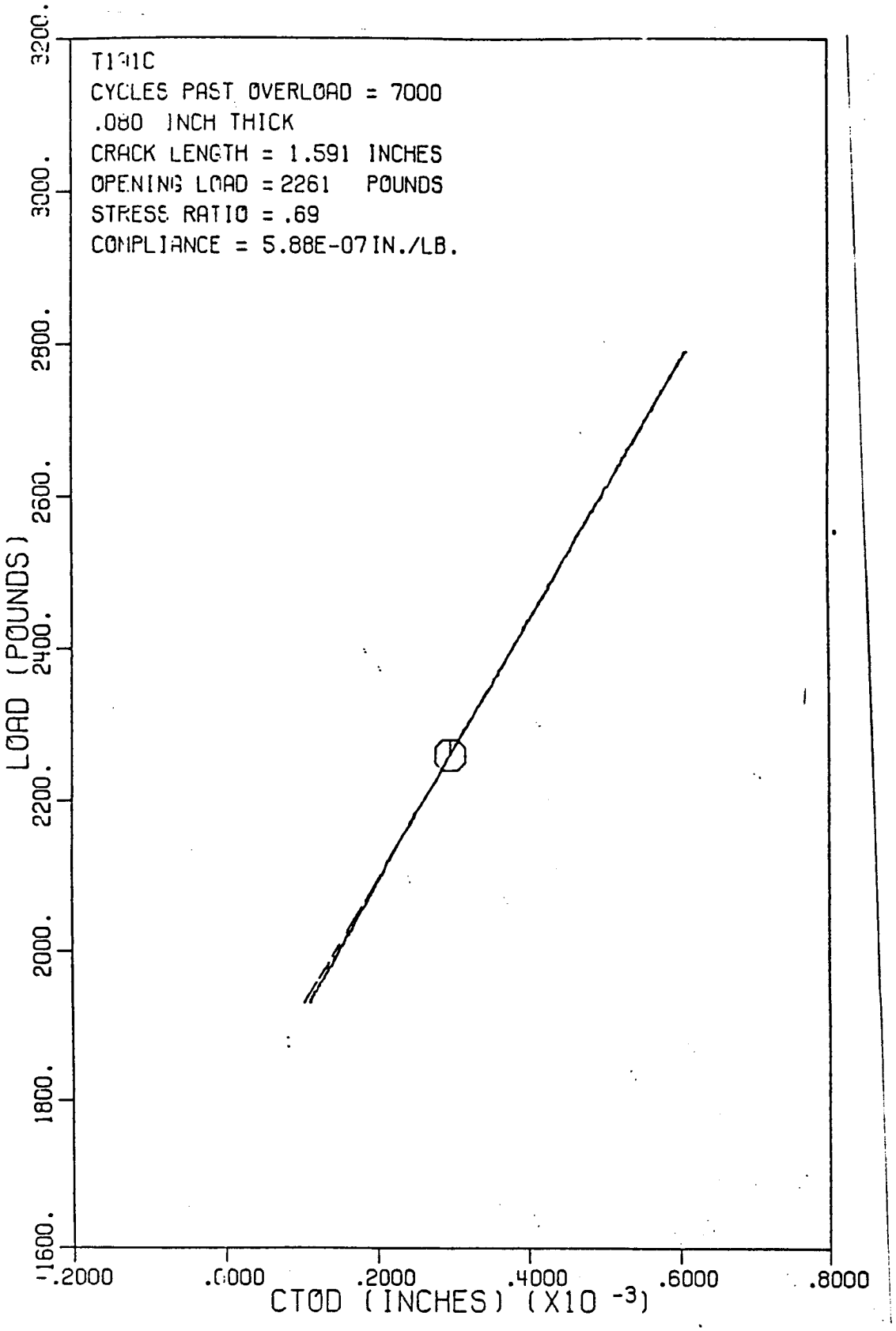

Figure E9. Load versus crack opening displacement 7000 cycles after mixed mode overload: $Q_{ol} = 1.50$.

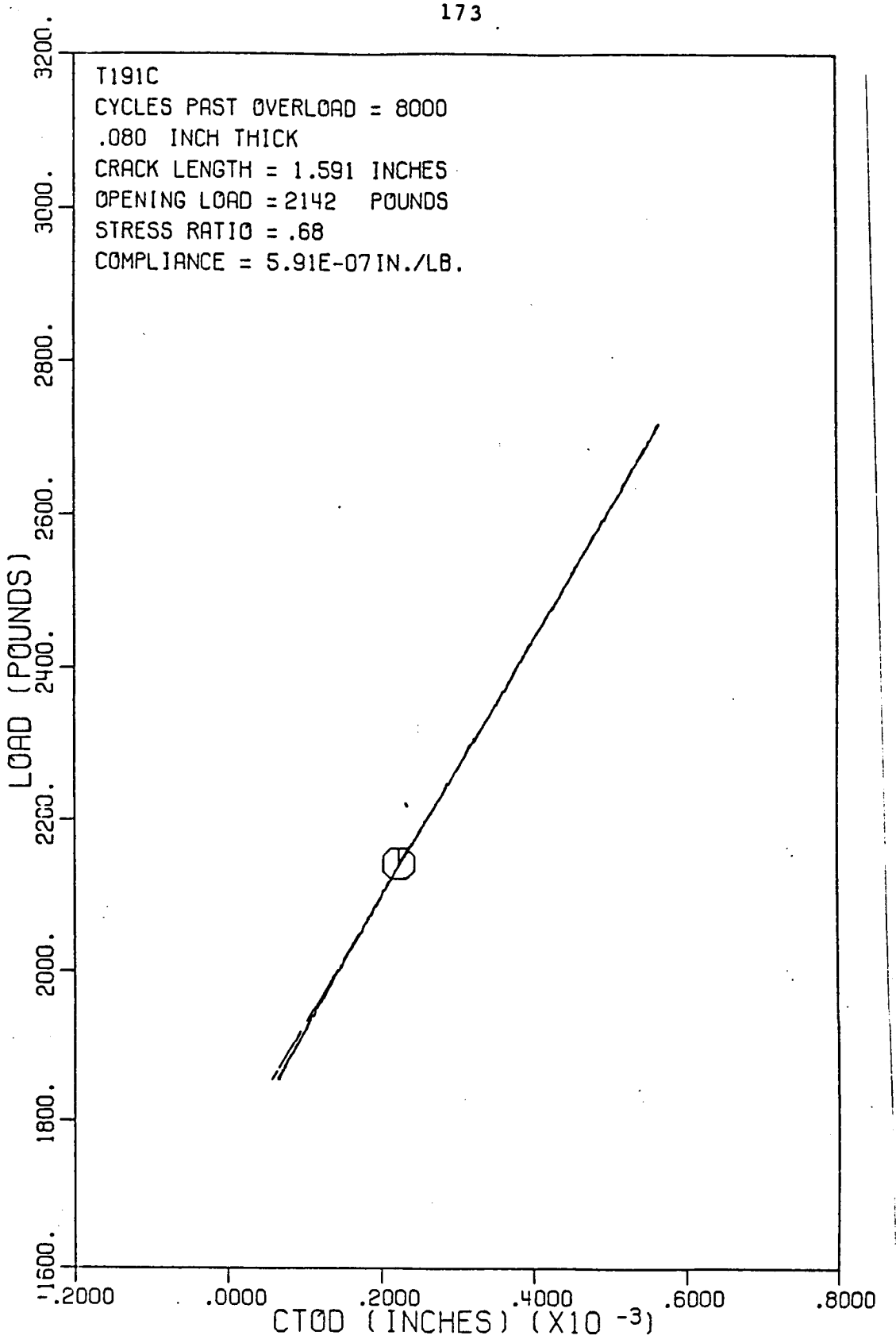

Figure E10. Load versus crack opening displacement 8000 cycles after mixed mode overload: Q_{ol} = 1.50.

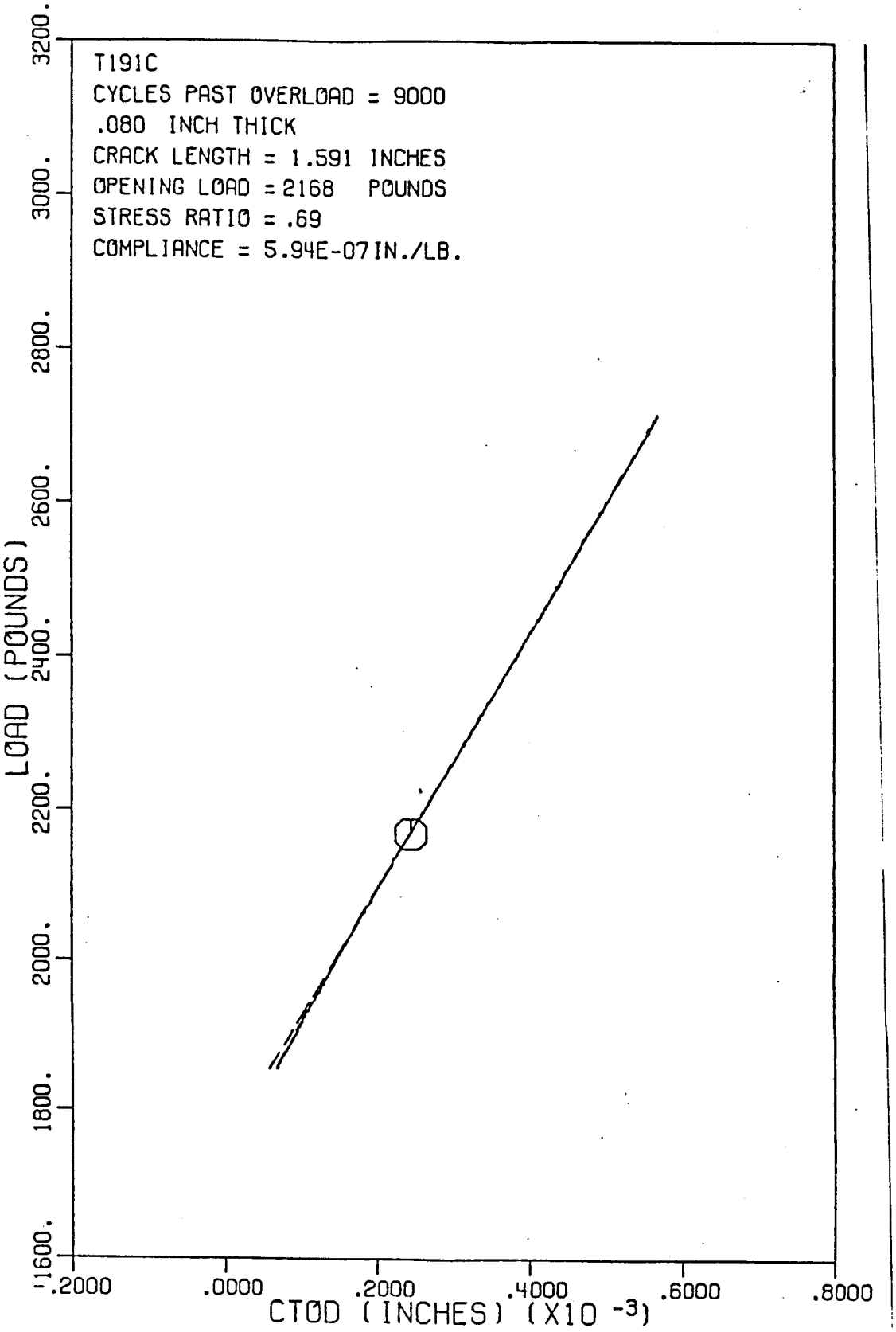

Figure E11. Load versus crack opening displacement 9000 cycles after mixed mode overload: Q_{ol} = 1.50.

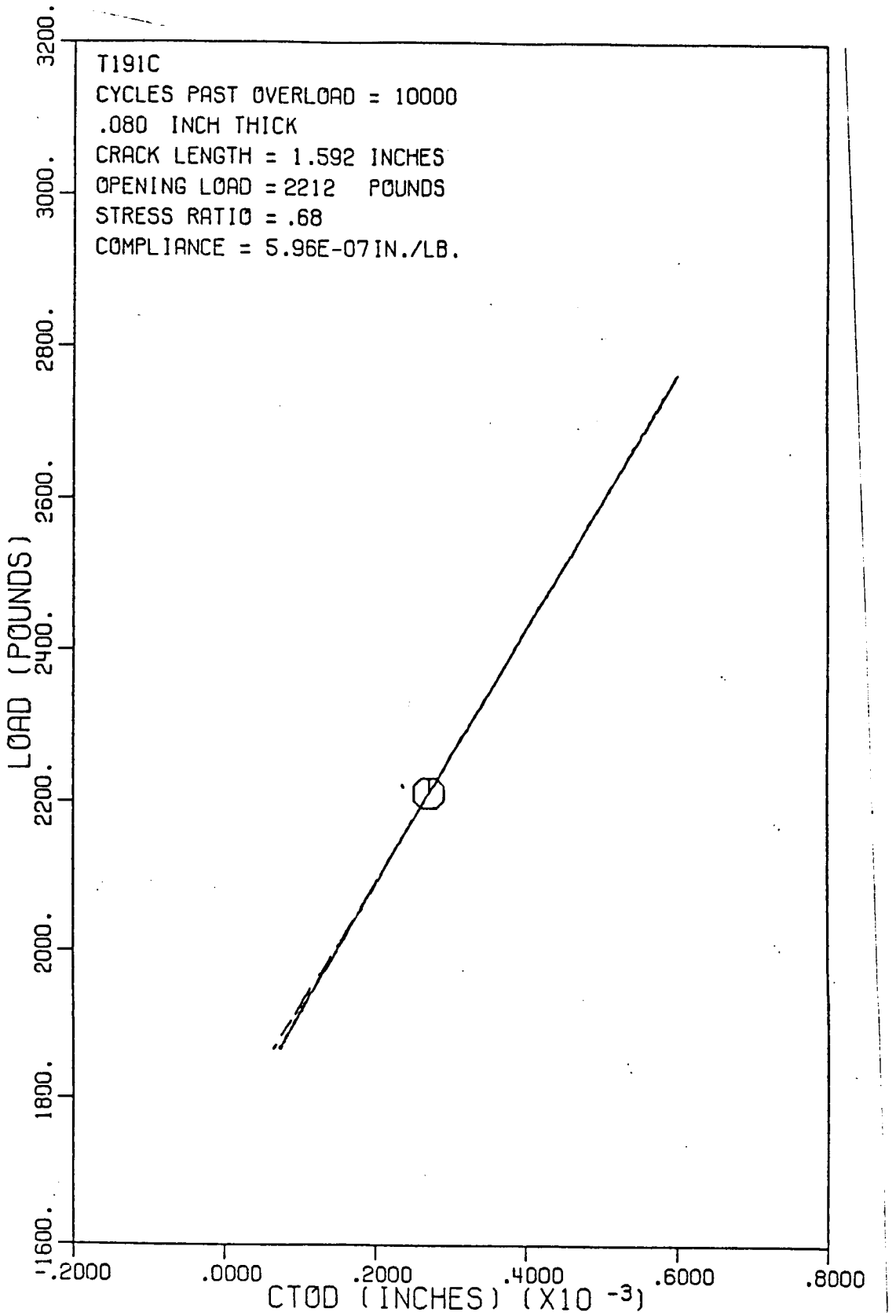

Figure E12. Load versus crack opening displacement 10000 cycles after mixed mode overload: Q_{ol} = 1.50.

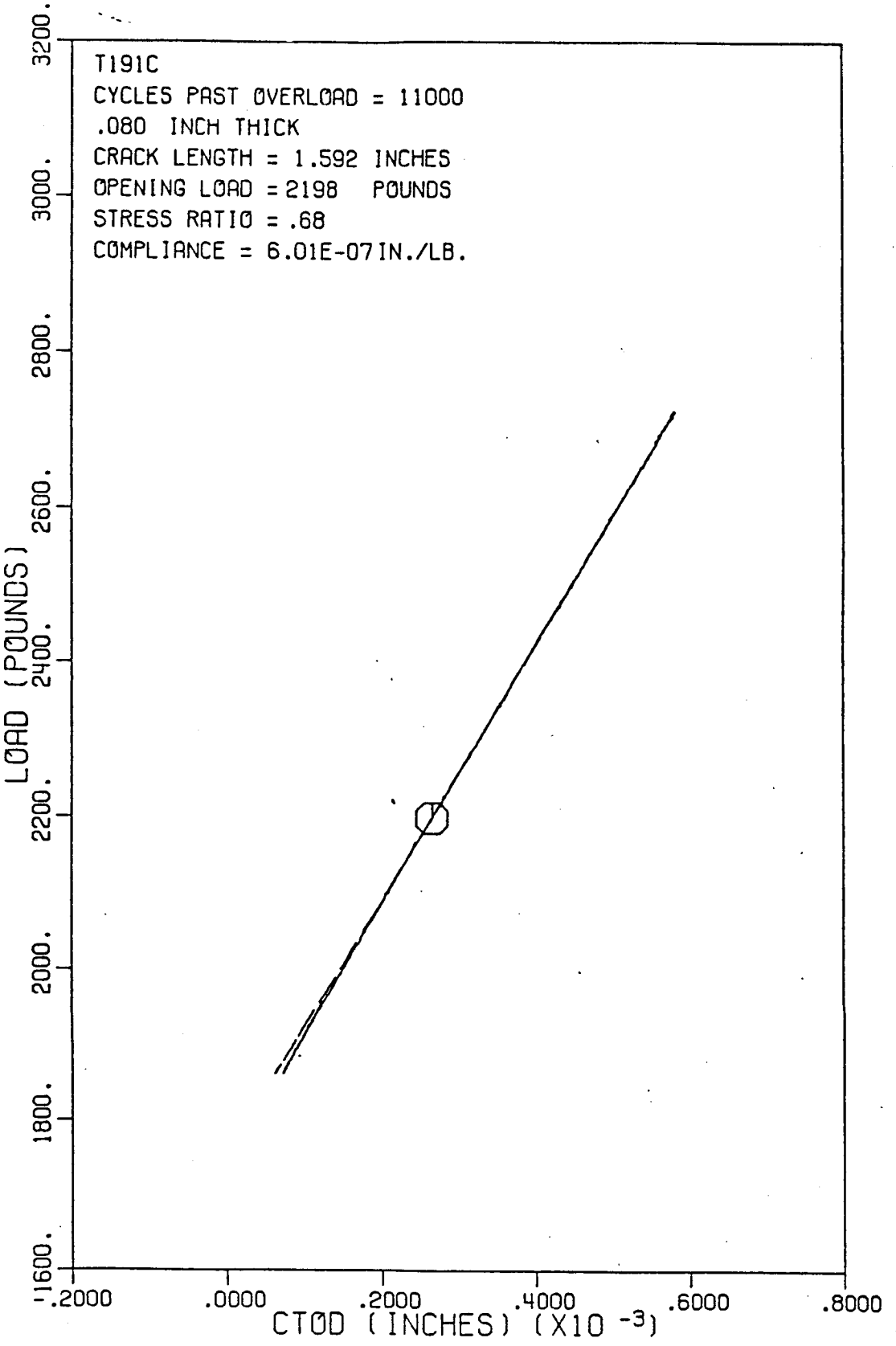

Figure E13. Load versus crack opening displacement 11000 cycles after mixed mode overload: Q_{ol} = 1.50.

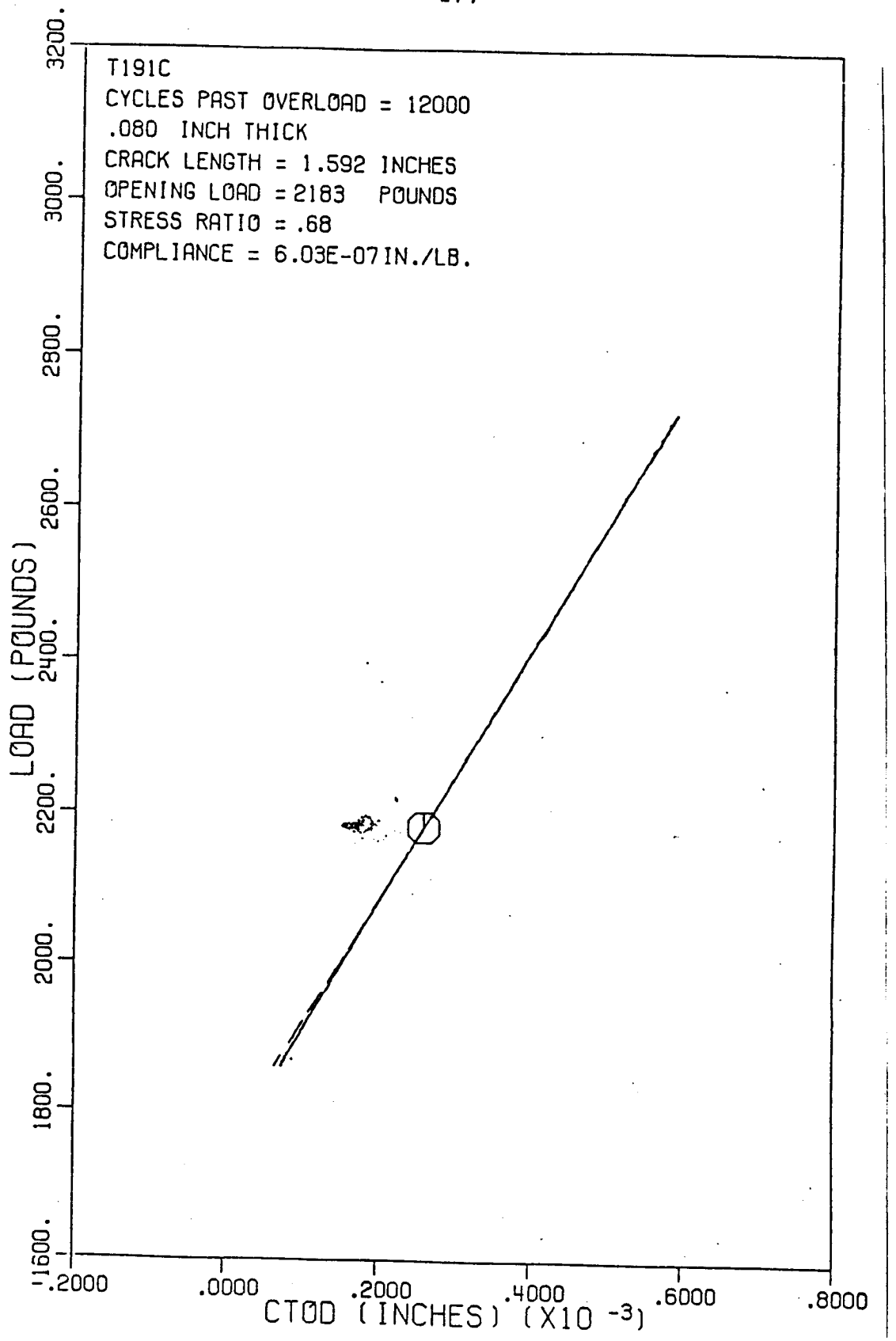

Figure E14. Load versus crack opening displacement 12000 cycles after mixed mode overload: Q_{o1} = 1.50.

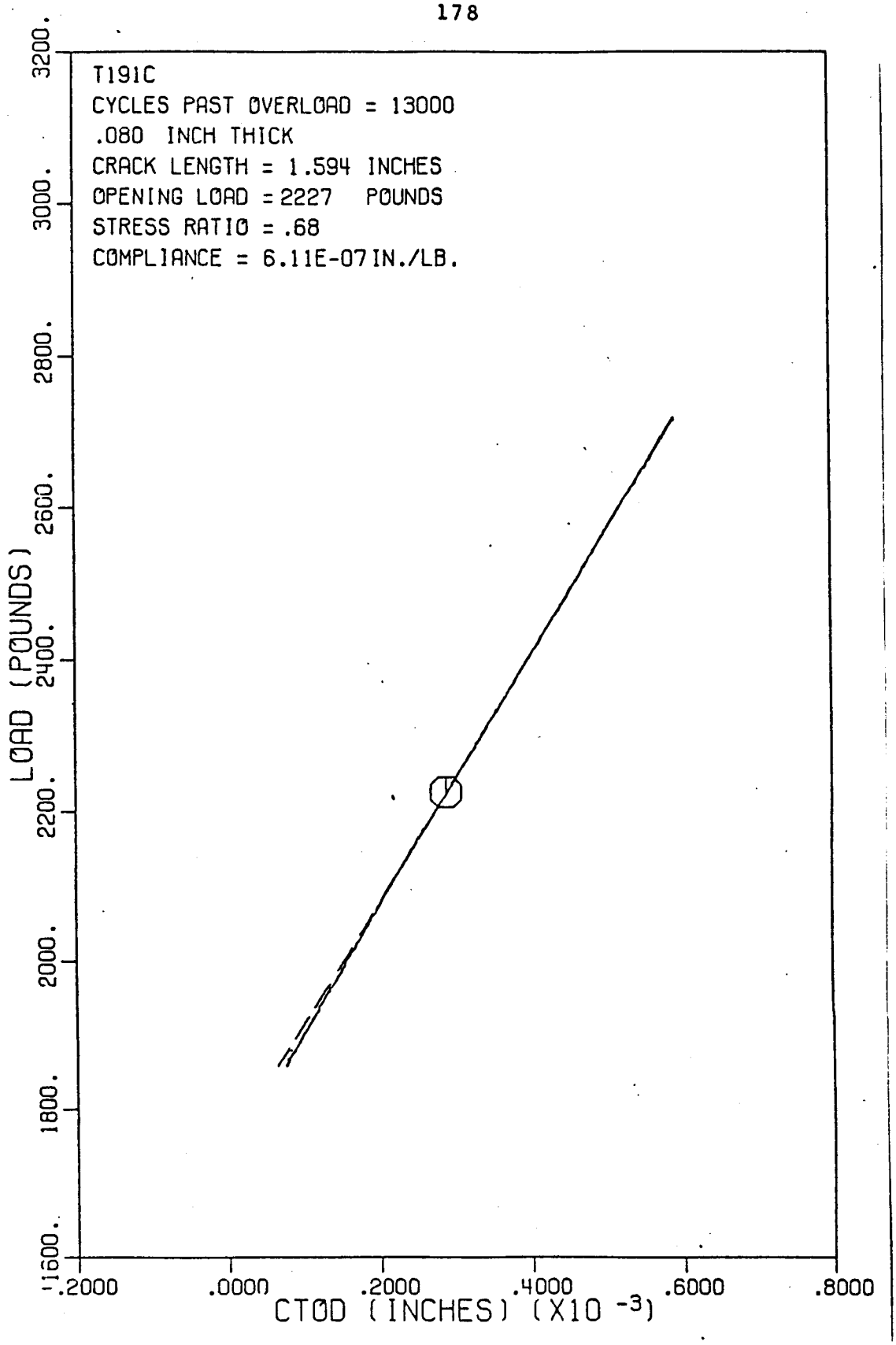

Figure E15. Load versus crack opening displacement 13000 cycles after mixed mode overload: Q_{ol} = 1.50.

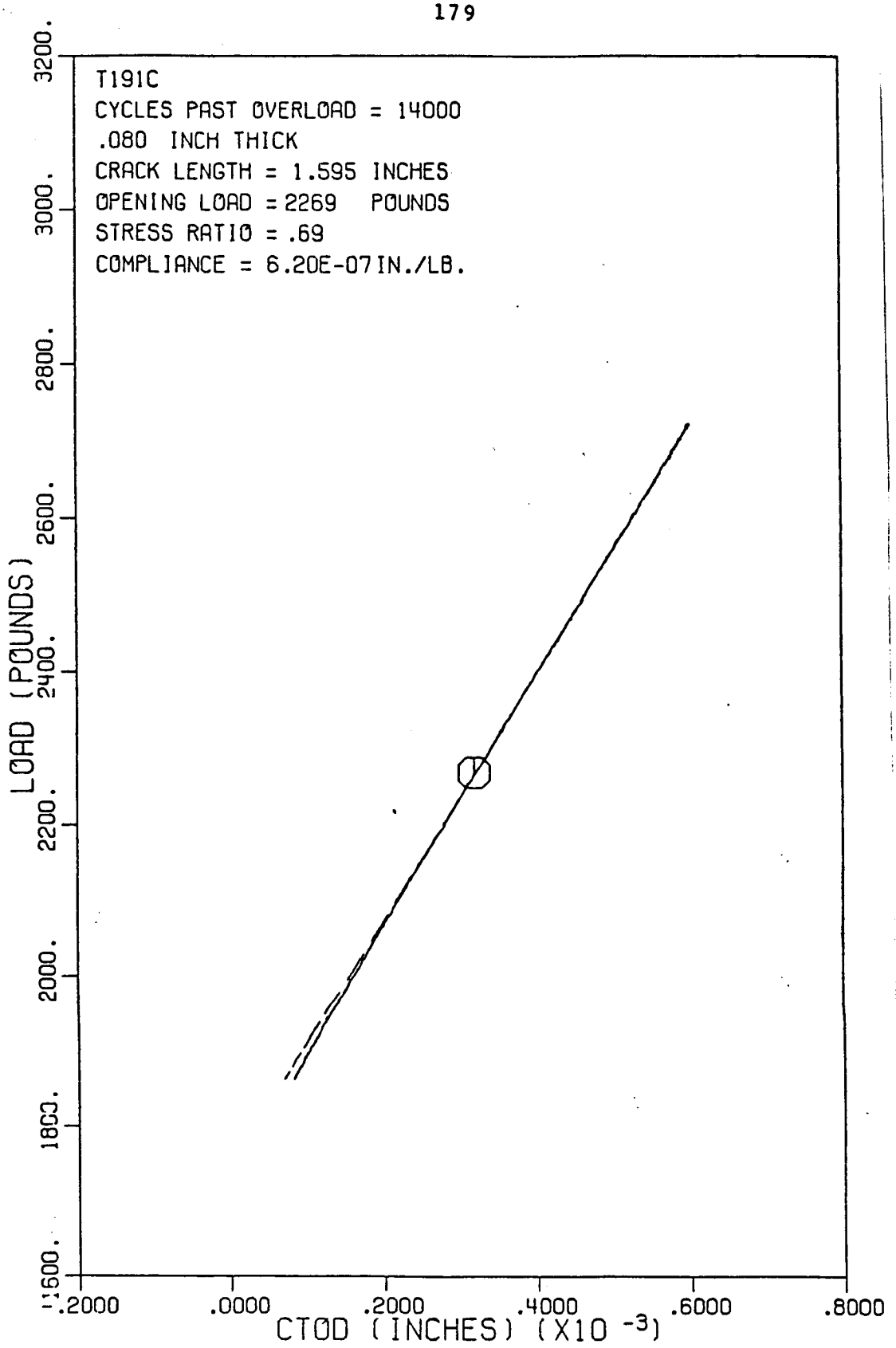

Figure E16. Load versus crack opening displacement 14000 cycles after mixed mode overload: Q_{ol} = 1.50.

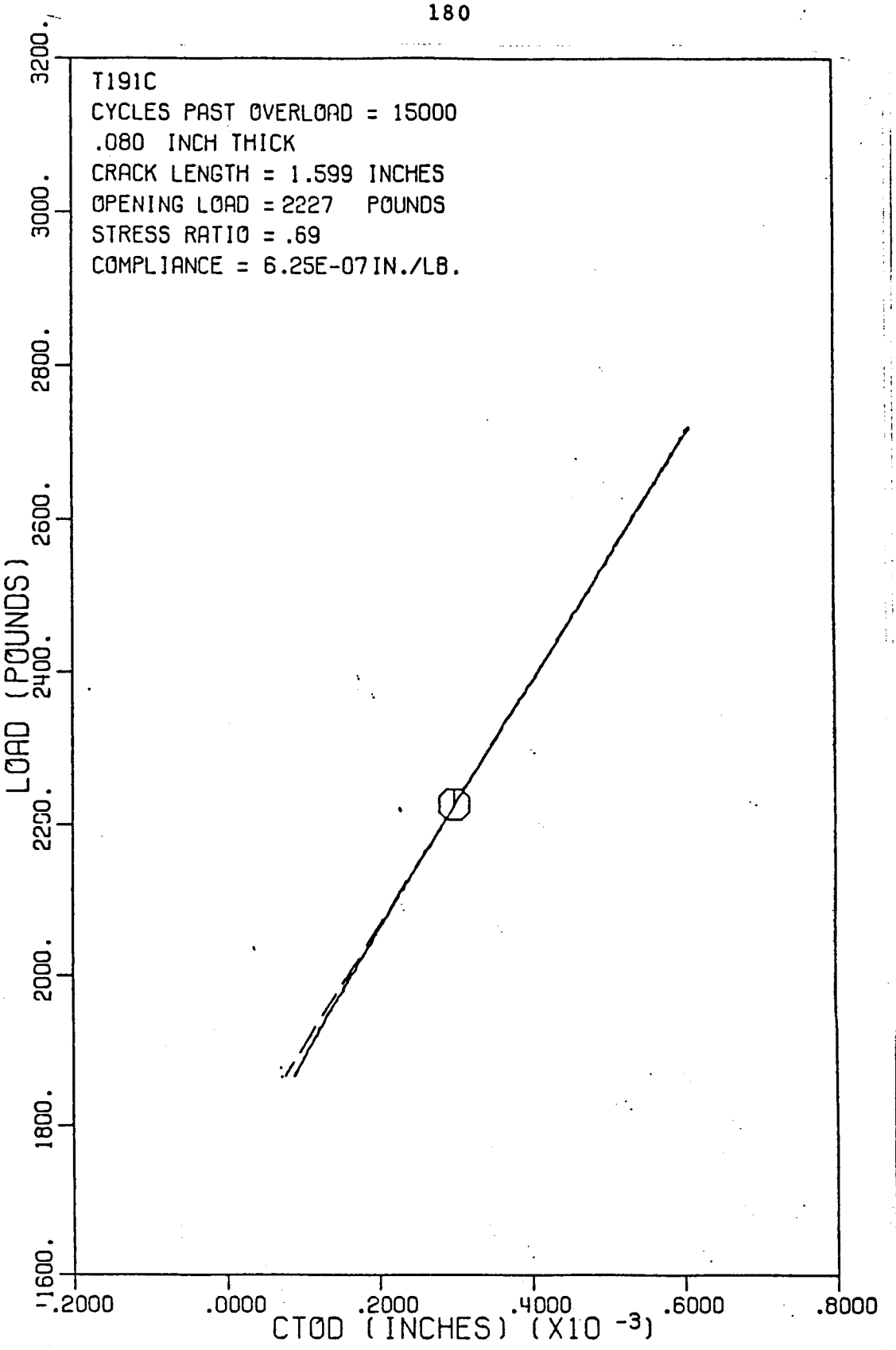

Figure E17. Load versus crack opening displacement 15000 cycles after mixed mode overload: $Q_{ol} = 1.50$.

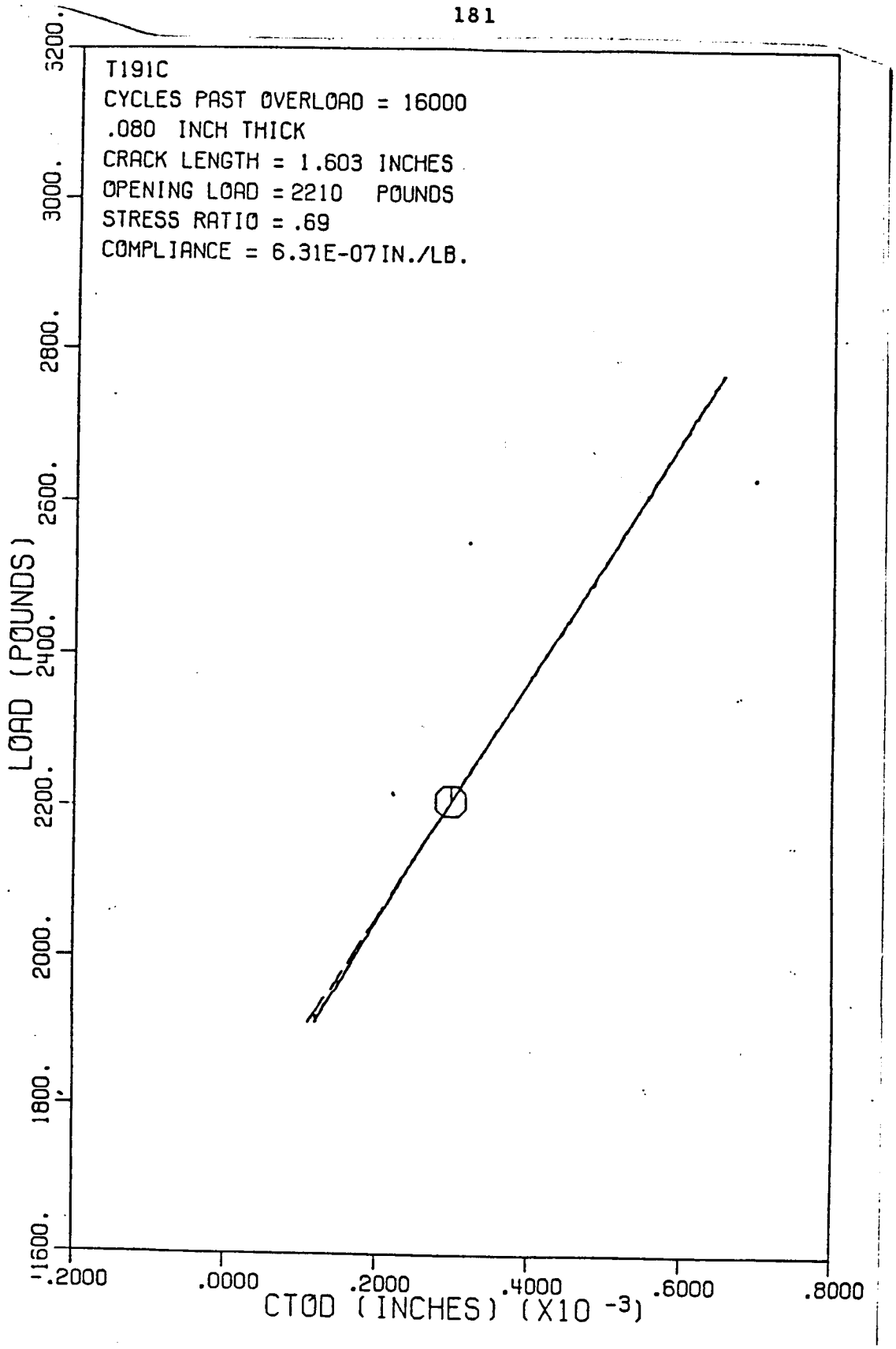

Figure E18. Load versus crack opening displacement 16000 cycles after mixed mode overload: $Q_{ol} = 1.50$.